Representative Volumes and Multi-scale Modelling of Quasi-brittle Materials

Representative Volumes and Multi-scale Modelling of Quasi-brittle Materials

PROEFSCHRIFT

ter verkrijging van de graad van doctor
aan de Technische Universiteit Delft,
op gezag van de Rector Magnificus prof.dr.ir. J.T. Fokkema,
in het openbaar te verdedigen ten overstaan van een commissie,
door het College voor Promoties aangewezen,

op maandag 23 januari 2006 te 10.30 uur

door Inna Mikhailovna Gitman
Master in Applied Mathematics, Perm State Technical University
geboren te Kaluga, Rusland

Dit proefschrift is goedgekeurd door de promotor:

Prof.dr.ir. L.J. Sluys

Samenstelling promotiecommissie:

Rector Magnificus	Voorzitter
Prof.dr.ir. L.J. Sluys	Technische Universiteit Delft, promotor
Prof.dr. N. Bićanić	University of Glasgow, United Kingdom
Prof.dr.ir. J. Carmeliet	Katholieke Universiteit Leuven, België
Prof.dr.ir. M.G.D. Geers	Technische Universiteit Eindhoven
Prof.ir. A.C.W.M. Vrouwenvelder	Technische Universiteit Delft
Dr.ir. M.A. Gutiérrez	Technische Universiteit Delft
Dr.ir. H.E.J.G. Schlangen	Technische Universiteit Delft

cover design: Inna M. Gitman
ISBN 90-64641-22-6

Contents

1 Introduction

Composite materials are becoming increasingly popular in modern engineering applications. The progress in civil engineering, aerospace industry, biomechanics and many other branches of technology increases the role of these materials. In the scope of this contribution the definition of a composite material can be given as *a material that is a combination of at least two mechanically distinct materials, with a distinct interface separating the components, created to obtain properties that cannot be achieved by any of the components acting alone (Schaffer et al. [87]).* Even if a material appears to be *homogeneous* (from Latin *homogeneus*: homo — same, similar and genos — kind, type; i.e. uniform in structure or composition throughout) on a higher scale of observation, it normally has a *heterogeneous* (from Latin *heterogeneus*: hetero — different and genos — kind, type; i.e. composed of parts having different characteristics or properties) composite structure on lower levels of observation. In the context of this manuscript the homogeneous structure of the material on the higher observation level will be denoted as the macro-structure of the material, and the higher observation level will be called the macro-level. The heterogeneous description of the material corresponds to the meso-structural description and this lower observation level will be called the meso-level.

Regarding the mechanical modelling, a composite material can be defined as a heterogeneous medium with effective properties. One of the central problems in mechanics is the problem of estimating these effective characteristics. It allows to represent any heterogeneous medium by some homogeneous medium with known overall properties and to use existing mathematical tools to describe its behaviour. At the same time, the analysis of the mechanical behaviour of composites allows not only to *define* these effective properties but also to obtain information about the deformation of material according to the real structure of composites and its components.

The overall goal of this contribution is to introduce a tool to describe the mechanical behaviour of a material with a composite structure. In other words, a representation of the composite material is formulated that supplies knowledge about effective mechanical properties according to the real structure of the material and on the basis of that to describe, explain and predict the response of the composite. As a special case of composites, quasi-brittle materials will be analysed in this thesis. The attention will be focused on the mechanical loading. Furthermore, this mechanical loading will consist of linear and nonlinear stages. Particular focus will be put on the so-called softening (post-peak) stage. The material in the post-peak regime is known to develop localised deformations, e.g. strain localisation. Properties of a material undergoing strain localisation are considerably different and special approaches are needed in order to describe its behaviour. A mechanical model, in which multiple scales are considered, will be introduced in this thesis, which can capture and represent such a material.

1.1 Mechanical models

Every model is built on three foundations:

- the goal of the model;
- the modelling approach;
- the parameters of the model.

In the scope of this contribution let us define the mechanical model using the above three categorisations.

The goal of the model

According to the different goals two types of mechanical models can be introduced: **descriptive** and **optimisational** (Ashihmin et al. [5]). The idea of a **descriptive** model is to formulate evolution laws for relevant parameters. As it follows from the name, these models are describing and explaining the behaviour of a modelled object. **Optimisational** models usually are introduced in order to define an optimal parameter of a modelled object for a certain criterion of interest.

In this manuscript the attention will be focused on the description of the mechanical behaviour of a composite material. Thus a **descriptive** model will be built. Once this **descriptive** model is accomplished, it could serve as the basis for an **optimisational** model in which the structure of the composite is optimised. However, this is beyond the scope of the present study.

The modelling approach

Two approaches can be distinguished in order to formulate a mechanical model of the material: **macrostructural** and **mesostructural** (in this thesis the focus is on the mesostructural, rather than microstructural or nanostructural, description of the material). **Macrostructural** models are built on the basis of empirical data describing the behaviour of a mechanical object. The knowledge of detailed material behaviour, i.e. the geometrical configuration and constitutive response of all material components, if more than one, is not essential here. The **mesostructural** approach on the contrary allows to construct models to describe and explain the detailed material behaviour on the basis of the internal structure of a mechanical object. The formulation of linear/non-linear models to *describe the overall response* of composites corresponds to the **macrostructural** approach. On the other hand, the detailed description of a composite by accounting for internal material components with their own constitutive properties represents the **mesostructural** approach. An alternative, third approach is the **macro-meso** or **multi-scale** approach. The idea of this approach is to consider a material on several levels simultaneously: for instance the mesoscopic level, which takes care of the actual structure of a composite material, and the macroscopic level, describing the behaviour of the composite material as homogeneous with effective properties.

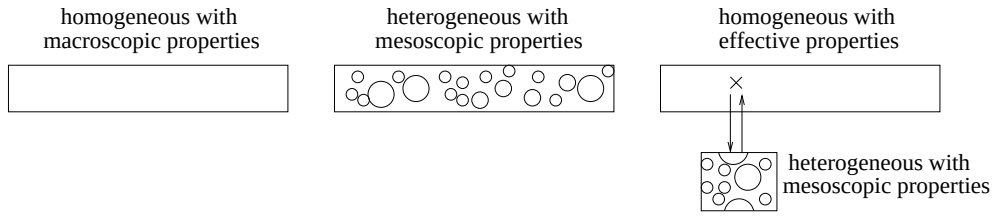

Figure 1.1: Left: macrostructural approach, middle: mesostructural approach, right: multi-scale approach

The inherent heterogeneous nature of a composite is taken into account differently in the three approaches, see also fig. 1.1:

- The **macrostructural** approach corresponds to a homogeneous description of the material, whereby all material properties are defined explicitly and assigned particular values in order to describe certain phenomena. Thus, the mesoscopic processes are accounted for by additional macrostructural parameters, for example length- or time-scale parameters.
- In the **mesostructural** approach, the material is described as a heterogeneous medium. As in the macrostructural approach, all properties are defined explicitly, but now these properties differ for each material component.
- Finally, in the **multi-scale** approach both homogeneous and heterogeneous descriptions are employed. On the macro-level the composite will be described as a homogeneous material and on the meso-level as a heterogeneous material.[1] On the meso-level the material properties are defined explicitly for each individual material component. The material properties on the macro-level do not appear explicitly, but they follow as effective properties via the meso-macro connection.

In this contribution, the main focus will be on the multi-scale approach. This approach is often denoted as *hierarchical*, i.e. a single material point is understood as belonging to the homogeneous material on the macro-level and, at the same time, to the heterogeneous material on the meso-level.

The parameters of the model

The nature of the parameters appearing in the model depends on the modelling approach that is pursued.

[1] In this work, a two-level multi-scale approach will be taken, whereby the higher level of observation is denoted as the macro-level and the lower level as the meso-level. In other studies, multi-scale approaches involve micro and/or nano-levels of observations (Ghoniem and Cho [33], Zohdi et al. [115], etc.).

- **Macrostructural approach**. It is well-established that the classical problem statements for a homogeneous continuum are not suited to describe effects that occur on a lower scale of observation. Therefore it has been proposed to extend the classical formulation by incorporating additional gradients of certain state variables, see for instance Aifantis [1, 2], de Borst and Muhlhaus [23], Lasry and Belytschko [58], Mühlhaus and Aifantis [72], Peerlings [77], Schreyer and Chen [88], Sluys [92]. The information from the lower level enters the macrostructural continuum via one or more additional material constants, usually in the form of so-called length-scale parameters or time-scale parameters. The latter could be related to viscosity if first-order time derivatives are taken into account de Borst and Sluys [24], or micro-structural inertia in case of second-order time derivatives Aifantis [3], Rubin et al. [86], Vardoulakis and Aifantis [106], Wang and Sun [109]. For certain transient analyses *both* length-scales and time-scales are included in the continuum description Aifantis [3], Askes and Metrikine [7], Metrikine and Askes [65], which allows for a realistic description of wave dispersion.

- **Mesostructural approach**. In a mesostructural approach, the relevant parameters are of the same nature as in the macrostructural approach, the difference being that they are now defined for each material component separately. Again, length- and time-scales may appear that represent a lower level of observation; this lower level would then be the micro-level or the nano-level.

- **Multi-scale approach**. Alternatively, when the scales of observation interact, the various scales can be studied simultaneously in a *multi-scale* analysis. The lower and higher scales interact by coupling the kinematics and the various stresses and forces of the two levels. Apart from the material parameters of the meso-level, one of the key parameters in the multi-scale description is then the considered size of this meso-level. Traditionally, this size is viewed within the concept of a Representative Volume Element (RVE). The meso-level cell employed in multi-scale analysis is assumed to be an RVE, and as such the size of the RVE is a relevant model parameter in these approaches.

The *model parameter* RVE size from the multi-scale technique and the *material parameters* length-scale and time-scale from the macrostructural continuum approach are related to each other. Such links have been established for materials with a periodic micro-structure by means of continualisation methods, e.g. [7, 65]. More general case of random micro-structure has been treated by Gitman et al. [35, 36, 37] where the aforementioned links have also been obtained. In Kouznetsova et al. [54] for the case of microstructurally *homogeneous* material a similar link has been established independently. These links will be used in the identification and quantification of the macrostructural length-scale and time-scale parameters in this study.

1.2 Outline

Following a *state of the art* overview given in Chapter 2, three main parts of this contribution can be distinguished: Chapter 3 continues the discussion started above on the parameters appearing in the macrostructural and multi-scale approaches. The detailed analysis of the RVE size is presented in Chapter 4, where also the issue of *existence* of an RVE is covered for the pre-peak and post-peak loading stages. Finally, the multi-scale material description is the subject of Chapter 5.

In Chapter 3 links are established between the phenomenological material parameters of the macrostructural approach and the model parameter of the RVE size that appears in the multi-scale approach. By means of analytical homogenisation, the appearance (if any) of macrostructural length- and time-scale parameters in so-called local and non-local homogenisation schemes is addressed. Whereas the links between macroscopic length- and time-scales with the RVE size have been derived for periodic media already (as mentioned above), here the extension is made towards general, randomly heterogeneous composites.

Chapter 4 deals with the detailed analysis of the RVE size. A statistical procedure based on the first and the second statistical moments (mathematical expectation and standard deviation) is introduced to clarify the question of the RVE existence in the pre-peak and post-peak stages of the material response. A novel method to define the RVE size, if existent, is presented. The influence of deterministic and stochastic test and material parameters on the RVE size is studied. In order to analyse the effect of stochastical characteristics, a novel stochastic stability (DH–stability) concept is formulated and employed. The issues of periodic boundary conditions and periodic material are also addressed in this Chapter. Parallel to the RVE size investigation, the Size Effect theory for the case of heterogeneous materials is discussed, and a link with the issue of RVE size existence is established.

Once the question of the RVE size is clarified, a multi-scale analysis is formulated in Chapter 5. Firstly, the local homogenisation scheme of Chapter 3 is taken. The dependence of the results with respect to the macro-level discretisation parameter (finite element size) and the meso-level model parameter (RVE size) is studied in detail. These issues are also addressed for the non-local homogenisation scheme, after which an alternative multi-scale procedure is formulated. This new procedure exhibits results that are reliable and insensitive to the macro-level discretisation and to the meso-level model parameter.

Finally, conclusions and possible perspectives on future research are addressed in Chapter 6 of the dissertation.

2 State of the art

In this Chapter an overview of the relatively modern field of the multi-scale modelling of composite materials is presented. The Chapter is divided into two sections: the first one deals with the research in the direction of multi-scale approaches and the second one discusses the knowledge about Representative Volumes, which is an important modelling parameter in multi-scale analysis.

2.1 Multi-scale approaches

A general framework to link material properties at two levels of description, incorporating both physical and geometrical nonlinearities, was suggested in 1984 by Hill [48]. He described the material as heterogeneous on one level, while on the other hand he considered the macroscopic behaviour to be homogeneous. In the 1980s and the 1990s the interest in multi-scale approaches was increasing rapidly, with the applications ranging from concrete-like composites Zimmermann et al. [114] to polycrystalline materials Miehe et al. [68] and porous media Trukozko and Zijl [99]. Since the same material point is considered on two levels of observation simultaneously, this approach is also called *hierarchical*, and in this thesis the term *multi-scale* should be understood as being hierarchical.

In order to provide a categorisation of the various strategies that are used in multi-scale analysis, a main distinction is made between those approaches that lead to *closed-form expressions* on the macro-level and those approaches that do not. In the former, analytical techniques are used in combination with continualisation or homogenisation, and they are treated in Section 2.1.1. The latter are denoted here as computational homogenisation techniques, and they are discussed in Section 2.1.2.

2.1.1 Analytical continualisation and homogenisation

Analytical multi-scale techniques comprise continualisation and homogenisation. The main difference between the two is the representation of the material on the meso-level: in continualisation techniques the material is modelled on the meso-level as a discrete medium consisting of masses and springs, e.g., whereas in homogenisation techniques the meso-level material representation is a heterogeneous continuum. Thus, continualisation indicates that a discrete model is translated into a (homogeneous) continuum model, and homogenisation indicates that a heterogeneous continuum is translated into a homogeneous continuum.

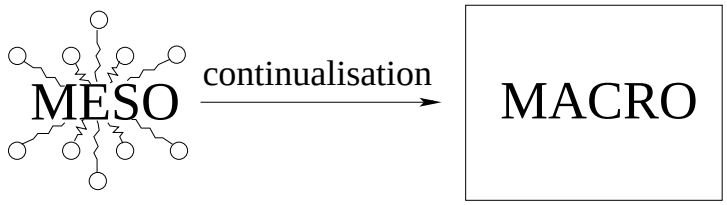

Figure 2.1: Analytical continualisation

Analytical continualisation

The philosophy of continualisation approaches, illustrated in fig. 2.1, can be summarised as:

- **meso-level:** the material is described as a heterogeneous discrete system consisting of masses and springs, possibly extended with dashpots or frictional elements if nonlinear behaviour is to be modelled. Often, a regular discrete lattice geometry is assumed, for instance patterns of hexagons or squares in two-dimensional problems;
- **up-scaling:** links are established between the variables of the discrete model and the corresponding variables of the continuum. These links are commonly referred to as the kinematic hypothesis if displacements are concerned, and static hypothesis in case of forces. Taylor series are used to translate the difference relations of the discrete model into differential relations of the continuum;
- **macro-level:** the material is described as a homogeneous continuum whereby all material coefficients are expressed in terms of mesostructural properties, such as the stiffness of the springs. The order of the continuum depends on the truncation of the Taylor series mentioned above: the lowest truncation possible leads to a classical continuum, but so-called higher-order continua may be derived by taking higher-order derivatives of the Taylor series into account. In the latter case, the higher-order coefficients can be expressed in terms of the interparticle distance of the discrete model.

Classical and higher-order continua were derived by Chang and Gao [21] and Mühlhaus and Oka [71]. Later, Suiker et al. [96] elaborated upon these works. Random particle packings were considered, by which the constitutive coefficients on the macro-level were obtained as summations over all interparticle contacts within the considered volume. Isotropy of the resulting macroscopic continuum was addressed by Askes and Metrikine [8].

A continuum model including micro-inertia for heterogeneous materials on the micro-level under dynamic loading was proposed by Wang and Sun [109]. The macro-level strain and stress are defined as the volume averages of the strain and stress fields in the unit cell. Although the conventional definitions of *volume-averaged* stresses and strains

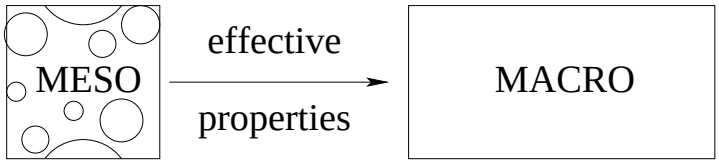

Figure 2.2: Analytical homogenisation

are adopted in their formulation, the *local* dynamic equations of motion are used. As a result, the macro strain energy density and the macro kinetic energy density contain the micro-inertia. Consequently, when Hamilton's principle is employed to obtain the macro equations of motion, an effective body force term appears in the macro equations of motion. This effective body force which is absent from the conventional continuum mechanics formulation, contains the micro-inertia effect.

Another continualisation procedure was proposed by Metrikine and Askes [65]. The kinematic coupling between the displacements of the discrete model and the continuum was formulated as a weighted average. The obtained continuum description was automatically equipped with micro-inertia as well as higher-order stiffness contributions [7, 65].

Analytical homogenisation

Analytical homogenisation is mostly performed as follows (see also fig. 2.2):

- **meso-level:** the material is described as a heterogeneous continuum. The boundary value problems are solved, for instance by means of the finite element method;
- **up-scaling:** the meso-level solutions are translated into effective properties for the macro-level.
- **macro-level:** the material is considered to be homogeneous. A specific format for the constitutive relations on the macro-level is assumed. Macroscopic constitutive constants appear in the form of effective properties, obtained from the meso-level.

Similar to continualisation, the macroscopic constitutive relations are obtained in closed form with quantitative information from the meso-level. In the analytical homogenisation approaches as given above, the format of the macroscopic constitutive relation must be given a priori[1].

Analytical homogenisation procedures are an efficient modelling tool for elastic materials. A standard elasticity format was used by Guedes and Kikuchi [42] to determine the effective elastic constants of general composite materials. Peerlings and Fleck [79] have proposed a strain-gradient approach to describe the materials behaviour. They determined

[1] In Chapter 3 an alternative analytical homogenisation technique is discussed, that does not rely upon a priori assumptions of the macro-level constitutive relation. However, it must be assumed that local perturbations of stiffness and strain remain small.

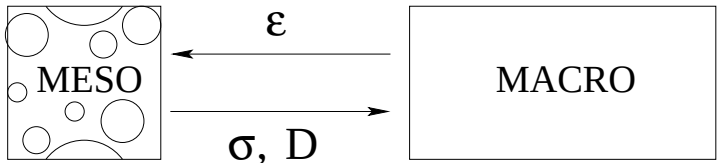

Figure 2.3: Computational homogenisation

all elastic constants (classical and higher-order) as effective properties from a number of boundary value problems solved on periodic microstructures. A micromechanical-based approach has also been used by Fatemi et al. [30]. They derived the effective Cosserat elastic moduli of cellular solids using analytical homogenisation. They assumed that on the micro-level the "cell wall" material is classically elastic and on the macro-level it behaves as a homogeneous Cosserat-type solid. To derive the effective elastic Cosserat constants, a Cosserat homogenisation technique has been used. Kinematic boundary conditions in terms of displacement and rotation were applied on the representative material sample (RVE). The coefficients of the overall Cosserat elastic tensors for the equivalent homogeneous medium have been determined by relating the resulting Cauchy stress and couple stress tensors (from the response of the material sample) to the applied strain and curvature tensors.

More recently, also nonlinear material behaviour has been modelled with analytical homogenisation approaches, see for instance van der Sluis [101]. However, the complexity of the problem increases significantly due to the choices available for the a priori assumed macroscopic constitutive relation.

Note 1 *The term 'analytical homogenisation' can be understood in two ways: either an analytical procedure is followed, or the result of the procedure is an analytical (i.e. closed-form) expression. Here, the latter meaning is implied. However, the approach followed in Chapter 3 is analytical in terms of procedure as well as results.*

2.1.2 Computational homogenisation

Instead of analytical continualisation or homogenisation, computational homogenisation (fig. 2.3) can be used. The difference of this approach from the one discussed above is the absence of an explicitly defined constitutive equation on the macro-level. The macroscopic constitutive relation is implicitly provided by the macro-meso-macro connection. The concept of computational homogenisation can be summarised as follows:

- **macro-level computation:** the material is described as homogeneous with *effective properties* but it does not require any constitutive assumption;
- **down-scaling:** to every integration point of the discretised macro-level a meso-level unit cell is assigned. The macro-level strain field is translated into meso-level displacement boundary conditions;

- **meso-level computations:** the material is described as heterogeneous with a particular composite structure. Each component of the structure has its own constitutive assumption. A boundary value problem is solved for each meso-level unit cell with the boundary conditions as given from the macro-level input. The boundary value problem can be solved in different manners, the most popular being the finite element method (Feyel and Chaboche [31], Kouznetsova et al. [52], Miehe et al. [68], Smit et al. [93], Terada and Kikuchi [98]), sometimes in its specific format of the Voronoi cell finite element method (Ghosh et al. [34], Kanit et al. [50], Lee and Ghosh [59, 60]). Alternatively, Fast Fourier Transforms could be used (Michel et al. [66]).

- **up-scaling:** homogenisation is performed on the meso-level response in terms of reaction forces and stiffness relations, which results in the *effective properties* of the homogeneous material to be transfered to the macro-level.

A multi-scale finite element model has been developed by Lee and Ghosh [60] and Ghosh et al. [34] for the elastic-plastic analysis of heterogeneous (porous and composite) materials by combining an asymptotic homogenisation theory. Modelling the behaviour of structures reinforced by long fibre SiC/Ti composite materials with a periodic microstructure, Feyel and Chaboche [31] have used the multi-scale approach in order to take heterogeneities into account in the behaviour between the fibre and matrix.

A multi-scale approach was also applied in biomechanics in order to predict local cell deformations in engineered tissue constructs. For instance, Breuls et al. [18] have simulated the compression of a skeletal muscle tissue to construct and study the influence of microstructural heterogeneity on local cell deformations. Cell deformations are predicted from a detailed nonlinear finite element analysis of the microstructure, consisting of an arrangement of cells embedded in matrix material. Effective macroscopic tissue behaviour is derived by a computational homogenisation procedure.

Recently, some advances have been made in the formulation of multi-scale methods. Different homogenisation schemes within a multi-scale approach have been studied extensively by Kouznetsova [55]. Damage evolution in masonry structures has been modelled by Massart [64] with the help of multi-scale modelling framework, in which the equilibrium equations were solved together with a diffusion-type equation on both levels.

The computational homogenisation approach as outlined above bears some similarities with the 'substructuring' technique. In the substructuring technique, the macroscopic domain is split into a number of adjacent but non-overlapping subdomains. The macroscopic boundary value problem is reformulated accordingly. For each subdomain, effective stiffness properties are derived, after which the subdomains are assembled into a macroscopic formulation. The differences with computational homogenisation are

- in computational homogenisation, the unit cell is assigned to a macroscopic integration point, i.e. an infinitely small material point, whereas in substructuring the subdomains are related to finite-size parts of the macroscopic domain;

- computational homogenisation does not require that the individual unit cells are adjacent or non-overlapping. However, it should be emphasized here, that in order

to exploit the computational homogenisation procedure fully, the individual unit cell of the meso-level should be significantly smaller than the macroscopic volume associated with this meso-level unit cell;

- in substructuring, the macroscopic effective properties are directly formulated in terms of forces and the corresponding stiffness properties, whereas in computational homogenisation the transition is made from meso-level forces and structural stiffness to macro-level stresses and material stiffness.

The substructuring approach has been applied to multi-scale mechanics by Zohdi et al. [115]. In Chapter 5 a new homogenisation principle will be formulated that combines aspects of substructuring and the computational homogenisation technique outlined above.

2.2 Representative Volume Element

The connection between the macro- and meso-level is traditionally viewed via the concept of a Representative Volume Element (RVE). Indeed, it is appealing to describe the macroscopic structure with the help of a much smaller specimen, which is still large enough to be constitutively valid. This specimen, which is small enough on one hand and large enough on the other hand, has been referred to as an RVE. Generally in applications it is assumed that an RVE exists and that the size of it is initially prescribed. However, the existence of an RVE for the class of quasi-brittle materials is one of the major questions to be answered.

2.2.1 Definitions

In order to answer the question of existence and start developing the procedure to find a representative size, an RVE should be properly defined. Some definitions of an RVE, used by scientists for different purposes, are listed below.

- The RVE is "a sample that (a) is structurally entirely typical of the whole mixture on average, and (b) contains a sufficient number of inclusions for the effective overall moduli to be effectively independent of the surface values of traction and displacement, so long as these values are *macroscopically uniform*" (Hill [46]).

- An RVE is "the minimal material volume, which contains statistically enough mechanisms of deformation processes. Increasing of this volume should not lead to changes of evolution equations for field-values, describing these mechanisms" (Trusov and Keller [100]).

- The RVE "must be chosen *sufficiently large* compared to the microstructural size for the approach to be valid" (Drugan and Willis [26]).

- The RVE is "the smallest material volume element of the composite for which the usual spatially constant *overall modulus* macroscopic constitutive representation is

a sufficiently accurate model to represent mean constitutive response" (Drugan and Willis [26]).

- "The RVE is a model of the material to be used to determine the corresponding effective properties for the homogenised macroscopic model. The RVE should be large enough to contain sufficient information about the microstructure in order to be representative, however it should be much smaller than the macroscopic body. This is known as the Micro-Meso-Macro principle" (Hashin [45]).

- "The RVE is defined as the minimum volume of laboratory scale specimen, such that the results obtained from this specimen can still be regarded as representative for a continuum" (van Mier [102]).

- "The size of the REV should be large enough with respect to individual grain size in order to define overall quantities such as stress and strain, but this size should also be small enough in order not to hide macroscopic heterogeneity" (Evesque [28]).

All definitions reveal that the RVE should contain enough information on the microstructure and should be sufficiently smaller than the macroscopic structural dimensions. Thus a separation of scales should be possible. As Ostoja-Starzewski [76] pointed out,

- "in order to determine an RVE it is necessary to have (a) statistical homogeneity and ergodicity of the material; these two properties assure the RVE to be statistically representative of the macro response, and (b) some scale L of the material domain, sufficiently large relative to the micro-scale d (inclusion size) so as to ensure the independence of boundary conditions".

In fact, Ostoja-Starzewski [76] also noted that

- "the RVE is very clearly defined in two situations only: i) unit cell in a periodic microstructure, and ii) volume containing a very large (mathematically infinite) set of micro-scale elements (e.g. grains), possessing statistically homogeneous and ergodic properties".

Periodic microstructures could be treated by continualisation or homogenisation methods, as discussed in Section 2.1. However, for the more general case of random heterogeneous materials, the quantitative definition of Wildemann et al. [113] can be used:

- the subvolume V_L with characteristic size L (fig. 2.4) is called an RVE of the volume V if an averaged function

$$\bar{g} = \frac{1}{V_L} \int_{V_L} g(r) \mathrm{d}r \tag{2.1}$$

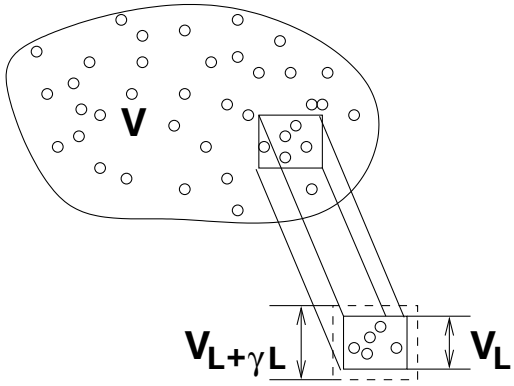

Figure 2.4: RVE definition according to Wildemann et al. [113]

exists and limited, and if for any positive small number δ such a positive number $\gamma(\delta)$ exists that

$$\left| \frac{1}{V_{L+\gamma L}} \int\limits_{V_{L+\gamma L}} g(r)\mathrm{d}r - \frac{1}{V_L} \int\limits_{V_L} g(r)\mathrm{d}r \right| < \delta \tag{2.2}$$

where function $g(r)$ is continuous everywhere inside phases V_1 and V_2. It is also necessary to make sure that $L >> l_\omega$), where l_ω is the characteristic size of the constituents (Wildemann et al. [113]).

Note 2 *Traditionally, RVE sizes are defined as a minimum size of a microstructural cell that fulfills the requirement of statistic homogeneity. As such, it is a* **lower bound***: large microstructural cells behave similarly while smaller microstructural cells do not.*

Note 3 *Here, an RVE (representative volume element) and an REV (representative elementary volume) refer to the same concept. Usually, the solid mechanics community uses the term RVE while the fluid mechanics community prefers the term REV.*

2.2.2 Quantification

In literature the concept of an RVE was introduced to correlate the effective or macroscopic properties of materials with the properties of the microscopic constituents and microscopic structures of the materials. However, today little quantitative knowledge is available about minimum RVE sizes of various engineering materials.[2] Several attempts

[2]Here the RVE size is understood as a one-dimensional length, two-dimensional area or three-dimensional volume depending on the particular application. In the scope of this contribution, the RVE size will be used as a two-dimensional area, if not stated otherwise.

have been made in order to determine the size of an RVE. For instance, Lemaitre [61] suggested that the three-dimensional RVE size should roughly be 0.1mm for metallic materials, 1mm for polymers, 10mm for woods and 100mm for concrete. The RVE size for the gneissic rock mass was found (Wang et al. [108]) to be around 12.5 m. However, to be on the conservative side, the RVE size to express the hydraulic behaviour of the gneissic rock mass was selected as 15 m.

The general point of view is to connect the size of a representative volume of the heterogeneous material to the size of inclusions (inclusions, reinforcements, grains, etc.). Van Mier and van Vliet in their experiments with concrete, for example, suggest the size of the RVE to be approximately equal to at least 3–5 times (van Mier [102], van Vliet [105]) or 7–8 times (van Mier [103]) the largest inclusion particle size. Also working with concrete, Bažant and Novák [13] proposed to take the size of the representative volume $V = l^{n_d}$ where n_d is the number of spatial dimensions and l the characteristic length of the material, which equals to 2.7–3.0 times the maximum inclusion size (Bažant and Oh [14], Bažant and Pijaudier-Cabot [15]).

Ren and Zheng [82, 83] introduced a definition of minimum RVE size based on the concept of nominal modulus, and determining numerically the minimum RVE sizes of more than 500 cubic polycrystals in the plane stress problem, under the assumption that all grains in a polycrystal have the same square shape (simple polycrystal model). They found that the minimum RVE sizes for effective elastic moduli have a roughly linear dependence on crystal anisotropy degrees. According to [82] with an error of 5% almost all of the tested materials have an RVE size of 20 or less times as large as the grain size. Together with a large overview of existing determined RVE sizes for different material types, Evesque and Adjemian [29] suggested that the minimum RVE contains in general 10 grains, though for the special case of stick-slip analysis they proposed to use an RVE containing at least 10^7 grains. On the other extreme of the range, Drugan and Willis derived for reinforced elastic composite the minimum RVE size to be equal to only twice the reinforcement diameter (Drugan and Willis [26]).

While most researchers relate the RVE size to the dimensions of the inclusions, the various suggestions for the RVE size in terms of the inclusion size differ by at least two orders of magnitude. Other parameters play a role in the quantification of the RVE size, such as for instance the volume fraction of the inclusions or the difference in stiffness between inclusions and matrix material. To assess the influence of these and other parameters, a closer look at the various quantification procedures should be taken.

RVE based on effective properties: numerical-statistical approaches

A number of approaches have been suggested in literature to analyse the RVE size numerically. They normally use multiple realisations for the meso-level unit cell, a finite element simulation of the unit cells and a statistical procedure to analyse the results. A typical example is provided by Kanit et al. [50], whose methodology can be summarised as follows:

- generate different realisations of the microstructure for 4–5 different sample sizes;

- submit each microstructure to loading conditions and, for instance, periodic boundary conditions, and record the obtained effective properties;
- compute mean value and variance of effective property for the considered volume sizes;
- set the desired precision for the estimation of effective property and a number of realisations; use the model to define the final RVE size.

Other numerical-statistical approaches based upon setting a tolerance for the scatter in the results are given by Ashihmin and Povyshev [6], Vinogradov [107]. A refinement to these approaches was proposed by Evesque [28]: an RVE will be the minimum volume, whose characteristics fluctuate in an *uncorrelated manner* and from which one is able to describe the macroscopic quantities and their fluctuations from its distribution characteristics.

Related to the above approach is the use of Monte-Carlo simulations. The idea of Ostoja-Starzewski [74] was to consider Hooke's law as being either controllable by strains or stresses, and to check for which sizes the two responses begin to coincide. His method requires an explicit computational mechanics solution of a number of realisations of possible microstructures, sampled in a Monte-Carlo sense, which in turn allows a determination of statistics of both bounds. In a follow-up work (Ostoja-Starzewski [75]) the stiffness difference between inclusions and matrix as well as the aspect ratio of the inclusions were varied. It was shown that with inclusion stiffness decreasing and their slenderness growing, the RVE tends to be very large. Gusev [43] generated statistically independent realisations of a periodic elastic composite with a disordered unit cell made up of 8, 27, and 64 non-overlapping identical spheres, after which Monte-Carlo runs were employed. By construction, all studied Monte-Carlo realisations had the same inclusion fraction. Overall elastic constants of these periodic Monte-Carlo realisations were then calculated numerically. It appears that the scatter in the individual elastic constants obtained with a few dozen spheres in the disordered unit cell is already remarkably small. The averages obtained with varying numbers of spheres are practically stationary. Thus, according to [43] based on only a few Monte-Carlo realisations, one can accurately predict the overall elastic constants of the studied periodic composite.

RVE based on effective properties: analytical approach

An estimation of the RVE size can also be done analytically. Drugan and Willis [26] employed an explicit nonlocal constitutive equation. They consider averaged strain fields that vary with position, and determine at which wave-length this variation will cause the nonlocal term in the constitutive equation to produce a non-negligible correction to the local term. On the basis of that they made an estimate of a minimum RVE size. They obtain the quantitative results for the type of composite for which it is possible to render the nonlocal constitutive equation completely explicit: namely, two-phase composites consisting of an isotropic matrix reinforced (or weakened) by a random dispersion of isotropic spherical particles. Analytically derived explicit expressions were obtained for

the RVE sizes in tensile and shear loading cases. The results of the study allowed to estimate the size of the RVE as approximately two times as large as the particle diameters for any reinforcement concentration level with high accuracy (95%). With exceptionally high accuracy (99%) they were able to show the RVE size to be approximately as large as 4.5 times the particle diameter.

RVE based on experimental observations

There have been many attempts to define the size of an RVE experimentally. Experimental analysis often involves selection of a particular sample geometry for mechanical testing and subjecting the specimen to image analysis after testing is complete. It is often assumed that the test specimen is representative of the material under investigation, but as it was mentioned by Graham and Yang [41] this may only be determined by examining the length scale of fluctuations in heterogeneous entities which control the material response. In order to obtain meaningful results, a sufficient number of particles or volume of material must be included in both experimental and image analysis.

A methodology has been developed by Shan and Gokhale [89] to arrive at a sufficiently small micro-structural size that can be referred to as an RVE of a non-uniform microstructure of a ceramic matrix composite (CMC) containing a range of fibre sizes, and fibre-rich and -poor regions at the length scale of about 100 μm. Their RVE contains about 250 fibres of 14 μm diameter average size. The absolute size of the RVE is 0.1 mm^2. The proposed [89] methodology involves

- a combination of quantitative characterisation of geometry and spatial arrangement of micro-structural features using stereological and image analysis techniques;
- development of a computer model of the micro-structure that is statistically similar to the real micro-structure;
- numerical simulations of micro-mechanical response on computer-simulated microstructural windows of different sizes containing 60-2000 fibres;
- numerical simulations on large-area high-resolution digital image of the composite micro-structure containing about 2000 fibres.

The RVE has the micro-structure that is statistically similar to that of the CMC having fibre-rich and -poor regions. The Young's modulus of this RVE is very close to the Young's modulus of the composite. The modelled RVE has a local stress distribution that is comparable to that in the real composite under similar loading conditions.

Romero and Masad [84] presented a theoretical background on the statistical requirements for an RVE. An image analysis technique using X-ray tomography was used to determine the RVE by measuring the volume at which the aggregate percentage becomes independent of the size of the volume analysed and reaches a constant value. The aggregate percentage was derived from different areas of two-dimensional images of asphaltic concrete.

Graham and Yang [41] mentioned one other length scale dependent phenomenon. They have noticed, that defining an RVE of the material after damage and/or localisation of deformation has occurred is not straightforward; an RVE may even not exist. Nevertheless, some attempts were made to construct a representative volume in the presence of softening and damage. Although there were trials both numerical (Lacy et al. [57]) and experimental (Graham and Yang [41]) to estimate such a representative volume, the conclusions were not promising. It can be explained recalling the fact, that a softening material is developing a localisation zone and thus loses its statistical homogeneity. According to the RVE definition, an RVE cannot be found if statistical homogeneity is lost.

2.3 Discussion

The remainder of this thesis will be centered around three main questions. They are concerned, respectively, with establishing links between parameters of different modelling approaches, with the existence and quantification of the RVE, and the formulation of a homogenisation scheme that is valid in all loading stages.

1. As has been discussed in this Chapter, different modelling approaches can be used to describe material behaviour at multiple scales. Obviously, it is possible to use different approaches for the same material, and an interesting question would then be how the parameters of the various models are related to one another. In other words, links are sought between the parameters of different models. The main advantage of the macrostructural (or phenomenological) approach is its efficiency: the information of the lower levels of observation is captured by additional constitutive parameters. However, the identification and experimental validation of these parameters is not always straightforward, which is due to their phenomenological nature. On the other hand, the multi-scale approach offers an improved accuracy and an explicit meso-structural background to the effective properties on the macro-level.

   Establishing a link between the parameters of the macrostructural approach and the multi-scale approach offers mutual advantages. The detailed knowledge of the meso-level material behaviour that is present in multi-scale approaches can be used to provide a meso-mechanical motivation for the phenomenological parameters in the macrostructural approach. Conversely, a better understanding of the model parameters in the multi-scale approach can be obtained if they are linked with material parameters from the macrostructural approach.

   In Chapter 3, analytical homogenisation will be performed. Local and non-local homogenisation schemes are discussed. In the non-local scheme a length-scale (in statics and dynamics) and a time-scale (in dynamics only) appear automatically in the macroscopic equations. As a result, a macrostructural modelling approach is obtained. However, in the homogenisation an RVE is used, and the relation between this RVE size and the macrostructural length- and time-scales will be studied.

2. The RVE size is an important parameter not only in multi-scale approaches, but also in macrostructural approaches. Therefore, the proper determination of the RVE size is of importance. Moreover, if a quantification of the RVE size is provided, also macrostructural length-scales (and time-scales) are obtained. It is known from literature that length-scales play an important role in the objective description of the softening behaviour of material [77, 92]. The inclusion of higher-order gradient terms, accompanied with above mentioned length-scales, can prevent loss of uniqueness and mesh-dependence of the solution. However, it has also been noted by Graham and Yang [41] and Lacy et al. [57] that possibly RVEs do not exist in softening. This issue needs thorough investigation.

   Furthermore, a unified RVE size determination procedure has not been established. Several different procedures have been proposed and used to generate quantitative knowledge on the RVE size, but it is still difficult to compare RVE sizes (*i*) in different loading stages, (*ii*) with different material properties and (*iii*) in different test set-ups. Thus, a systematic approach to determine RVE size is needed. Such an approach is formulated and used in Chapter 4. On the basis of a combined numerical-statistical procedure the existence of an RVE is verified in different loading stages (including the pre-peak and post-peak stages in the macroscopic stress-strain relation). It turns out that an RVE does exist in the pre-peak loading stage but ceases to exist in the post-peak regime.

   As a next step, if an RVE exists a procedure is outlined to quantify its size. The sensitivity of the RVE size to model parameters (such as loading scheme and boundary conditions) and material parameters (both deterministic and stochastic) is verified.

3. Once the issues of RVE existence and RVE size determination have been addressed, the multi-scale framework is completely formulated. In Chapter 5 this multi-scale procedure is employed. First, the local homogenisation scheme, as introduced in Chapter 3, is studied. Reliable results are obtained in the pre-peak loading stages. However, the RVE non-existence in the post-peak regime has a detrimental influence on the results — the structural response depends strongly on the finite element discretisation employed on the macro-level as well as on the size of the meso-level unit cell.

   Therefore, an alternative homogenisation scheme is needed that does not suffer from these two disadvantages in the post-peak regime. As a first option, a non-local homogenisation scheme, known from literature, can be used. This scheme has been proposed, formulated and implemented by Kouznetsova [55]. Although this scheme solves the issue of macro-level mesh dependence, the meso-level cell size dependence still remains. For this reason, a new homogenisation technique is developed. The usual assumption in computational homogenisation that the mesostructural cell size corresponds to an infinitely small material point on the macro-level is dropped in this novel homogenisation scheme. The structural response does not depend on the macro-level mesh size and the meso-level cell size if this new scheme is used.

3 Analytical homogenisation

As it was already mentioned in the Introduction and Section 2.1, in order to describe and analyse the behaviour of heterogeneous materials, different approaches can be used. First of all these approaches can be classified with respect to the scale of interest: one can be interested in a material as such (macrostructural approach), or one can be interested in processes which are taking place at a lower, more detailed level (mesostructural approach).

On one hand, a mono-scale approach on macroscopical level, i.e. a macrostructural approach is commonly used in nowadays mechanics. There are different variations of mono-scale procedures, but the general philosophy, as it has been mentioned in Chapter 1, is that the material considered on the macro-level and all information about its mesostructure is taken into account by means of *material parameters*: a so-called length-scale — the representation of the underlying mesostructure (de Borst and Muhlhaus [23], Geers et al. [32], Mühlhaus and Aifantis [72], Peerlings [77], Sluys [92]), or less common, a time-scale – related to inertia, viscosity, which are relevant in time-dependent processes (Rubin et al. [86], Wang and Sun [109]). Usually only one of the parameters, either length- or time-scales is present in the model, though the *royal road* requires both length- and time-scales in the material description (Aifantis [3], Askes and Metrikine [7], Metrikine and Askes [65], Mindlin [70], Vardoulakis and Aifantis [106])[1].

On the other hand, when the various scales interact, a multi-scale analysis could give a better approximation of the real response of the material. The big advantage of the multi-scale analysis is that one can take the lower-scale influences into account explicitly in order to describe the higher-scale response and vice versa. The idea of the multi-scale routine could be presented as an interaction between macro-level (full macroscopic structure) and meso-level (a unit cell, representing the material on a lower level of interest). Here, a unit cell is taking part in the multi-scale procedure as a *model parameter* and it is described with the help of a Representative Volume Element (RVE) concept.

A link between the two approaches can be established (Gitman et al. [35, 36, 37]). In particular, links exist between the *model parameter* RVE-size from the multi-scale technique and *material parameters* length-scale and time-scale from the macrostructural approach. As it was mentioned in Chapter 1 somewhat similar link between the RVE-size and the length-scale parameter has already been established in literature: the case of material with a periodic micro-structure has been addressed by Askes and Metrikine [7], Metrikine and Askes [65], and the case of microstructurally homogeneous material has been treated by Kouznetsova et al. [54]. However, in the latter work, the question

[1] It should be noted, that a time-scale parameter can also be expressed as a length-scale parameter divided by a velocity (normally the velocity of the infinitely long waves). Thus, instead of one length-scale parameter and one time-scale parameter, the model can also be equipped with two independent length-scale parameters.

of finding the RVE size of homogeneous material still remains: traditionally, as it was mentioned in Chapter 2, RVE sizes are defined as a **lower bound** of possible representative sizes, and for the case of homogeneous material such a size would be considered as zero. Here a more general case of random meso-structure will be treated. An analytical homogenisation scheme will be used to derive these links.

3.1 Scale transition

Here, a distinction should be made between first-order homogenisation techniques and second-order homogenisation techniques. This terminology was introduced by Kouznetsova et al. [53] in a numerical sense. Here, these two techniques will be referred to as local and non-local homogenisation. Below, the terms first-order/local homogenisation and second-order/non-local homogenisation techniques will be used in an analytical context (first-order/local analytical homogenisation and second-order/non-local analytical homogenisation techniques). If we consider the case with only values of stresses and strains (in other words in a case of local constitutive equations), then first-order/local homogenisation is used. On the other hand, if gradients of these quantities are also taken into account (in case of nonlocal constitutive equations) second-order/non-local homogenisation is performed.

Consider the equilibrium equation at meso-level in an RVE:

$$\sigma^{\mathrm{m}}_{ij,j} = 0 \tag{3.1}$$

where σ is the stress tensor, the superscript m denotes the meso-level and an index following a comma denotes a derivative with respect to the corresponding spatial coordinate. By means of volume averaging, eq. (3.1) is rewritten as

$$\frac{1}{V_{\mathrm{rve}}} \int\limits_{V_{\mathrm{rve}}} \sigma^{\mathrm{m}}_{ij,j} \, \mathrm{d}V = 0 \tag{3.2}$$

in which V_{rve} is the volume of the RVE. Switching the order of integration and differentiation gives

$$\left(\frac{1}{V_{\mathrm{rve}}} \int\limits_{V_{\mathrm{rve}}} \sigma^{\mathrm{m}}_{ij} \, \mathrm{d}V \right)_{,j} = 0 \tag{3.3}$$

The macroscopic stress σ^{M} is defined as the volume average of the mesoscopic stress σ^{m}, denoted as $\sigma^{\mathrm{M}}_{ij} = \langle \sigma^{\mathrm{m}}_{ij} \rangle$. Thus,

$$\left(\frac{1}{V_{\mathrm{rve}}} \int\limits_{V_{\mathrm{rve}}} \sigma^{\mathrm{m}}_{ij} \, \mathrm{d}V \right)_{,j} = \langle \sigma^{\mathrm{m}} \rangle_{,j} \equiv \sigma^{\mathrm{M}}_{ij,j} \tag{3.4}$$

A general mesoscopic constitutive equation $\sigma_{ij}^{\mathrm{m}} = D_{ijkl}^{\mathrm{m}} \varepsilon_{kl}^{\mathrm{m}}$ is assumed. Substitution into eq. (3.4) yields

$$\sigma_{ij,j}^{\mathrm{M}} = \left(\frac{1}{V_{\mathrm{rve}}} \int\limits_{V_{\mathrm{rve}}} D_{ijkl}^{\mathrm{m}} \varepsilon_{kl}^{\mathrm{m}} \, \mathrm{d}V \right)_{,j} = 0 \tag{3.5}$$

where D^{m} and ε^{m} are the mesoscopic stiffness and the mesoscopic strain, respectively. From eq. (3.5) it follows that

$$\sigma_{ij}^{\mathrm{M}} = \frac{1}{V_{\mathrm{rve}}} \int\limits_{V_{\mathrm{rve}}} D_{ijkl}^{\mathrm{m}} \varepsilon_{kl}^{\mathrm{m}} \, \mathrm{d}V \tag{3.6}$$

Next, linearisations of the mesoscopic stiffness and strain are performed around the values at the centre of the RVE. The origin of the coordinate system x is assumed to be positioned in the centre of the RVE. In particular,

$$D_{ijkl}^{\mathrm{m}} = D_{ijkl}^{\mathrm{M}} + D_{ijkl,o}^{\mathrm{M}} x_o \tag{3.7}$$

$$\varepsilon_{kl}^{\mathrm{m}} = \varepsilon_{kl}^{\mathrm{M}} + \varepsilon_{kl,p}^{\mathrm{M}} x_p \tag{3.8}$$

which is valid as long as perturbations remain small with respect to the average values. The values of mesoscopic stiffness and mesoscopic strain (and their derivatives) at the origin of the RVE correspond to the macroscopic values, as is explained below. The first-order and the second-order homogenisation schemes are obtained for different truncations of the above series.

3.2 Local homogenisation scheme

A local homogenisation scheme is obtained when the derivatives in eq. (3.7) and (3.8) are ignored. Then, from eqs. (3.6) it follows that

$$\sigma_{ij}^{\mathrm{M}} = \frac{1}{V_{\mathrm{rve}}} \int\limits_{V_{\mathrm{rve}}} D_{ijkl}^{\mathrm{M}} \varepsilon_{kl}^{\mathrm{M}} \, \mathrm{d}V \tag{3.9}$$

It must be realised that D_{ijkl}^{M} and $\varepsilon_{kl}^{\mathrm{M}}$ are the values of D_{ijkl}^{m} and $\varepsilon_{kl}^{\mathrm{m}}$ evaluated at the centre of the RVE. Therefore, they are constant and can be taken out of the indicated integration, so that

$$\sigma_{ij}^{\mathrm{M}} = D_{ijkl}^{\mathrm{M}} \varepsilon_{kl}^{\mathrm{M}} \tag{3.10}$$

which explains why the mesoscopic stiffness and strain evaluated at the origin of the RVE coincide with the macroscopic stiffness and the macroscopic strain.

It can be seen from eq. (3.10) that in the first-order homogenisation method no length-scale parameter appears on the macroscopic level. In contrast, the constitutive equations retain their classical format. The same holds for the equilibrium equations upon substituting eq. (3.10) into eq. (3.5).

3.3 Non-local homogenisation scheme

A non-local homogenisation scheme requires the inclusion of the derivative terms from eqs. (3.7) and (3.8). Now the constitutive relation (3.6) is rewritten as

$$\begin{aligned}\sigma_{ij}^{\mathrm{M}} = \tfrac{1}{V_{\mathrm{rve}}} \int\limits_{V_{\mathrm{rve}}} \left(D_{ijkl}^{\mathrm{M}} + D_{ijkl,o}^{\mathrm{M}} x_o\right) \left(\varepsilon_{kl}^{\mathrm{M}} + \varepsilon_{kl,p}^{\mathrm{M}} x_p\right) \,\mathrm{d}V = \\ \tfrac{1}{V_{\mathrm{rve}}} \int\limits_{V_{\mathrm{rve}}} \left(D_{ijkl}^{\mathrm{M}} \varepsilon_{kl}^{\mathrm{M}} + D_{ijkl,o}^{\mathrm{M}} \varepsilon_{kl}^{\mathrm{M}} x_o + D_{ijkl}^{\mathrm{M}} \varepsilon_{kl,p}^{\mathrm{M}} x_p + D_{ijkl,o}^{\mathrm{M}} \varepsilon_{kl,p}^{\mathrm{M}} x_o x_p\right) \,\mathrm{d}V\end{aligned} \tag{3.11}$$

Furthermore, it is noted that for arbitrary integration domains V, it holds that

$$\begin{aligned}\int\limits_V D_{ijkl,o} \varepsilon_{kl,p} x_o x_p \,\mathrm{d}V = \\ -\int\limits_V \left(D_{ijkl} \varepsilon_{kl,op} x_o x_p + D_{ijkl} \varepsilon_{kl,p} x_{o,o} x_p + D_{ijkl} \varepsilon_{kl,p} x_o x_{p,o}\right) \,\mathrm{d}V \\ + \oint\limits_S n_o D_{ijkl} \varepsilon kl, p x_o x_p \mathrm{d}S\end{aligned} \tag{3.12}$$

where n_o is a normal vector to surface of domain S. This is also assumed to hold within the RVE, thus

$$\begin{aligned}\sigma_{ij}^{\mathrm{M}} = \frac{1}{V_{\mathrm{rve}}} \int\limits_{V_{\mathrm{rve}}} \big(D_{ijkl}^{\mathrm{M}} \varepsilon_{kl}^{\mathrm{M}} + D_{ijkl,o}^{\mathrm{M}} \varepsilon_{kl}^{\mathrm{M}} x_o + D_{ijkl}^{\mathrm{M}} \varepsilon_{kl,p}^{\mathrm{M}} x_p - D_{ijkl}^{\mathrm{M}} \varepsilon_{kl,op}^{\mathrm{M}} x_o x_p \\ - D_{ijkl}^{\mathrm{M}} \varepsilon_{kl,p}^{\mathrm{M}} x_{o,o} x_p - D_{ijkl}^{\mathrm{M}} \varepsilon_{kl,p}^{\mathrm{M}} x_o x_{p,o}\big) \,\mathrm{d}V\end{aligned} \tag{3.13}$$

Here, the boundary term, i.e. the surface integral is canceled as a result of the assumption of periodic boundary conditions. As in the local homogenisation scheme, the macroscopic quantities are identified with their mesoscopic counterparts evaluated at the centre of the RVE. Therefore they can be taken out of the integral. Afterwards, the second, third, fifth and sixth term in the right-hand-side of eq. (3.13) consist of uneven functions integrated over a symmetric domain, therefore they vanish. Furthermore, the fourth integral can be evaluated by denoting the length of the RVE by L. In a two-dimensional context $V_{\mathrm{rve}} = L^2$ and

$$\int\limits_{V_{\mathrm{rve}}} x_o x_p \,\mathrm{d}V = \int\limits_{-\frac{1}{2}L}^{\frac{1}{2}L} \int\limits_{-\frac{1}{2}L}^{\frac{1}{2}L} x_o x_p \,\mathrm{d}x \,\mathrm{d}y = \frac{1}{12} L^4 \delta_{op} \tag{3.14}$$

With these elaborations, eq. (3.13) is rewritten as

$$\sigma_{ij}^{\mathrm{M}} = D_{ijkl}^{\mathrm{M}} \varepsilon_{kl}^{\mathrm{M}} - \frac{1}{12} L^2 D_{ijkl}^{\mathrm{M}} \varepsilon_{kl,pp}^{\mathrm{M}} = D_{ijkl}^{\mathrm{M}} \left(\varepsilon_{kl}^{\mathrm{M}} - \frac{1}{12} L^2 \nabla^2 \varepsilon_{kl}^{\mathrm{M}}\right) \tag{3.15}$$

Note that eq. (3.15) only contains the usual macroscopic parameters plus a coefficient that precedes the ∇^2-operator. This coefficient has the dimension of length squared and is univocally related to the dimensions of the RVE.

Eq. (3.15) bears close similarities with the phenomenological gradient elasticity model proposed by Aifantis and coworkers [4, 85]

$$\sigma_{ij} = D_{ijkl}\left(\varepsilon_{kl} - \ell^2\nabla^2\varepsilon_{kl}\right) \tag{3.16}$$

where ℓ is a macroscopic length-scale parameter. Comparing eqs. (3.15) and (3.16), the phenomenological parameter ℓ can be connected to the size of the RVE L via

$$\ell^2 = \frac{1}{12}L^2 \tag{3.17}$$

Thus, a mesoscopic interpretation is obtained for the phenomenological constant ℓ. In the numerical framework presented in Kouznetsova et al. [53] it was shown that a macroscopic length-scale emerges within a second-order homogenisation scheme. This length-scale is present in the entire loading regime, including the nonlinear stages. Eq. (3.17) aids in understanding this occurrence: the macroscopic length-scale is *proportional* to the RVE size.

Note 4 *For the general case of higher-order homogenisation, it can be shown that*

$$\sigma^M_{ij} = D^M_{ijkl}\left(\varepsilon^M_{kl} + \frac{(-1)^k L^{2k}}{(2k+1)k^2 2^{2k}}\nabla^{2k}\varepsilon^M_{kl}\right) \qquad \text{where } k \in \mathcal{N} \tag{3.18}$$

here, $2k$ is the order of the homogenisation.

3.4 Homogenisation and macroscopic time-scale parameter

Although the main focus of this study is on static loading cases, it is nevertheless worthwhile to examine the effect of second-order homogenisation on dynamic loading cases. As it turns out, macroscopic time-scales can be identified in a similar manner as macroscopic length-scales. To this end, the equation of motion on the meso-level is considered:

$$\sigma^{\mathrm{m}}_{ij,j} = \varrho^{\mathrm{m}}\ddot{u}^{\mathrm{m}}_i \tag{3.19}$$

here ϱ^{m} is the mass density. Volume averaging of eq. (3.19) leads to

$$\frac{1}{V_{\mathrm{rve}}}\int\limits_{V_{\mathrm{rve}}} \sigma^{\mathrm{m}}_{ij,j}\,\mathrm{d}V = \frac{1}{V_{\mathrm{rve}}}\int\limits_{V_{\mathrm{rve}}} \varrho^{\mathrm{m}}\ddot{u}^{\mathrm{m}}_i\,\mathrm{d}V \tag{3.20}$$

Changing the order of differentiation and integration yields

$$\left(\frac{1}{V_{\mathrm{rve}}}\int\limits_{V_{\mathrm{rve}}} \sigma^{\mathrm{m}}\,\mathrm{d}V\right)_{,j} = \frac{1}{V_{\mathrm{rve}}}\int\limits_{V_{\mathrm{rve}}} \varrho^{\mathrm{m}}\ddot{u}^{\mathrm{m}}_i\,\mathrm{d}V \tag{3.21}$$

In order to elaborate the right-hand-side of eq. (3.21), it is assumed that

$$\varrho^{\mathrm{m}} = \varrho^{\mathrm{M}} + \varrho^{\mathrm{M}}_{,o} x_o \tag{3.22}$$

$$\ddot{u}^{\mathrm{m}}_i = \ddot{u}^{\mathrm{M}}_i + \ddot{u}^{\mathrm{M}}_{i,p} x_p \tag{3.23}$$

where again the macroscopic values denote values that are evaluated at the centre of the RVE. Then, a procedure analogous to the one described in Section 3.3 is performed, and as a result

$$\frac{1}{V_{\mathrm{rve}}} \int\limits_{V_{\mathrm{rve}}} \varrho^{\mathrm{m}} \ddot{u}^{\mathrm{m}}_i \, \mathrm{d}V = \varrho^{\mathrm{M}} \ddot{u}^{\mathrm{M}}_i - \frac{1}{12} L^2 \varrho^{\mathrm{M}} \nabla^2 \ddot{u}^{\mathrm{M}}_i \tag{3.24}$$

In the elaboration of the right-hand side of eq. (3.21) first order derivatives of the inertia terms (mass and acceleration) have been considered. It is thus consistent to employ eq. (3.15), rather than eq. (3.10), for the left-hand-side of eq. (3.21). With these substitutions eq. (3.21) can be rewritten as

$$D^{\mathrm{M}}_{ijkl} \left(\varepsilon^{\mathrm{M}}_{kl,j} - \frac{1}{12} L^2 \nabla^2 \varepsilon^{\mathrm{M}}_{kl,j} \right) = \varrho^{\mathrm{M}} \left(\ddot{u}^{\mathrm{M}}_i - \frac{1}{12} L^2 \nabla^2 \ddot{u}^{\mathrm{M}}_i \right) \tag{3.25}$$

The last term on the right-hand-side is a mesoscopic inertia term and must not be confused with viscosity.

On the macro-level the equations of motion are normally written as $\varrho \ddot{u}_i = \sigma^{\mathrm{C}}_{ij,j}$, where σ^{C} is a (macroscopic) Cauchy stress tensor. For the formulation according to eq. (3.25) this stress can be written as

$$\sigma^{\mathrm{C}}_{ij} = D_{ijkl} \left(\varepsilon_{kl} - \frac{1}{12} L^2 \nabla^2 \varepsilon_{kl} \right) + \frac{1}{12} L^2 \varrho \ddot{\varepsilon}_{ij} \tag{3.26}$$

where the superscripts M have been dropped. For the particular case of elasticity, $D_{ijkl} = \lambda \delta_{ij} \delta_{kl} + \mu \delta_{ik} \delta_{jl} + \mu \delta_{il} \delta_{jk}$ where λ and μ are the Lamé constants. Eq. (3.26) can then be rewritten as

$$\begin{aligned} \sigma^{\mathrm{C}}_{ij} &= \lambda \delta_{ij} \left(\varepsilon_{kk} - \frac{1}{12} L^2 \nabla^2 \varepsilon_{kk} \right) + 2\mu \left(\varepsilon_{ij} - \frac{1}{12} L^2 \nabla^2 \varepsilon_{ij} + \frac{1}{24} \frac{\varrho}{\mu} L^2 \ddot{\varepsilon}_{ij} \right) \\ &= \lambda \delta_{ij} \left(\varepsilon_{kk} - \ell^2 \nabla^2 \varepsilon_{kk} \right) + 2\mu \left(\varepsilon_{ij} - \ell^2 \nabla^2 \varepsilon_{ij} + \tau^2 \ddot{\varepsilon}_{ij} \right) \end{aligned} \tag{3.27}$$

where ℓ is the macroscopic length-scale parameter defined earlier in eq. (3.17) and τ is a macroscopic time-scale parameter defined via

$$\tau^2 = \frac{1}{24} \frac{\varrho}{\mu} L^2 \tag{3.28}$$

Eqs. (3.26) and (3.27) bear large similarities with the higher-order gradient models proposed earlier, e.g. phenomenologically in [3, 106] or by means of continualisation in [7, 65]. As noted in these references, the time-scale parameter τ is concerned with the propagation velocity of the high-frequency waves. Indeed, for a realistic description of wave

dispersion it is necessary that both a length-scale parameter and a time-scale parameter are included in the macroscopic continuum formulation. However, in the remainder of this thesis only static loading cases will be considered.

Note 5 *To keep the above derivations transparent, it has been assumed that the same RVE has been used for the stiffness terms as well as for the inertia terms, cf. eq. (3.20). However, this is not strictly necessary. For instance, let* $V_2 > V_1 = V_{rve}$*, then for any generic quantity* a^m *it should hold that*

$$\frac{1}{V_1}\int_{V_1} a^m \, dV = \frac{1}{V_2}\int_{V_2} a^m \, dV \tag{3.29}$$

within a given error tolerance. A certain volume can be a Representative Volume V_{rve} *for one quantity while at the same time it is larger than the Representative Volume for another quantity. In particular,* L *in eq. (3.17) does not have to be equal to* L *in eq. (3.28).*

3.5 Discussion

The main difference between the second-order homogenisation technique compared to the first-order scheme is the automatic appearance of a length-scale parameter (and possibly a time-scale parameter) in a second-order scheme. These length- and time-scale parameters have been derived here as linear functions of the RVE size. However, the dependence of the length- and time-scale on the RVE size only makes sense if an RVE does exist. The question of (*i*) the existence of an RVE and (*ii*) its size determination (if an RVE exists) will be treated in Chapter 4.

The second-order homogenisation technique is valid as long as higher-order derivatives are negligible compared with the first-order derivatives, i.e. if deformations are relatively homogeneous. As it will be shown in Chapter 4, the existence of an RVE is strongly related to the deformations being (reasonably) homogeneous. The use of the first- and the second-order homogenisation techniques will be discussed in Chapter 5. Chapter 5 will also address modelling strategies that can be used in case an RVE ceases to exist.

4 RVE existence and size determination

As has been discussed in the previous Chapters, the RVE plays an important role in various modelling approaches. A detailed analysis of the Representative Volume Element concept is the subject of this Chapter. The analysis begins from addressing the question of an RVE existence. This issue will be treated on the basis of a statistical analysis of the behaviour of the tested unit cell in pre-peak and post-peak loading regimes. Two-dimensional plane strain assumption is used.

Once the question of an RVE existence will be answered, the procedure to find its size will be introduced. Several attempts have been made in literature to develop a procedure to determine the representative size (cf. Section 2.2 [6, 17, 19, 26, 69], etc.). An objective method to determine the size of the RVE will be presented below, see also Gitman et al. [38].

Furthermore, it will be tested how sensitive the RVE size is to changes in test parameters and material parameters.

4.1 Unit cell and implementational issues

In this thesis the investigation of a three phase material with matrix, inclusions (here, in the circular shape) and an interfacial transition zone (ITZ) surrounding each inclusion is addressed. Each material component has its own set of properties in terms of Young's modulus and Poisson's ratio. Here it is chosen that inclusions and ITZ have the highest and the lowest stiffness respectively. Sizes of inclusions are varied from [2.5mm .. 5mm] and the thickness of the ITZ has been chosen as 0.25 mm, i.e. 10% of the smallest diameter of the inclusions. The material components properties are presented in the tab. 4.1 and, unless mentioned otherwise, used throughout this thesis. The material with the above

Materials components properties	Inclusions	Matrix	ITZ
Young's modulus E [MPa]	30000	25000	20000
Poisson's ratio ν [-]	0.2	0.2	0.2

Table 4.1: Material components properties

properties could be the representation of a concrete[1], but generally, any three phase

[1] Although concrete has been chosen to be the analysed material, the properties mentioned in tab. 4.1 are not its accurate representation. Generally the stiffness contrasts of the three concrete components are higher than those mentioned in the table, however, as it will be shown in Section 4.5.1. these higher stiffness contrasts will result in much larger RVE sizes and as such larger unit cell sizes will

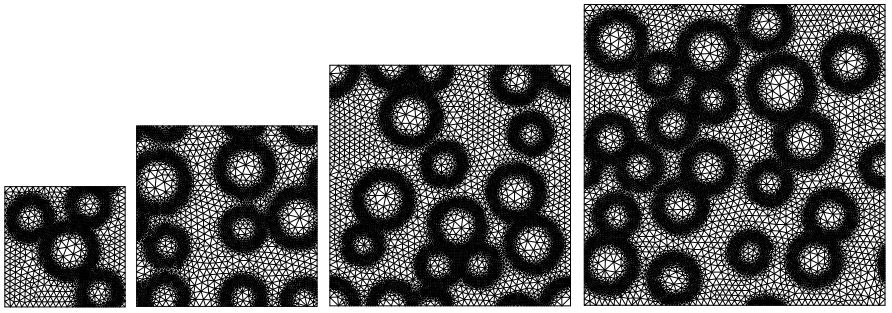

Figure 4.1: Sizes of the unit cell, from left to right $10\times10\text{mm}^2$; $15\times15\text{mm}^2$; $20\times20\text{mm}^2$; $25\times25\text{mm}^2$ ($\rho = 30\%$)

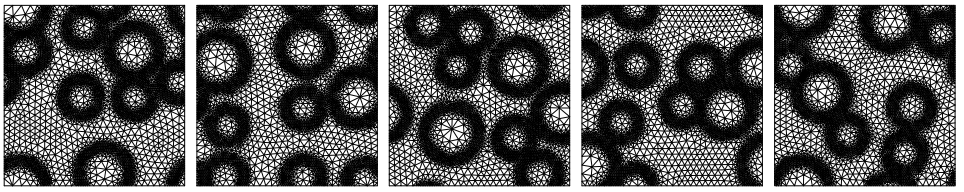

Figure 4.2: Different realisations of the unit cell for size $15\times15\text{mm}^2$, ρ=30%

composite material (or even two phase material with two out of three phases bearing the same properties) could be described.

In order to address the question of RVE existence, a statistical analysis has been employed. The statistical procedure is as follows: a series of numerical experiments for increasing sizes of the unit cell are made (fig. 4.1), and for each unit cell size different inclusion locations (with given value of volume fraction of inclusions) are considered (fig. 4.2). This is repeated for several values ρ of volume fractions of inclusions/aggregate density distributions (fig. 4.3).

have to be generated. The chosen width of the ITZ is in reality at least one order of magnitude lower than that mentioned in the table. This is motivated by considering this layer not strictly as an ITZ, but as an extended boundary between inclusions and matrix. The choice of this rather thick ITZ is dictated purely by numerical reasons: as at least two finite elements are desired to carry the ITZ properties the realistic width of the ITZ would lead to extremely small element sizes. As a consequence, this would increase enormously the time of the numerical analysis. Taking the ITZ as an extended boundary between inclusions and matrix is balanced by a rather high value of its stiffness in comparison with the stiffnesses of inclusions and matrix. In reality, the ITZ is a highly porous material and its stiffness should be much lower compared to the two other components.

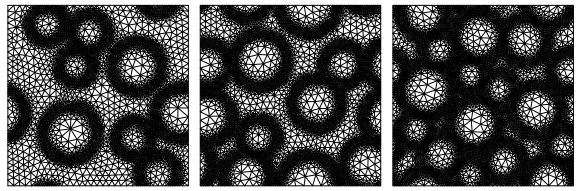

Figure 4.3: Volume fractions of inclusions, from left to right $\rho = 30\%$; $\rho = 45\%$; $\rho = 60\%$ for size 15×15 mm^2

Constitutive law: an elasticity-based gradient damage model (Lemaitre and Chaboche [62], Peerlings [77], Simone [90]) is used for the materials component description.

$$\sigma_{ij} = (1-\omega)D_{ijkl}\varepsilon_{kl} \tag{4.1}$$

where σ and ε are stresses and strains, respectively, D is the matrix of elastic stiffness and ω is a damage parameter. The damage depends on the history and in particular on the strain. A softening damage evolution law was used. More details on the gradient damage model can be found in Appendix A. As it has been shown by Peerlings and co-workers [78], this model provides mesh objective results. The crack initiation strains and length-scale parameters (which provide the link with the underlying micro-structure and, for simplicity, are here chosen to be equal for all three phases) are specified in tab. 4.2. The crack initiation strain of the inclusions has been chosen artificially high in order

Materials components properties	Inclusions	Matrix	ITZ
Crack initiation strain κ_0 [-]	0.5	5.0e-06	3.0e-06
Length-scale parameter l [mm]	0.63	0.63	0.63
Residual stress level α [-]	0.95	0.95	0.95
Slope of softening β [-]	1500	1500	1500

Table 4.2: Material components properties

to avoid the crack propagation through the inclusions.

Numerical tests. The finite element method is used to simulate the response of the unit cell, and three-noded triangular elements have been applied[2]. Each of the finite elements is assigned its own material properties corresponding to one of the three phases (see tab. 4.1). The size of the meso-level elements have been chosen accordingly to the length-scale parameter: the matrix element size has been taken 3 times smaller than the

[2]In the three-noded triangular element for gradient damage formulation both displacements and non-local equivalent strain are interpolated with linear shape-functions. See Simone et al. [91] for the suitability of this choice.

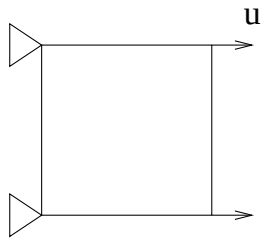

Figure 4.4: Tension test

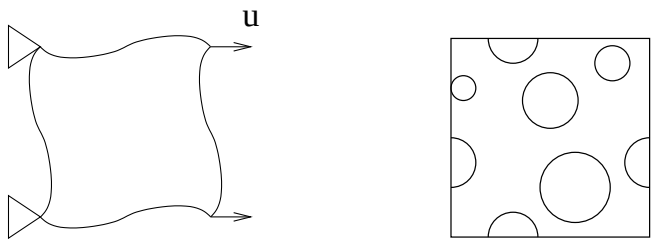

Figure 4.5: Left: periodic boundary conditions; right: material periodicity (no wall-effect)

length-scale parameter. The size of the ITZ elements were chosen smaller than the size of the matrix elements in order to capture the curvature of the crack in the neighbourhood of an inclusion. The size of the elements in inclusions has been taken much larger in order to save the computer time and bearing in mind the fact that the crack initiation strain of the inclusions has been chosen artificially high and as a consequence crack cannot propagate through the inclusion.

Tension tests have been performed for the series of samples (fig. 4.4). Both periodic boundary conditions and periodic material are employed.

- **Periodicity of boundary conditions** refers to specific mesh construction, where nodes on the top and on the bottom borders identically repeat their positioning before and after the deformation (the same applies to the nodes on the left and right borders, fig. 4.5–left). This behaviour is implemented via penalty functions. The versatility of periodic boundary conditions has been demostrated by van der Sluis [101] and Miehe and Koch [67].
- **Periodicity of material** is understood here as a material without *wall-effects* (fig. 4.5–right). However, the internal material structure, i.e. the positions of the inclusions, remains random[3]. By the term *wall-effect* we understand here the inability of inclusions to *penetrate* through the unit cell borders. The motivation of this is

[3]In contrast, Miehe et al. [69] describe periodic material as material without wall-effect and also with evenly distributed inclusions.

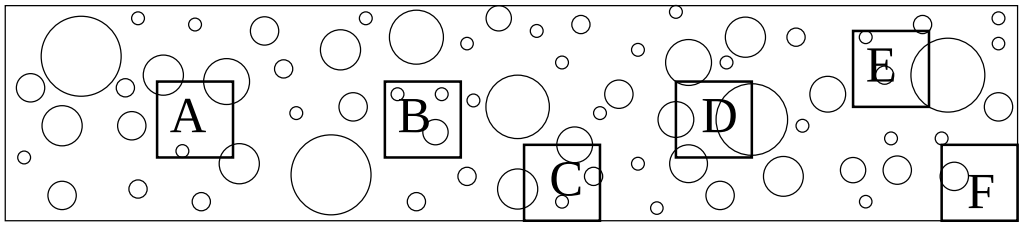

Figure 4.6: Wall-effect

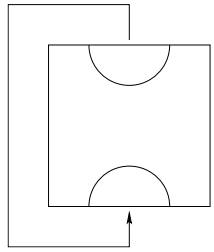

Figure 4.7: Avoiding wall-effects by invoking periodicity of the material

that an RVE is thought of as belonging to a larger sample, therefore wall-effect is not a realistic representation. According to the definition, an RVE is first of all a *representative* volume. Thus it should *represent* any part of the material. In fig. 4.6 several different situations have been displayed: samples **A**, **B**, **D** and **E** are valid in the context of periodicity of material. Although there are no inclusions crossing the edges in sample **B**, this should be considered a coincidence. On the contrary, the samples **C** and **F** are experiencing wall-effects: there are one or more edges which can not be crossed by inclusions. In this thesis, wall-effects are avoided by letting inclusions penetrate through the unit cell borders and also by letting them re-appear through the opposite edge. As such, *periodicity of the material* is obtained (fig. 4.7).

Below (fig. 4.8) results (in terms of stress – strain relations) are presented, corresponding to one of the realisations of different sample sizes with different volume fractions. These stress – strain relations have been obtained by normalising the force – displacement responses with respect to the size of the particular sample.

In fig. 4.9 volume fraction of inclusions 30% is further analysed. Four pictures, corresponding to four different sizes are presented, each of them showing five different realisations. It should be mentioned, that the same analysis of different realisations has been performed for aggregate densities 45% and 60%, although they are not shown here.

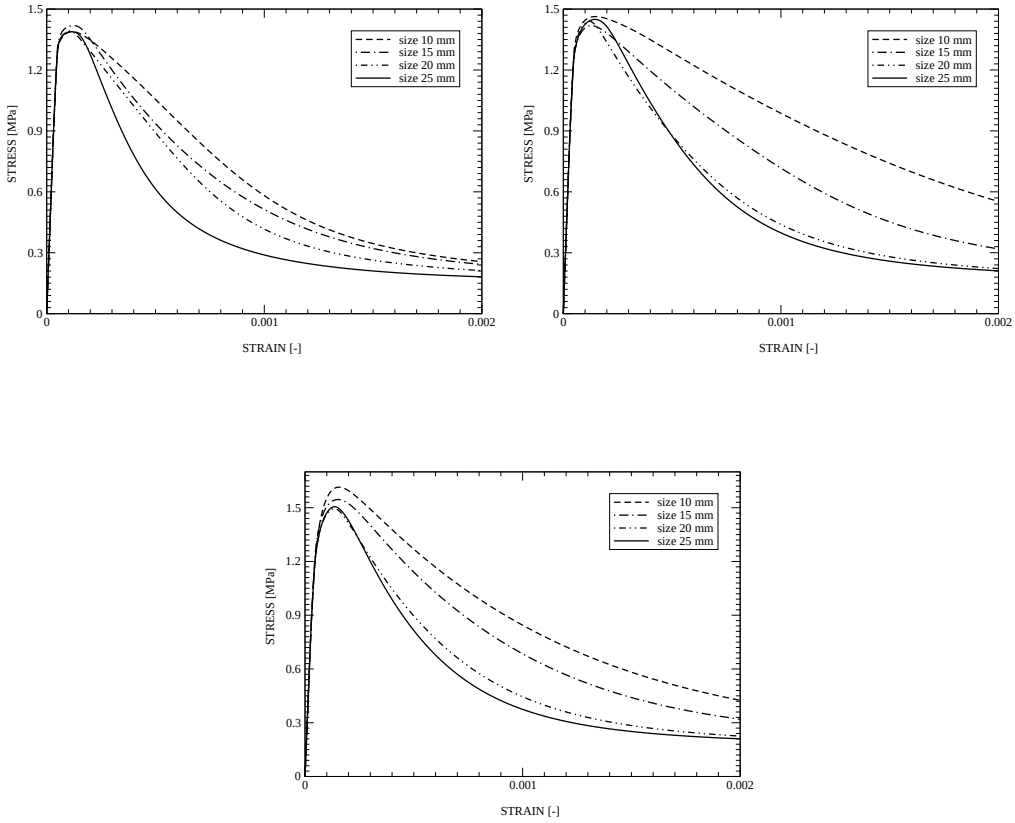

Figure 4.8: Sets of sample sizes for aggregate densities 30% (left-top), 45% (right-top) and 60% (middle-bottom)

4.2 RVE existence: statistical analysis

A statistical analysis, based on the mathematical expectation and standard deviation values has been performed on each set of results. All curves were analysed in several points, corresponding to elastic, hardening[4] and softening regions (fig. 4.11) with stiffness (slope) being the parameter of interest.

Although the conclusion could be drawn from fig. 4.9, that with increasing the size

[4]The term 'hardening' is normally used in metal plasticity, and it denotes the regime in the stress-strain curve between the end of the yield plateau (or, if the yield plateau is absent, the end of the elastic regime) and the peak. As such, hardening usually refers to *material* behaviour. In this Chapter, the term hardening will also be used in connection with the load-displacement response of the samples, since the load and the displacement are translated into stresses and strains. The term hardening thus denotes the nonlinear part of the pre-peak stress-strain curve.

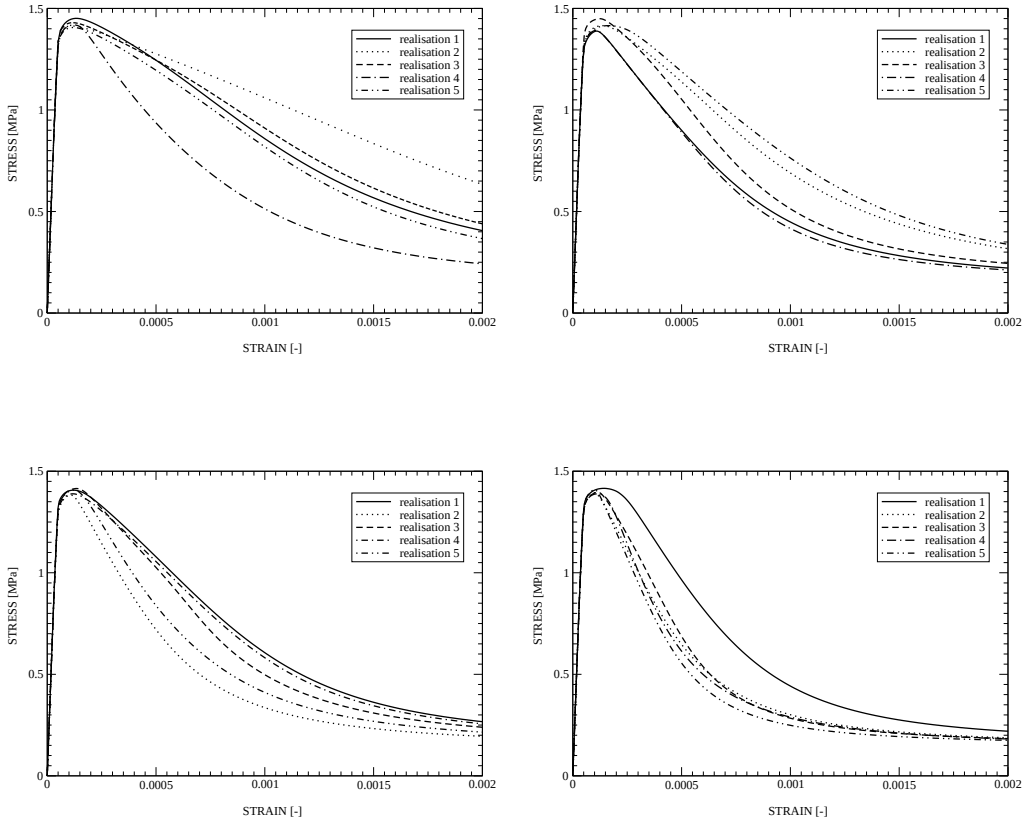

Figure 4.9: Different sizes of the unit cell, from left to right and from top to bottom $10\times10\text{mm}^2$; $15\times15\text{mm}^2$; $20\times20\text{mm}^2$; $25\times25\text{mm}^2$ ($\rho = 30\%$)

the difference in the slope values of different realisations is decreasing, i.e. the distance between curves is getting smaller, fig. 4.8 changes the picture: with increasing the size slope becomes steeper. Fig. 4.10 offers a better understanding of the situation. The three regimes presented in fig. 4.10 are linear-elastic (fig. 4.10-a), hardening (fig. 4.10-b) and softening (fig. 4.10-c). All curves (figs. 4.8, 4.9) are analysed by means of the mathematical expectation and standard deviation of the stiffnesses (value of slopes) in points corresponding to different regimes: linear-elasticity, hardening and softening with respect to size. In the linear-elastic case (fig. 4.10-a), the value of mathematical expectation (i.e. *average slope*) is practically constant with increasing the size, the standard deviation (i.e. *shifting of the slope from its average*) approaches to zero with increasing size. Material in hardening (fig. 4.10-b) shows the same trend: relatively constant mathematical expectation and approaching to the small constant of the standard deviation as size is increased.

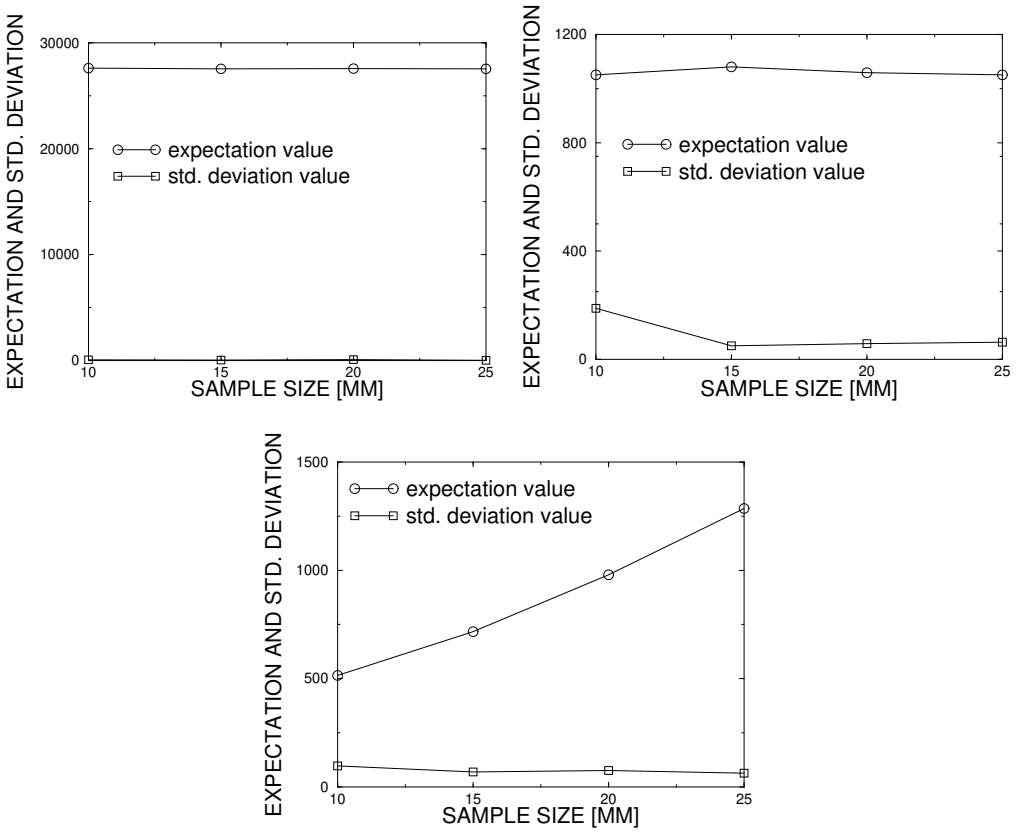

Figure 4.10: Expectation and standard deviation values for stiffness: linear elasticity (left) hardening (right) and softening (the bottom)

On the contrary, when in the softening regime (fig. 4.10-c), the standard deviation behaves qualitatively similar to linear elasticity and hardening (convergence to zero with respect to size), but the mathematical expectation steadily increases (it should be noted, that here all values are considered as absolute). In other words, with increasing size, the material behaves differently (here, more brittle).

This statistical analysis allows to make a conclusion about RVE existence. In the pre-peak regime, when the mathematical expectation shows stable constant behaviour with respect to size while the standard deviation converges with increasing size. Therefore, representative volumes can be found. However in softening, when the response of the material qualitatively changes with increasing size (which is shown with the help of mathematical expectation) there is no *representative* size, i.e. an RVE in softening cannot be found.

Schematically the dependence of the statistical information, and as the consequence

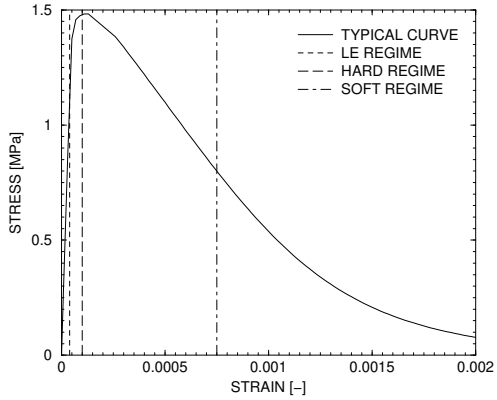

Figure 4.11: Typical curve: linear-elastic, hardening and softening regimes

the RVE existence, on the loading regime can be presented in tab. 4.3.

Results	pre-peak	post-peak
convergence of expectation	+	–
convergence of standard deviation	+	+
RVE existence	+	–

Table 4.3: RVE existence

The issue of the representative volume is analysed for different heterogeneous materials behaviour, namely linear elasticity, hardening and softening. Following the procedure, based on the statistical analysis of numerical experiments, it has been shown that the representative volume can be found with relatively high accuracy in cases of linear elasticity and hardening. In case of softening (fig. 4.10-c), as it was concluded earlier, a representative volume cannot be found.

Note 6 *It has been concluded that an RVE in softening material cannot be found. Theoretically, there is a possibility to use the RVE concept also in softening: one can consider the complete macro-structure as a Representative Volume. However, this description is of little practical use in computational mechanics.*

Note 7 *Above, the non-existence of an RVE in case of softening has been addressed from a statistical point of view, namely the non-convergence of the expectation for increasing cell sizes. However, a deterministic mechanical explanation can also be given, namely the occurrence of a size effect. This will be treated in detail in Section 4.6.*

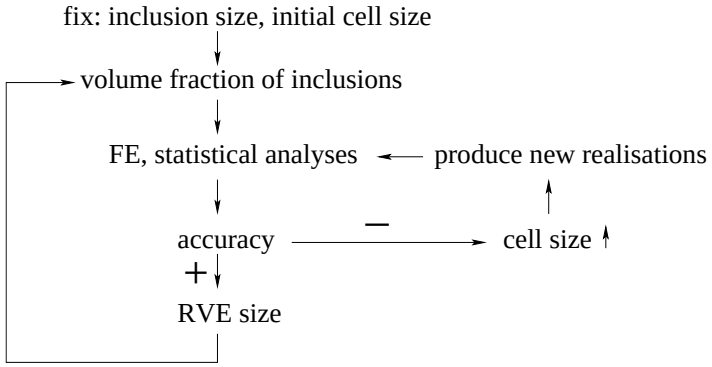

Figure 4.12: RVE size determination procedure. Block scheme

4.3 Theoretical description of the RVE determination

Once the question of an RVE *existence* is verified, its *size determination* is the next issue to address. Here a method to determine the size of the RVE is proposed (fig. 4.12). This block scheme reads as the sequence of steps:

1. Fix the maximum and minimum diameters of inclusions and the initial size of the unit cell tested (usually two times larger than the maximum diameter of inclusions).
2. Choose the volume fraction of inclusions.
3. For the tested volume fraction of inclusions generate several (minimum 5) realisations of the tested unit cell size.
4. Perform the Finite Element computation and present the results in the form of either load/displacement or stress/strain curve (dependent on the parameter of interest).
5. Perform the statistical analysis (see below for the details) of the obtained finite element results.
6. Compare the accuracy of the statistical analysis results with the desired accuracy and if the obtained accuracy is good enough the tested unit cell size is the RVE size, otherwise increase the unit cell size and go to 3.
7. Change the volume fraction of inclusions and go to 2.

For the statistical analysis of the numerical results different approaches can be used. The *variation coefficient* approach is one of them. Finding the variation coefficient as the ratio of the standard deviation of the investigated parameter to its mathematical expectation, it can be verified how the response of the single tested unit cell deviates

relatively from the mean of its class of realisations. Specifically, we have generated 5 unit cells for each volume fraction of inclusions and each unit cell size (see for instance fig. 4.2). The investigated sizes of the unit cell range from $10 \times 10\text{mm}^2$ to $25 \times 25\text{mm}^2$ (see fig. 4.1) and the dimensions of the inclusions follow a uniform distribution from [2.5 mm .. 5.0 mm]. The investigated parameter a_i is the average stress or the stiffness of the unit cell, although other parameters are also possible (cf. Stroeven et al. [94]). In this work the limiting value of variation coefficient $V_c = 0.16$ has been chosen, which is related to the 95% accuracy of the expected RVE size[5].

Note 8 *As can be deduced from the data given above, the smallest unit cell that is tested has a dimension which is twice the size of the largest inclusion. This hypothesis is widely used in literature: Drugan [25], Drugan and Willis [26] in their articles, working with elastic composites, derived quantitative estimates for the minimum RVE size, so they have shown that the minimum RVE size is twice the reinforcement diameter (cf. Section 2.2).*

4.4 RVE size sensitivity to test parameters

Traditionally, RVE sizes are thought of as being a property of the material under consideration. As such the size of the RVE should not depend on the specific loading scheme. Furthermore, in case an averaged response is required, the RVE size should ideally not depend on the specific quantity, such as stiffness or stress that is selected to represent. These two issues are verified in this section. The importance of the periodicity of both material and boundary conditions is also clarified in this section.

Note 9 *As mentioned, in this Section the* average *response (for instance average stress) is considered. Another option would be to consider the maximum (or minimum) value within the unit cell. Differences between these two approaches may arise, e.g. while increasing the unit cell size the* average stress *could remain constant whereas the* maximum stress *increases (Stroeven et al. [94]).*

Note 10 *In this and the following Section the attention will be focused only on linear elasticity (the entire loading regime is dealt with in terms of dissipated energy in Section 4.6).*

4.4.1 Tension versus shear

First, the tension tests were performed on the set of samples (fig. 4.13–left). For a given volume fraction of inclusions the statistical analysis (introduced in Section 4.3), based on the variation coefficient, gives the following results (fig. 4.14). Here, for the variation coefficient the stress averaged on the unit cell was chosen as the parameter of interest.

This size of the unit cell will be considered as a size of RVE with a given value of volume fraction of inclusions.

[5]For more details on this and related equivalent method see Gitman et al. [36, 38, 39]

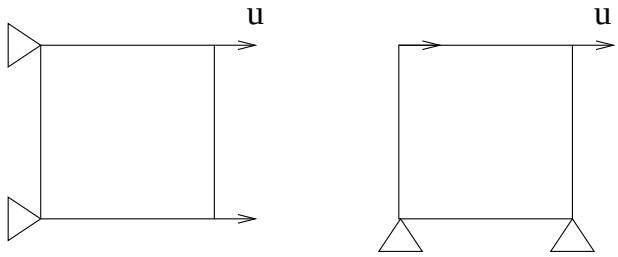

Figure 4.13: Left: tension test; right: shear test

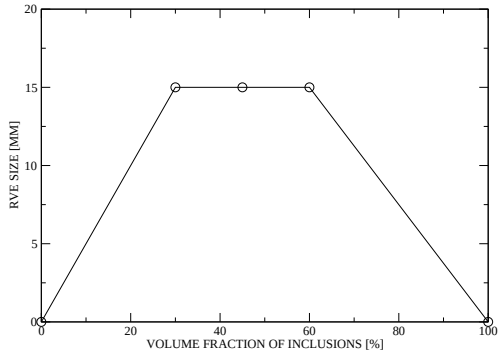

Figure 4.14: Tension test (accuracy 95%) RVE size versus volume fraction of inclusion

Note 11 *In order to improve the accuracy of the quantitative analysis, one should consider more intermediate sizes in between the sizes 10×10mm^2 and 15×15mm^2 in fig. 4.14. Similarly, the accuracy of fig. 4.14 can be improved by considering more intermediate values of the volume fraction of inclusions.*

The next step of the procedure is to make a graph, corresponding to the value of the RVE for different volume fractions of inclusions (fig. 4.14). These results allow us to find the size of the RVE with given volume fraction of inclusions of the material and accuracy. Corresponding values of the RVE for all different volume fractions of inclusions ρ are 15×15mm^2, except 0×0mm^2 for $\rho = 0\%$ and $\rho = 100\%$ (purely homogeneous materials). It should be emphasized again that the RVE size is understood here as a minimum size of a microstructural cell that fulfills the requirements i.e. a lower bound, larger microstructural cells behave similarly (cf. Section 2.2.1).

Next, shear tests have been performed on the same series of samples (fig. 4.13–right). Note, that again, as in the tension test, periodicity of boundary condition and material are used. The results are presented in fig. 4.15–left. The same accuracy as in the tension

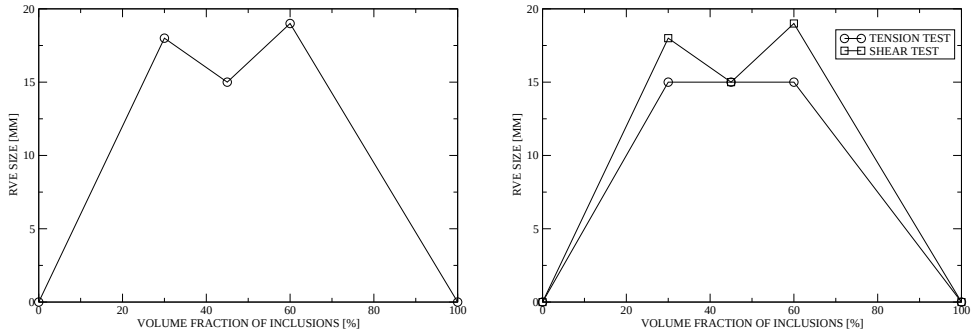

Figure 4.15: RVE in case of shear test (left); tension and shear tests comparison (right)

test is used. As for the tension test, in case of shear corresponding values of the RVE for different volume fractions of inclusions are:

- RVE size = 18×18 mm^2 for $\rho = 30\%$;
- RVE size = 15×15 mm^2 for $\rho = 45\%$;
- RVE size = 19×19 mm^2 for $\rho = 60\%$;
- RVE size = 0×0 mm^2 for $\rho = 0\%$ and $\rho = 100\%$ (purely homogeneous materials).

In fig. 4.15–right the results for tension and shear are compared. Although the number of realisations n was rather small, still a reasonable agreement between the two loading schemes was found.

Discussion: in the present results there is no significant sensitivity to the loading scheme. On the basis of the above analysis (fig. 4.15–right) we cannot conclude that the RVE size for linear elastic material depends on the loading scheme. Thus the value of the RVE is generally unique for the particular choice of the loading scheme. Note that this conclusion is restricted only to tension, compression, shear and the linear combination of these loading schemes.

4.4.2 Periodicity versus Non-periodicity

As it was mentioned in Section 4.2, two types of periodicity are considered: periodicity of material in terms of the wall-effect and periodicity of boundary conditions (fig. 4.5). The importance of both types of periodicity is addressed below.

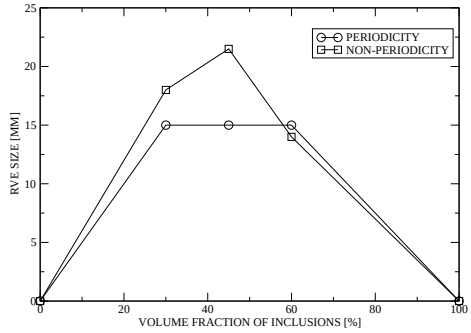

Figure 4.16: Tension test. Stress-based RVEs for material without wall-effect versus material with wall-effect; periodic boundary conditions are applied.

Periodic material. Material without wall-effect versus material with wall-effect have been tested. Periodic boundary conditions have been employed in both cases. The results for the tension test are presented in fig. 4.16. As it can be verified, in case of the tension test the difference in RVE sizes is not extremely large compared to the following shear test results (see below).

For the case of shear loading materials with and without wall-effect have also been compared. The results of the shear test in case of no wall-effect and existence of wall-effect (i.e. material periodicity versus material non-periodicity) are presented in fig. 4.17. The shear test of the material with wall-effect shows that reasonably accurate RVE size should be much larger than the maximum tested size of $25\times25\text{mm}^2$. As it follows from fig. 4.17, the only possible RVE sizes for the non-periodic material in case of shear test was found with an unacceptable low accuracy of 5% (i.e. 95% error). Increasing the accuracy to levels comparable with the no wall-effect tests will lead to extremely large RVE sizes, which have not been generated.

This brings us to the conclusion that in case of the tension test it is desirable but not essential to have material without wall-effect, but in case of shear test the absence of wall-effect is essential in order to describe realistic behaviour of the material. To understand the above observation one may think of a tension test in terms of prescribed deformations (for example horizontal stretching). In this case the restrained lateral deformation and the developed two normal stress components do not depend on particles penetrating (or not) the boundaries. Thus the issue of the material periodicity is not very essential in the tension case. On the contrary in case of shear, one could think of the test in terms of stiffnesses. Material without wall-effect guarantees that opposite sides of a specimen have more or less identical stiffnesses, however in case of material with wall-effect this is not necessary the case. As a result the scatter in the responses (and thus the RVE size) in case of non-periodic material is much larger than the one in the periodic material.

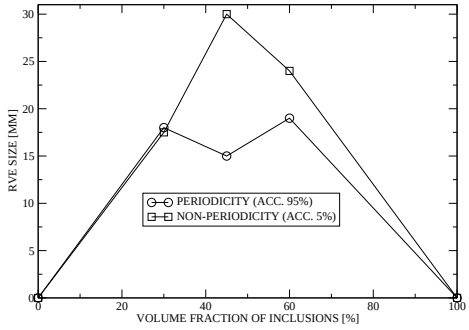

Figure 4.17: Shear test. Stress-based RVEs for material without wall-effect versus material with wall-effect; periodic boundary conditions are applied.

Periodic boundary conditions Next the issue of periodic boundary conditions versus non-periodic boundary conditions has been analysed. The results for the case of material without wall-effect and with periodic boundary conditions are presented in fig. 4.15–right (both tension and shear tests). Also tests have been performed for material without wall-effect and without periodic boundary conditions. Results show that for both tension and shear tests the RVE size should be extremely large (much larger than $25\times25\text{mm}^2$ – maximum size tested) once the accuracy 95% is required. In figs. 4.18 and 4.19, corresponding to the tension and shear tests respectively, together with the reference cases of periodicity the non-periodic curves are presented, corresponding to the much lower accuracy of 30%. Higher prescribed accuracy will lead to much larger size of the RVE in both tension and shear cases.

Discussion: two different types of periodicity have been analysed – periodicity of material in terms of wall-effect and periodicity of boundary conditions. Two different loading schemes have been compared – tension and shear. The results show that for the tension test the periodicity of boundary conditions influences the results drastically: the size of the RVE in the case of non-periodic boundary conditions is much larger than the RVE size for the material with periodic boundary conditions. On the contrary, RVE sizes for material with and without wall-effect are relatively similar. For the shear test results, the conclusion is opposite: the material periodicity seems to be more dominant than periodicity of boundary conditions. However in order to obtain a reliable results both material and boundary conditions periodicity are strongly recommended.

Note 12 *In the above study the issue of periodicity of boundary conditions has been analysed for the case of elastic material behaviour, however the offered methodology is general and can be used to analyse the periodicity question also in case of inelastic (but*

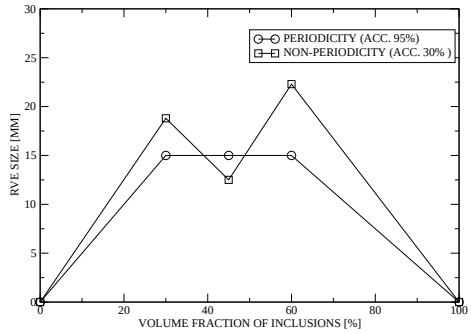

Figure 4.18: Tension test. Stress-based RVEs for material without wall-effect: periodic boundary conditions versus non-periodic boundary conditions.

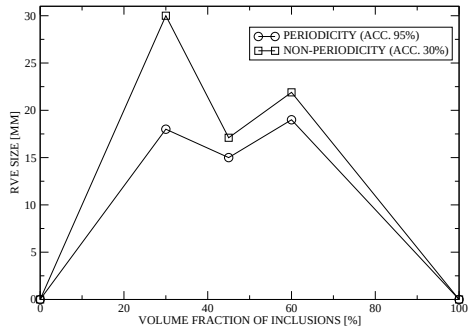

Figure 4.19: Shear test. Stress-based RVEs for material without wall-effect: periodic boundary conditions versus non-periodic boundary conditions.

pre-peak) material behaviour. The extension towards inelasticity is treated in Miehe and Koch [67], for instance.

4.4.3 Stiffness-based versus Stress-based RVE

In the previous paragraphs, the stress has been used as a parameter of interest. The second issue is to check whether the RVE size is a function of the parameter of interest. Two different parameters of interest were analysed: stress, averaged on a sample and stiffness, found by means of the slope of the stress – strain curve. The choice of these

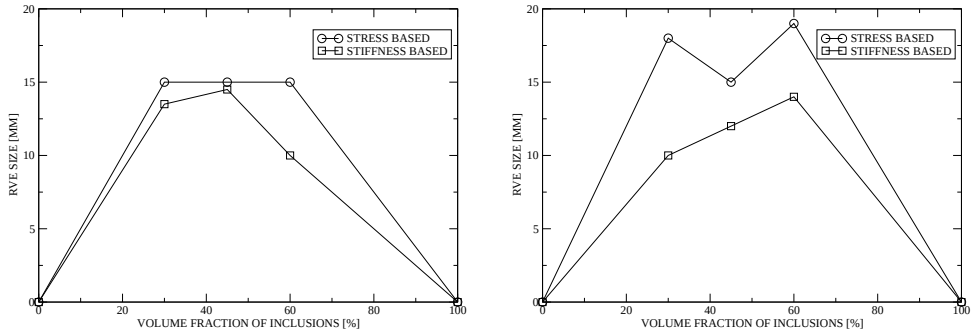

Figure 4.20: RVEs for stress and stiffness being parameters of interest in case of tension test (left); shear test (right)

parameters could be explained by their relevant role in multi-scale methods, where these are the two quantities that are "up-scaled". Therefore stiffness and averages of stress are extremely relevant in homogenisation techniques, as will be discussed in Chapter 5.

The results are presented in fig. 4.20. Again the accuracy was 95%, and both tension and shear loading cases were tested.

As it can be verified from fig. 4.20–left the parameters stress and stiffness lead to similar RVE sizes if tension loading is considered. For the case of shear loading (fig. 4.20–right) the differences are somewhat larger, especially for $\rho = 30\%$. However, for $\rho = 45\%$ and $\rho = 60\%$ the differences are again not significant.

Discussion: taking the stiffness or the stress as the parameter of interest does not lead to a significant change in RVE size.

4.5 RVE size sensitivity to material parameters

Further tests are performed in order to check how sensitive the size of the RVE is to changes in material parameters. Indeed, traditionally being considered as a material property (cf. references in Section 2.2.2), the RVE size should be highly affected by changes in material structure and in the mechanical properties of its components.

As was mentioned above, a three phase material is considered. Each component of the material has its own set of properties in terms of Young's modulus and Poisson's ratio. The structural property will be analysed mainly by means of the volume fraction of inclusions and not so much by the sizes of inclusions (we do realise that the size of inclusions plays an important role in RVE size determination, but here we focus on volume fractions of inclusions; the influence of the inclusions size appears here as the

influence of their minimum and maximum value).

In our statement of the problem, some parameters are assumed to be deterministic (e.g. Young's moduli and Poisson's ratios of the three phases) whereas others have a stochastic character: for example volume fraction of inclusions or minimum and maximum sizes of inclusions. These parameters are stochastic as a result of the sample generation process (it is very difficult or even impossible to reach exactly the desired deterministic value of volume fraction and minimum or maximum size of the inclusions in all samples).

4.5.1 Deterministic characteristics

The averaged response of a heterogeneous material is determined by the properties of its components. The hypothesis of Young's modulus and Poisson's ratio of each material phase influencing the size of the RVE is to be analysed in this section. Both Young's modulus and Poisson's ratio are considered to be deterministic.

Stiffness ratio variation

Firstly, we investigate the influence of changing the ratio of the Young's moduli of the three phases (Poisson's ratios were kept constant and for all three phases equal to 0.2).

	Analysis number (fig. 4.21)	Inclusions [MPa]	Matrix [MPa]	ITZ [MPa]
reference	1	30000	25000	20000
variation 1	2	35000	25000	15000
variation 2	3	250000	25000	2500
variation 3	0	25000	25000	25000

Table 4.4: Variations of Young's moduli

The reference case (first line of table 4.4) was chosen equal to the computations in the previous sections. The first variation involves a material with a *slightly larger* difference in Young's modulus of its components whereas the second variation deals with *significantly larger* differences in stiffness. The third variation corresponds to the case of a homogeneous material: Young's modulus of different phases are equal to each other. The results of these tests were compared in terms of the corresponding RVE sizes. In other words, the question *how an increase of the heterogeneity of the material will influence its RVE size* was addressed.

Tension tests were performed for all four different stiffness ratios. In fig. 4.21 the curves for stiffness-based RVE sizes are presented. The RVE size sensitivity of a variations in the stiffness ratio can be analysed. It was necessary to drop the prescribed accuracy from 95% to 75% in order to make a comparison between the four cases – 95% accuracy would lead to a very large RVE for the second variation. Thus, it can be concluded that increasing the differences in Young's modulus of different phases leads to larger RVE sizes.

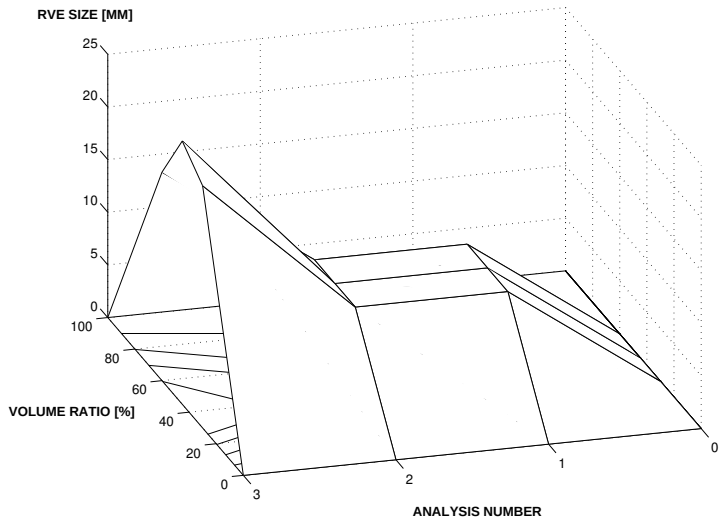

Figure 4.21: Tension test; stiffness-based RVE; sensitivity of RVE size to changing the stiffness ratios

Note, that smaller RVEs are found for the reference case compared to the previous Section, which is due to the a lower imposed accuracy. Also note, that in case of similar Young's modulus of all three components (matrix, inclusions and ITZ) – variation three (table 4.4) the material loses its heterogeneity and behaves as homogeneous. The RVE size of homogeneous material is zero.

Poisson's value sensitivity

The sensitivity of the RVE size to a variation of Poisson's ratio has also been studied. Different values of the Poisson's ratio were analysed (as shown in table 4.5), while the Young's moduli were kept as in the reference case (table 4.4).

	$\nu_{inclusions}$	ν_{matrix}	ν_{ITZ}
reference	0.2	0.2	0.2
variation 1	0.2	0.3	0.3
variation 2	0.05	0.45	0.45

Table 4.5: Poisson's ratios

In the same way as described above, tension tests were performed for all three different Poisson's ratios. Despite the fact that the variation coefficient decrease with increasing size of the unit cell, for the accuracy 95% s even the maximum variation coefficient

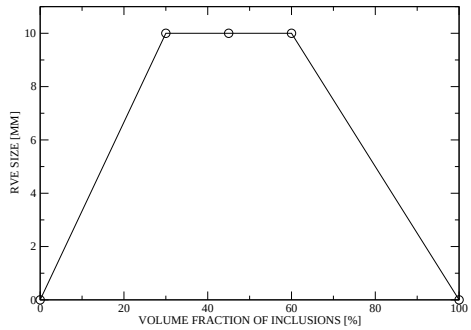

Figure 4.22: Tension test; Poisson's ratio-based RVE; sensitivity of RVE size to changing the Poisson's ratio

(corresponding to the smallest unit cell size in with Poisson's ratios of phases following the variation 2 from table 4.5) gives already far too small number. Variation coefficient was found of order 10^{-6} which is much smaller than the most accurate table value. Speculating on the results, and extrapolating the variation coefficient to the smaller sizes, can provide 95% accurate RVEs. But, bearing in mind, that the choice of the smallest unit cell was dictated by the fact that RVE should be at least twice the size of the largest inclusion, the results of the analysis showed no significant influence of the $\nu_{incl} : \nu_m : \nu_{ITZ}$ ratio on the RVE size. Thus, in case of stress-based RVE, the sizes $10{\times}10\text{mm}^2$ for volume fractions 30%, 45% and 60% and $0{\times}0\text{mm}^2$ for volume fractions 0% and 100% (fig. 4.22) can be an referred as RVE sizes, however that would not be the RVE in terms of its lower bound (cf. Section 2.2.2) anymore.

4.5.2 Stochastic characteristics

The influence of a small change in input data (particularly the volume fraction of inclusions ρ and/or sizes of inclusions d) on the size of the RVE occurs to be one of the important issues in the RVE investigation. This problem is especially important when those input data have a stochastic character. In this section, the attention is focused on the case where ρ and d have a stochastic character[6]. This type of problems is actually the problem of stability analysis: if small changes of input data lead to small changes of the solution, the solution is stable, otherwise it is unstable. In our case the problem becomes more difficult, as *stochastic* input data is considered, and as a consequence the solution also has a *stochastic* character.

[6] As it has been intended to analyse both deterministic and stochastic material parameters the choice has been made to take Young's modulus and Poisson's ration as deterministic parameters with the volume fraction of inclusions and sizes of inclusions are taken as stochastic parameters.

DH–stability concept

In nowadays mechanics several approaches exist to deal with stability of uncertain systems, most of them based on modified Lyapunov stability: Lyapunov stability in probability, Lyapunov stability in means, almost sure Lyapunov stability, etc. (Kozin [56]). All these concepts are based on the fact, that input data (initial/boundary conditions, geometry, etc.) have a deterministic character. However, in our case, as far as dealing with stochastic character of both input data (here: volume fraction of inclusions and size of inclusions) and solution (lower bound of the RVE size) these concepts are not sufficient. We propose here an enhanced concept of stochastic stability which would take into account the uncertainty of input data together with solutions. This new concept is called *DH–stability* (Gitman and Gitman [40]).

In order to formulate a definition of stability in "Direct Hit" terms (or answer the question: how adequate is the initial guess?) we need to introduce probability spaces (Jaynes [49]).

We consider a general mechanical process with initial data x_0, boundary conditions x_{b} (in terms of displacement and/or tractions), a right-hand-side that includes effects of loads f, and operator A that acts on the displacement (e.g. stiffness operator).

Probability spaces Let (Ω_i, F_i, P) be the probability space for initial conditions. Here Ω_i is a set of events associated with a probability P. We will identify an elementary event $\omega \in \Omega_i$ with the initial conditions of the problem in a deterministic sense.

Let us define a proximity confidence level $\pi^{\delta_i}_{\Omega_i}$ for events $\omega_1, \omega_2 \in \Omega_i$ as follows:

$$\forall \omega_1, \omega_2 \in \Omega_i : \quad \pi^{\delta_i}_{\Omega_i}(\omega_1, \omega_2) = P(\|\omega_1 - \omega_2\| < \delta_i) \tag{4.2}$$

which quantifies the probability that the norm of $\omega_1 - \omega_2$ is smaller than a user-defined value δ_i.

The probability space for boundary values is introduced similarly as (Ω_b, F_b, P), where the elementary event $\omega \in \Omega_b$ will be identified with the boundary conditions of the problem in a deterministic sense, in other words ω with proximity confidence level $\pi^{\delta_b}_{\Omega_b}$

$$\forall \omega_1, \omega_2 \in \Omega_b : \quad \pi^{\delta_b}_{\Omega_b}(\omega_1, \omega_2) = P(\|\omega_1 - \omega_2\| < \delta_b) \tag{4.3}$$

For the right-hand-sides we define (Ω_f, F_f, P), where the elementary event $\omega \in \Omega_f$ is identified with the right-hand-side of the problem in a deterministic sense, or ω with proximity confidence level $\pi^{\delta_f}_{\Omega_f}$

$$\forall \omega_1, \omega_2 \in \Omega_f : \quad \pi^{\delta_f}_{\Omega_f}(\omega_1, \omega_2) = P(\|\omega_1 - \omega_2\| < \delta_f) \tag{4.4}$$

Finally, the probability space for operators will be (Ω_A, F_A, P), where the elementary event $\omega \in \Omega_A$ is identified with the operator of the problem in a deterministic sense, thus ω and proximity confidence level $\pi^{\delta_A}_{\Omega_A}$

$$\forall \omega_1, \omega_2 \in \Omega_A : \quad \pi^{\delta_A}_{\Omega_A}(\omega_1, \omega_2) = P(\|\omega_1 - \omega_2\| < \delta_A) \tag{4.5}$$

If we denote the probability space for solutions as (Γ, F, P), then the elementary event $\gamma \in \Gamma$ will be identified with the solution of the problem in a deterministic sense, in other words γ with proximity confidence level $\pi^{\varepsilon}_{\Gamma}$

$$\forall \gamma_1, \gamma_2 \in \Gamma : \quad \pi^{\varepsilon}_{\Gamma}(\gamma_1, \gamma_2) = P(\|\gamma_1 - \gamma_2\| < \varepsilon) \tag{4.6}$$

Assuming that ω_2 and γ_2 exist and correspond to the reference solution $\hat{\omega}$ and $\hat{\gamma}$, respectively, let us formulate the criterion of DH–stability.

DH-stability formulation To define the stability in "direct hit" terms it is necessary to define a solution of the stochastic problem, which we will denote as a conventional $\varepsilon - \delta$ solution. As the $\varepsilon - \delta$ solution we will conceive a set of such solutions $x(t)$, that $\forall t \quad : \quad \|x - \hat{x}\| < \varepsilon$, if the perturbations (of initial conditions, boundary conditions etc.) are located in the δ-neighbourhood. Here $\hat{x}$ is the solution corresponding to $\delta = 0$, i.e. the unperturbed (or reference) solution. Suppose, that the set of such solutions is not empty, the stability in a stochastic sense can be defined as follows:

assign a confidence level for input data (initial conditions $\hat{x_0}$, boundary conditions $\hat{x_b}$, right-hand-side $\hat{f}$ and operators $\hat{A}$ of the problem) $P^{**} \in [0, 1]$ and a confidence level for the solution $P^* \in [0, 1]$. Now, if for any number $\varepsilon > 0$ such a number $\delta(\varepsilon) > 0$ can be found, that as far as the following condition

$$\begin{aligned} &(\pi^{\delta}_{\Omega_i}(x_0, \hat{x_0}) \geq P^{**}) \wedge (\pi^{\delta}_{\Omega_b}(x_b, \hat{x_b}) \geq P^{**}) \wedge \\ &\wedge (\pi^{\delta}_{\Omega_f}(f, \hat{f}) \geq P^{**}) \wedge (\pi^{\delta}_{\Omega_A}(A, \hat{A}) \geq P^{**}) \end{aligned} \tag{4.7}$$

is fulfilled $\forall t$, the inequality

$$\pi^{\varepsilon}_{\Gamma}(x, \hat{x}) \geq P^* \tag{4.8}$$

is fulfilled for any $t > t_0$, then the unperturbed process is DH-stable.

In terms of ω and γ the definition of DH–stability can be rewritten as follows:

assign confidence levels $P^*, P^{**} \in [0, 1]$; the unperturbed solution to the problem corresponding to $\hat{\omega}$ is said to be DH–stable (on confidence levels P^*, P^{**}) if for any $\varepsilon > 0$ there is $\delta(\varepsilon) > 0$ such, that if $\pi^{\delta}_{\Omega}(\omega, \hat{\omega}) \geq P^{**}$ then $\pi^{\varepsilon}_{\Gamma}(\gamma, \hat{\gamma}) \geq P^*$, where $\Omega = \Omega_i \times \Omega_b \times \Omega_f \times \Omega_A$

The idea of the definitions above can be seen as follows: if the inequalities (4.7) are fulfilled (in the sense of proximity confidence level of the corresponding space events) and in any point of time the perturbed process is located in the ε –neighbourhood of the nonperturbed process with probability P^{**} (in a sense of proximity confidence level of the solution space events), then the nonperturbed deformation process is stable with the probability P^*.

Note 13 *The classical (Lyapunov) definition of stability in a deterministic sense can be retrieved from eqs. (4.7)-(4.8), by taking* $P^* = P^{**} = 1$. *On the other hand, Lyapunov stability in probability, Lyapunov stability in means, almost sure Lyapunov stability, p-stability etc. are all referred only to* P^* *[56, 95, 97].*

A short overview of the known stability concepts reads:

- *Lyapunov Stability*

  $IF \ \forall\, \varepsilon > 0 \ \ \exists\, \delta(\varepsilon) > 0 :$
  $\quad if \ \ \|x_0\| < \delta \ \ then \ \ \sup_{t \geq t_0} \|x(t; x_0, t_0)\| < \varepsilon$
  $THEN \quad Stability$

- *Lyapunov Stability in Probability*

  $IF \ \forall\, \varepsilon > 0, \varepsilon' > 0 \ \ \exists\, \delta(\varepsilon, \varepsilon') > 0 :$
  $\quad if \ \ \|x_0\| < \delta \ \ then \ \ P(\sup_{t \geq t_0} \|x(t; x_0, t_0)\| > \varepsilon') < \varepsilon$
  $THEN \quad Stability\ in\ Probability$

- *DH-stability*

  $IF \ \forall\, \varepsilon > 0; \quad P^*, P^{**} \in [0, 1] \quad \exists\, \delta(\varepsilon, P^*, P^{**}) > 0 :$
  $\quad if \ \ P(\|x_0\| < \delta) \geq P^{**} then \ \ P(\sup_{t \geq t_0} \|x(t; x_0, t_0)\| < \varepsilon) \geq P^*$
  $THEN \quad DH–Stability$

Being derived from the general setting of the DH–stability problem, the following issue is of special interest: assuming a proximity confidence level for the obtained solution (set by the user) find the proximity confidence level of the input data that satisfies the proximity confidence level of the solution. In other words the problem can be reduced to a determination of the minimum value $P^{**} = P^{**}(P^*)$, which ensures that the conditions eqs. (4.7)-(4.8) are satisfied (see also Appendix B).

DH–stable RVE

Now, consider the problem of the RVE size quantification. The evidence of a properly defined RVE size is the requirement that small changes in volume fraction and size of inclusions lead to small changes of the RVE size. In other words, the issue of a properly defined RVE size is coupled to a stability analysis. As both parameters (volume fraction and size of inclusions) have a stochastic character, the problem of the stochastic stability investigation can be formulated in the following way:
for given δ_i *and* ε *and user-specified values of probabilities* P^* *and* P^{**} *the stochastic (DH–)stable RVE should be found with a given probability distribution of the above values.* Here we require a maximum deviation $\delta_1 = 0.05\%$ in the volume fraction of inclusions, maximum deviations $\delta_2 = 0.01$mm and $\delta_3 = 0.01$mm in maximum and minimum diameter of inclusions, respectively. Furthermore, we require a maximum deviation $\varepsilon = 0.05$mm in the size of the RVE. Both probabilities P^* and P^{**} were taken equal to 95%. The information above can be presented in the form of a system of equations:

$$P^{**} = P(\|\rho - \hat{\rho}\| < 0.0005) \geq 0.95 \tag{4.9a}$$

$$P^{**} = P(\|d_{\max} - \hat{d}_{\max}\| < 0.01) \geq 0.95 \tag{4.9b}$$

$$P^{**} = P(\|d_{\min} - \hat{d}_{\min}\| < 0.01) \geq 0.95 \tag{4.9c}$$

$$P^{*} = P(\|L_{\text{rve}} - \hat{L}_{\text{rve}}\| < 0.05) \geq 0.95 \tag{4.9d}$$

here ρ and $\hat{\rho}$ are dimensionless, $d_{\max}$, $\hat{d}_{\max}$, $d_{\min}$, $\hat{d}_{\min}$, L_{rve} and $\hat{L}_{\text{rve}}$ have a dimension of mm.

The first three expressions in the system eqs. (4.9a–4.9c) correspond to the geometrical input data, the validity of which is ensured by the accuracy of the sample preparation, i.e. volume fraction of inclusions was allowed to vary ±0.05% from the deterministic values (30%, 45% and 60%); the maximum and minimum diameter of inclusions were allowed to vary ±0.01mm from the deterministic vales (2.5 mm and 5.0 mm, respectively). Thus, with an accuracy of 0.95[7], it can be stated that the samples characteristics lie in the specified ranges.

As for the expression (4.9d), a further explanation should be given. Equation (4.9d) claims that with an accuracy $P^* = 0.95$ the RVE sizes of the deterministic (unperturbed, i.e. corresponding to the deterministic volume fraction of inclusions 30%, 45% and 60%) and perturbed (i.e. corresponding to variations of ±0.05% volume fraction) values lie within 0.05mm from each other. The validity of this last statement could be shown in the following way: let us consider the tension test with the stiffness based RVE (fig. 4.23), and let (for the sake of simplicity) the volume fraction of inclusions be 60% (the same analysis can be made for any volume fraction in this curve). Then, the limit cases, when expression (4.9d) is still valid, correspond to the perturbed values of volume fraction equal to 59.95% and 60.05%. According to the curve on fig.4.23, the values of the RVE size corresponding to the perturbed volume fractions are equal to $10.015 \times 10.015\text{mm}^2$ and $9.987 \times 9.987\text{mm}^2$, respectively. The unperturbed value of the RVE size, i.e. the RVE size corresponding to exactly 60% volume fraction of inclusions, is $10.000 \times 10.000\ \text{mm}^2$. The difference between the deterministic RVE size and the RVE sizes corresponding to the perturbed volume fractions is 0.015mm for $\delta_1 = -0.05\%$ and 0.013mm for $\delta_1 = +0.05\%$. More formally, $\|L_{\text{rve}} - \hat{L}_{\text{rve}}\| = \max_{\text{i}}(L^{\text{i}}_{\text{rve}} - \hat{L}_{\text{rve}}) = 0.015\text{mm}$ in terms of length of the RVE. In both cases the difference is less than the allowed deviation 0.05mm (4.9d). As for the accuracy, the curve in fig. 4.23 corresponds to the prescribed 0.95 accuracy. Thus, as all entries of system eqs. (4.9) are fulfilled, the stochastically DH–stable RVE is found for the given test and parameter of interest.

Another parameter test was also of interest: the allowed perturbation for the volume fraction of inclusion δ_1, it was given that $\delta_1 = 0.05\%$. But in reality, the allowed deviation could be as large as $\delta_1 = 1.0\%$. In this case $\varepsilon = 1.0\text{mm}$. Coming back to fig. 4.23, it is

[7] As it was stated above, $P^{**} = P^{**}(P^*)$, the probability of the results, i.e. the accuracy of the variation coefficient analysis, is $P^* = 0.95$. The simplest way to define P^{**} is to state $P^{**} = P^*$ and then the accuracy P^{**} is also 0.95.

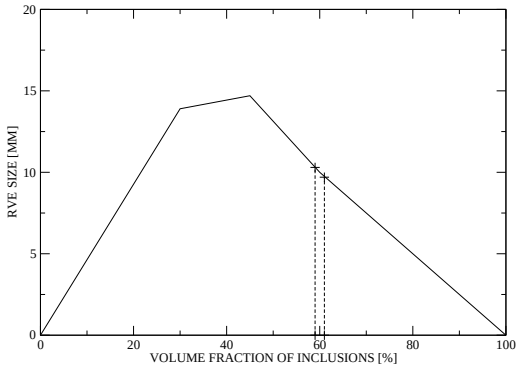

Figure 4.23: Stiffness based RVE for tension case

possible to retrieve the sizes of the RVE, corresponding to the limit cases of volume fraction 59% and 61%. Those sizes are 10.3×10.3 mm^2 and 9.7×9.7 mm^2, respectively. Again the maximum differences $\|L_{\mathrm{rve}} - \hat{L}_{\mathrm{rve}}\| = \max_{\mathrm{i}}(L^{\mathrm{i}}_{\mathrm{rve}} - \hat{L}s_{\mathrm{rve}}) = 0.3$ mm is less than $\varepsilon = 1.0$mm. So that the solution is DH–stable.

Furthermore, it is interesting to analyse how the probability P^* influences the result. Fig. 4.24 shows the RVE size curves for the case of different accuracy P^*, namely 90%, 95% and 97.5%. According to the figure, the higher the accuracy, the larger the RVE size should be. In terms of DH–stability, sizes above the curve corresponding to the given accuracy are DH–stable, as eq. (4.9d) is satisfied there. On the contrary sizes below the curve are DH–unstable, as eq. (4.9d) is violated. This statement is in good agreement to the RVE size properties known from literature.

On the basis of the above analysis the **DH-stability–enhanced definition of an RVE** can be formulated (Gitman et al. [39]), namely
an RVE is a stochastically DH–stable representation of statistically homogeneous material. The size of the RVE depends on the type of material. This size should be large enough for the constitutive relations valid for the material to hold, i.e. be representative, and small enough compared with the structural size.

4.6 RVE existence versus Deterministic Size Effect

As it was mentioned above in Section 4.2, the statistical analysis of series of samples in softening showed that the response of the material qualitatively changes with increasing size (fig. 4.10–bottom: expectation values). On the other hand, the phenomenon that the response of a specimen changes with increasing size is also known as the *size effect* (Weibull [110], Weibull [111], Weibull [112], Bažant [10], Bažant [11], Bažant and Yavari [16], Carpinteri et al. [20], Duan et al. [27], Karihaloo [51], van Mier [104]) etc.

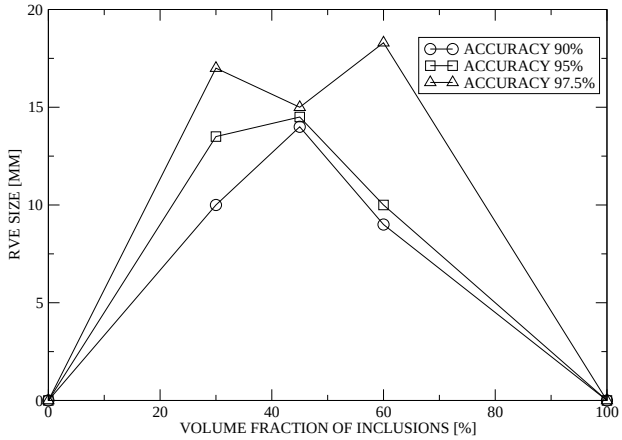

Figure 4.24: Stiffness-based RVE for tension case. A variation of accuracy

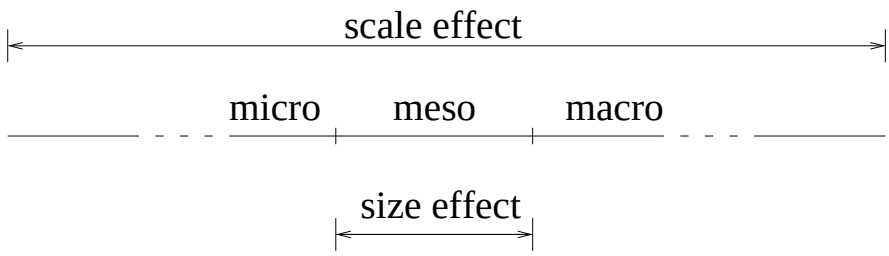

Figure 4.25: Scale and size effects

In the context of this manuscript several assumptions are made:

- we are working within one scale (see fig. 4.25), i.e. meso-level: different scales would lead to the introduction of different constitutive relations;
- as we are working within the meso-level, the material under consideration should have a heterogeneous structure (here: three-phase material);
- all samples should have the same geometry.

The deterministic size effect (Bažant [10], Bažant [11], Bažant and Yavari [16], Duan et al. [27]) can be caused by:

- different material overall properties due to the ratio between the structural size and the fracture zone, and/or

- the influence of the boundary (Duan et al. [27]).

The extension of the deterministic size effect theory to the class of materials with explicitly defined inclusions and matrix is discussed below. Here we treat deterministic size effects in terms of the dissipated energy.

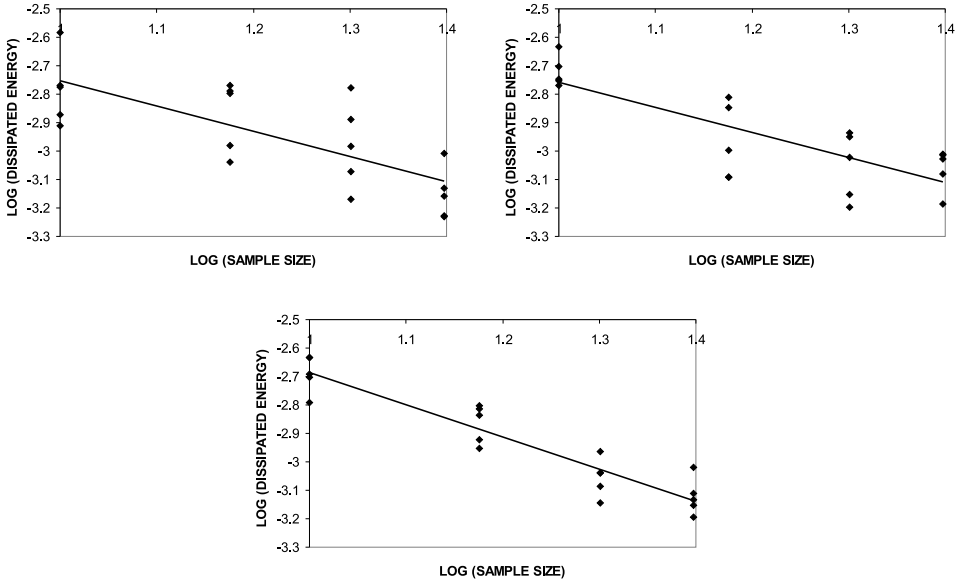

Figure 4.26: Energy based deterministic size effect. Least-square fit for volume fraction 30% (top left), 45% (top right) and 60% (bottom)

The results presented in fig. 4.26 show the dissipated energy values in case of a tension test. The three curves describe a linear fit between different realisations corresponding to different sample sizes for volume fractions of inclusions equal to 30% (fig. 4.26–top left), 45% (fig. 4.26–top right) and 60%(fig. 4.26–bottom). The value of the dissipated energy has been evaluated as the area under the stress-displacement curves. As it follows from the graph, the fracture energy value is decreasing with respect to increasing sample size. The values of the slopes in the logarithmic coordinates are very close to each other and approximately equal to -1, which corresponds to an inverse proportionality of the dissipated energy with the sample size. This inverse proportionality towards the size can be explained as follows:

- the value of the dissipated energy is obtained from integrating the average stresses with respect to the average strains;

- whereas the reaction forces are different for all sizes, the stresses are obtained by

averaging the forces over the samples' cross sections and are, therefore, similar for all sizes;

- the average strains are obtained from dividing the displacements (similar for all sizes) by the sample length, and as a result they are inversely proportional to the sample size;
- thus, as a result, the dissipated energy is inversely proportional to the sample size.

These trends are also observed in fig. 4.8.

Generally speaking, whenever the occurrence of a size effect is observed, the effects of statistical and deterministic size effects should be distinguished. The deterministic size effect has been discussed above in terms of dissipated energy, but a statistical size effect is also present in terms of strength. The strength of a specimen is largely determined by the stress concentration factors that occur upon loading. Stress concentration factors increase in the neighbourhood of an inclusion, more so if this inclusion is relatively large, and even more so if two large inclusions are close to one another. A statistical size effect thus appears as a result of increasing the probability of the "weakest link" (Weibull [110, 111, 112]): the larger the sample, the higher the probability of two large inclusions in contact, and therefore the higher the probability of failure initiation. Therefore, this statistical size effect relates to a *strength* size effect.

However, the statistical strength size effect is not related to the lack of RVE existence, since the strength size effect is related to the peak of the stress-strain diagram whereas the RVE ceases to exist after the peak in the stress-strain diagram. On the other hand, the considered deterministic size effect has been derived in terms of *dissipated energy*, and it therefore concerns the entire stress-strain diagram. The issue of the RVE non-existence for softening materials is confirmed by the existence of a deterministic size effect. It should be realised, however, that this argument may not be inverted: absence of any size effect does not imply existence of an RVE.

5 Computational homogenisation

In this Chapter the main steps of the computational hierarchical multi-scale procedure (sf. Section 2.1.2) are presented. First of all the material is considered on the higher level (macro-level). Then in order to improve the accuracy of the response (in the regions of critical activity) the meso-level is analysed. Finally, the results from the meso-level are transferred back to the macro-level.

The meso-macro connection is used as a constitutive equation on the macro-level. Thus, instead of an explicit formulation of the stress-strain relation, data from the meso-level is considered. The main idea of the hierarchic multi-scale technique is as follows: the strain from the macro-level goes directly in the form of essential boundary conditions to the meso-level, where the material behaviour is simulated (assuming the material to be a heterogeneous continuum), after which the reaction forces to the essential boundary conditions are transformed by means of a homogenisation technique as stresses back to the macro-level. Schematically, the procedure is presented in figs. 5.1-5.2. In fig.5.1 a typical test is presented: the one-dimension bar with an imperfection is loaded in tension. In fig. 5.2 the block-scheme of the multi-scale procedure is shown, in which (1) corresponds to the *down-scaling* and transforms the macroscopic strain value into the displacement boundary condition at meso-level; (2) represents the *up-scaling* mechanism, through computational homogenisation.

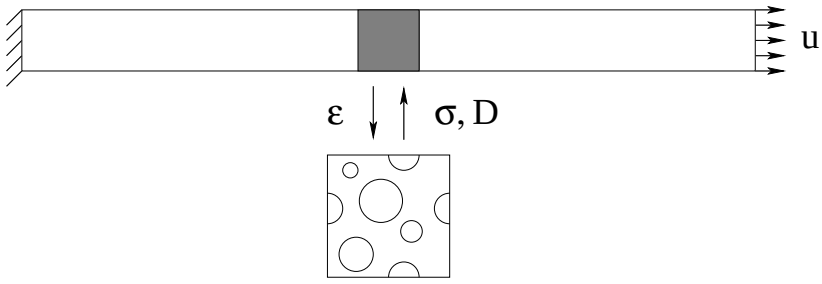

Figure 5.1: Multi-scale procedure. Tension bar

The sequential steps in the multi-scale scheme as mentioned in fig. 5.2 will be discussed in the following:

Macro-level: on the macro-level the material is assumed to have a homogeneous structure, so the constitutive response of the material are averaged. The mechanical loading

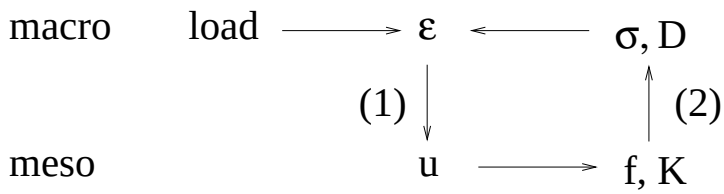

Figure 5.2: Multi-scale procedure: down-scaling(1) and up-scaling (2)

is applied at macro-level and it should be in equilibrium with the internal forces which are computed from the stresses, which are computed at meso-level.

Macro-meso connection: the idea of a macro-meso connection is, that after analysis of the structure at macro-level, in each integration point the meso-level is considered. The macroscopic strain field is translated into essential boundary conditions in terms of the vertex displacements of the meso-level cell in the following way:

$$u^{\mathrm{TR}} - u^{\mathrm{BL}} = \varepsilon^{\mathrm{M}}(x^{\mathrm{TR}} - x^{\mathrm{BL}}) \tag{5.1}$$

where indices TR and BL denote top and right versus bottom and left cell boundaries. The choice is dictated by the direction of the normal to the boundary vector in Cartesian coordinates with the origin in the centre of the meso-level unit cell. The traction boundary conditions reads now:

$$f^{\mathrm{TR}} = -f^{\mathrm{BL}} \tag{5.2}$$

Here the normal vector n has been used via $f_j = n_i\sigma_{ij}$, and the negative sign in the right-hand-side of eq. (5.2) follows from the fact that the normal vector is defined as outwards. Periodic boundary conditions, chosen here, imply that both eq. (5.1) and eq. (5.2) are satisfied.

The displacements of the four corner nodes can be presented as

$$u^1_{\mathrm{x}} = 0 \qquad u^1_{\mathrm{y}} = 0 \tag{5.3a}$$

$$u^2_{\mathrm{x}} = \varepsilon^{\mathrm{M}}_{\mathrm{xx}} L^{\mathrm{m}}_{\mathrm{x}} \qquad u^2_{\mathrm{y}} = \frac{1}{2}\gamma^{\mathrm{M}}_{\mathrm{xy}} L^{\mathrm{m}}_{\mathrm{x}} \tag{5.3b}$$

$$u^3_{\mathrm{x}} = \frac{1}{2}\gamma^{\mathrm{M}}_{\mathrm{xy}} L^{\mathrm{m}}_{\mathrm{x}} + \varepsilon^{\mathrm{M}}_{\mathrm{xx}} L^{\mathrm{m}}_{\mathrm{x}} \qquad u^3_{\mathrm{y}} = \frac{1}{2}\gamma^{\mathrm{M}}_{\mathrm{xy}} L^{\mathrm{m}}_{\mathrm{y}} + \varepsilon^{\mathrm{M}}_{\mathrm{yy}} L^{\mathrm{m}}_{\mathrm{y}} \tag{5.3c}$$

$$u^4_{\mathrm{x}} = \frac{1}{2}\gamma^{\mathrm{M}}_{\mathrm{xy}} L^{\mathrm{m}}_{\mathrm{y}} \qquad u^4_{\mathrm{y}} = \varepsilon^{\mathrm{M}}_{\mathrm{yy}} L^{\mathrm{m}}_{\mathrm{y}} \tag{5.3d}$$

where $\varepsilon^{\mathrm{M}}_{\mathrm{xx}}$, $\varepsilon^{\mathrm{M}}_{\mathrm{yy}}$ and $\gamma^{\mathrm{M}}_{\mathrm{xy}}$ are macro-level strain components, $L^{\mathrm{m}}_{\mathrm{x}}$ and $L^{\mathrm{m}}_{\mathrm{y}}$ are horizontal and vertical dimensions of the meso-level cell, u is the meso-level displacement with bottom indices showing the corresponding degree of freedom and top indices representing the

corner node number – here the numbering starts from the left bottom corner and goes anti-clockwise. Periodicity both of material and boundary conditions (cf. Section 4.2) is employed to link the displacements of opposite edges. As it has been shown in Section 4.2 abandoning either periodicity of material or periodicity of boundary conditions will lead to larger sizes of the meso-level, which can strongly influence the results of the multi-scale computation. Thus both material periodicity and periodicity of boundary conditions are used.

Meso-level: at meso-level a heterogeneous material is considered; here a three-phase material is investigated. The first phase consists of inclusions (stiff); the second phase is the matrix (less stiff) and the third phase is the interfacial transition zone between inclusions and matrix (least stiff zone). Each of these phases has its own properties (E – Young's modulus, ν – Poisson's ratio etc., cf. Chapter 4, tab. 4.2). The cracking mechanism in the meso-level is caused by mechanical loading only.

The formulation of the problem on the meso-level is set by the same boundary value problem as defined in section 4.1 with the same gradient-enhanced constitutive model (see Appendix A). The essential boundary conditions are given in (5.3) with the periodic boundary conditions linking both displacement components of opposite edges. Again, fracture at the meso-level can take place in the aggregate, in the cement paste or in the interfacial transition zone (ITZ).

Meso-macro connection: the stresses and tangent moduli at macro-level are computed from their associated quantities at meso-level. Thus, instead of an *explicit* formulation of the macro-level constitutive equation, information from the meso-level is used.

In order to keep the meso-macro relation consistent, bearing in mind the homogeneous description of the material at macro-level and heterogeneous material definition at meso-level, the procedure of homogenisation should be carried out.

The average value of stresses in the meso-level can be computed via (cf. Section 3.2)

$$< \sigma^{\mathrm{m}} > = \frac{1}{V_{\mathrm{m}}} \int_{\Omega} \sigma^{\mathrm{m}} dV \tag{5.4}$$

The average value of the stress in the meso-level $< \sigma^{\mathrm{m}} >$ is equal to the value of the stress in the macro-level σ^{M} in the considered integration point at macro-level (eq. 5.5):

$$\sigma^{\mathrm{M}} = < \sigma^{\mathrm{m}} > \tag{5.5}$$

In order to obtain the macro-level stiffness matrix the following steps are performed:

- the meso-level stiffness matrix is rewritten in the form of

$$\begin{bmatrix} K_{ff} & K_{fp} \\ K_{pf} & K_{pp} \end{bmatrix} \begin{bmatrix} \delta u_f \\ \delta u_p \end{bmatrix} = \begin{bmatrix} 0 \\ \delta f_p \end{bmatrix} \tag{5.6}$$

Here δu_p and δf_p correspond to the values of iterative displacements and residual forces of the *prescribed* nodes, respectively, i.e. the four corner nodes of the meso-level; δu_f consists of the iterative displacements of the *free* nodes (the rest of the nodes in the discretised meso-level). Furthermore, for a converged solution $\delta f_f = 0$.

- eq. (5.6) can then be rewritten as

$$K^{\mathrm{M}} \cdot \delta u_p = \delta f_p \tag{5.7}$$

where

$$K^{\mathrm{M}} = K_{pp} - K_{pf} K_{ff}^{-1} K_{fp} \tag{5.8}$$

- thus for the prescribed boundary nodes it can be written

$$\sum_j K_{ij}^{\mathrm{M}} \cdot \delta u_p^j = \delta f_p^i \tag{5.9}$$

with i and j being the corner node numbers

- then the expression for the stress can be presented as

$$\delta\sigma^{\mathrm{M}} = \frac{1}{V_{\mathrm{m}}} \sum_i \delta f_p^i \mathbf{x}^i = \frac{1}{V_{\mathrm{m}}} \sum_i \sum_j (K_{ij}^{\mathrm{M}} \cdot \delta u_p^j) \mathbf{x}^i \tag{5.10}$$

- bearing in mind that

$$\delta u_p^j = \mathbf{x}^j \cdot \delta\varepsilon^{\mathrm{M}} \tag{5.11}$$

- it is possible now to rewrite the stress in the form

$$\delta\sigma^{\mathrm{M}} = \frac{1}{V_{\mathrm{m}}} \sum_i \sum_j (K_{ij}^{\mathrm{M}} \cdot \mathbf{x}^j \cdot \delta\varepsilon^{\mathrm{M}}) \mathbf{x}^i = \frac{1}{V_{\mathrm{m}}} \sum_i \sum_j (\mathbf{x}^i K_{ij}^{\mathrm{M}} \mathbf{x}^j)^{\mathrm{C}} : \delta\varepsilon^{\mathrm{M}} \tag{5.12}$$

- Thus, the macro-level constitutive tangent stiffness D^{M} on the meso-level can be presented now as:

$$D^{\mathrm{M}} = \frac{1}{V_{\mathrm{m}}} \sum_i \sum_j \mathbf{x}^i K_{ij}^{\mathrm{M}} \mathbf{x}^j \tag{5.13}$$

note that here $\mathbf{x}^i = (x^i, y^i)$ is the position vector of node i.

With values of stresses and stiffnesses in each macro-level integration point the analysis of the macro-level is continued.

Note 14 *The values of the stress and stiffness following the above procedures are computed only after the meso-level finite element calculation is converged.*

Note 15 *The macroscopic stresses can be found from equations (5.4-5.5), or by translating the reaction forces to the prescribed displacements given in (5.3) in a similar way as K^M is translated into D^M.*

The key issue in this multi-scale procedure is the size of the meso-level. In Chapter 4 the question of the RVE size determination is analysed in detail. Once the size of the RVE is found the multi-scale procedure can be performed. Here, every meso cell size is considered to be an RVE unless mentioned otherwise.

Macrohomogeneity principle. The meso-macro transition should satisfy the macrohomogeneity condition, known also as the Hill-Mandel condition [46, 47, 55]. Following Hill's procedure the energy density

$$2U = \sigma_{ij}^{\mathrm{M}} \varepsilon_{ij}^{\mathrm{M}} \tag{5.14}$$

should then fulfill

$$\sigma_{ij}^{\mathrm{M}} \varepsilon_{ij}^{\mathrm{M}} = \frac{1}{V_{\mathrm{m}}} \int_{\Omega} \sigma_{ij}^{\mathrm{m}} \varepsilon_{ij}^{\mathrm{m}} \mathrm{d}V \tag{5.15}$$

In order to evaluate eq. (5.15), let us consider first the right-hand-side:

$$\frac{1}{V_{\mathrm{m}}} \int_{\Omega} \sigma_{ij}^{\mathrm{m}} \varepsilon_{ij}^{\mathrm{m}} \mathrm{d}V = \frac{1}{V_{\mathrm{m}}} \int_{\Omega} \sigma_{ij}^{\mathrm{m}} \nabla_i^s u_j \mathrm{d}V \tag{5.16}$$

Here the relation between strain and displacement has been used: $\varepsilon_{ij} = \nabla_i^s u_j$. It can be written that

$$\sigma_{ij}^{\mathrm{m}} \nabla_i^s u_j = \nabla_i^s (\sigma_{ij}^{\mathrm{m}} u_j) - (\nabla_i^s \sigma_{ij}^{\mathrm{m}}) u_j \tag{5.17}$$

where the second term on the right-hand-side vanishes as a result of the meso-level equilibrium. It is now possible to rewrite eq. (5.16)

$$\frac{1}{V_{\mathrm{m}}} \int_{\Omega} \sigma_{ij}^{\mathrm{m}} \nabla_i^s u_j \mathrm{d}V = \frac{1}{V_{\mathrm{m}}} \int_{\Omega} \nabla_i^s (\sigma_{ij}^{\mathrm{m}} u_j) \mathrm{d}V = \frac{1}{V_{\mathrm{m}}} \int_{\Gamma} f_j u_j \mathrm{d}S \tag{5.18}$$

Note, that the Gauss divergence theorem has been used as well as $f_j = n_i \sigma_{ij}$ As it has been mentioned above, periodic boundary conditions have been used (eqs. (5.1–5.2)). As such eq. (5.18) can be elaborated as

$$\begin{aligned}
&\frac{1}{V_{\mathrm{m}}} \int_{\Gamma} f_j u_j \mathrm{d}S = \frac{1}{V_{\mathrm{m}}} \int_{\Gamma^{TR}} f_j^{TR} u_j^{TR} \mathrm{d}S + \frac{1}{V_{\mathrm{m}}} \int_{\Gamma^{BL}} f_j^{BL} u_j^{BL} \mathrm{d}S = \\
&\frac{1}{V_{\mathrm{m}}} \int_{\Gamma} f_j^{TR} (u_j^{TR} - u_j^{BL}) \mathrm{d}S = \frac{1}{V_{\mathrm{m}}} \int_{\Gamma} f_j^{TR} (x_i^{TR} - x_i^{BL}) \mathrm{d}S \varepsilon_{ij}^{\mathrm{M}} = \\
&\frac{1}{V_{\mathrm{m}}} \int_{\Gamma} f_j x_i \mathrm{d}S \varepsilon_{ij}^{\mathrm{M}}
\end{aligned} \tag{5.19}$$

Considering eqs. (5.4) and (5.5)

$$\sigma_{ij}^{\mathrm{M}} = \frac{1}{V_{\mathrm{m}}} \int_{\Omega} \sigma_{ij}^{\mathrm{m}} \mathrm{d}V \tag{5.20}$$

and using the meso-level equilibrium condition $\nabla_k \sigma_{kj}^{\mathrm{m}} = 0$ and the equality to $\nabla_k^s x_i = \delta_{ki}$, it is possible to write

$$\sigma_{ij}^{\mathrm{m}} = (\nabla_k^s \sigma_{kj}^{\mathrm{m}}) x_i + \sigma_{kj}^{\mathrm{m}} (\nabla_k^s x_i) = \nabla_k^s (\sigma_{kj}^{\mathrm{m}} x_i) \tag{5.21}$$

Substitution of eq. (5.21) into eq. (5.20) and applying the Gauss divergence theorem leads to

$$\frac{1}{V_{\mathrm{m}}} \int_{\Omega} \sigma_{ij}^{\mathrm{m}} \mathrm{d}V = \frac{1}{V_{\mathrm{m}}} \int_{\Omega} \nabla_k^s (\sigma_{kj}^{\mathrm{m}} x_i) \mathrm{d}V = \frac{1}{V_{\mathrm{m}}} \int_{\Gamma} f_j x_i \mathrm{d}S = \frac{1}{V_{\mathrm{m}}} \int_{\Gamma} f_j x_i \mathrm{d}S \tag{5.22}$$

With derived relation (5.22), eq. (5.19) can now be elaborated as

$$\frac{1}{V_{\mathrm{m}}} \int_{\Gamma} f_j x_i \mathrm{d}S \varepsilon_{ij}^{\mathrm{M}} = \sigma_{ij}^{\mathrm{M}} \varepsilon_{ij}^{\mathrm{M}} \tag{5.23}$$

Thus the macrohomogeneity condition (5.15) is satisfied.

5.1 Local multi-scale modelling

In Chapter 3 analytical homogenisation techniques have been discussed. Here, computational homogenisation will be used. First, local multi-scale modelling will be treated. Here, by means of *local* modelling it will be assumed that only local values of strain, stress and stiffness are considered in the integration point at the macro-level. At the macro-level the material is assumed to be homogeneous. The mechanical loading is applied at the macro-level and it should be in equilibrium with the internal forces which are computed from the stresses at the meso-level.

5.1.1 Tension bar

As a representative example of the multi-scale procedure, a tension bar as shown in fig. 5.1 is analysed. On the macro-level, a one-dimensional bar with length $L = 600$ mm and cross-sectional area $A = 1$ mm^2 is considered (fig. 5.3). The material is considered to be homogeneous with an imperfection in the middle of the macro-structure (10% reduction in cross-section). The macro-level is discretised by means of linear one-dimensional elements with one integration point per element. Every macroscopic integration point of the discretised bar has an equivalent on the meso-level. On the meso-level, the material is considered to be heterogeneous: matrix with inclusions, surrounded by an interfacial transition zone. Each of these components has its own mechanical properties. Periodic

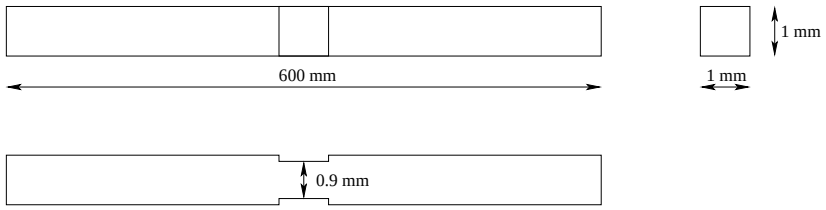

Figure 5.3: Macro-level

Materials components properties	Inclusions	Matrix	ITZ
Young's modulus E [MPa]	30000	25000	20000
Poisson's ratio ν [-]	0.2	0.2	0.2
Crack initiation strain κ_0 [-]	0.5	5.0e-06	3.0e-06
Length-scale parameter l [mm]	0.63	0.63	0.63
Residual stress level α [-]	0.999	0.999	0.999
Slope of softening β [-]	1500	1500	1500

Table 5.1: Material components properties at meso-level

boundary conditions together with material periodicity (see Chapter 4 for details) are used on the meso-level. At meso-level material parameters were chosen as presented in tab. 5.1. Again as in Chapter 4, crack initiation strain of the inclusions has been chosen artificially high in order to avoid the crack propagation through the inclusions and the length-scale parameters, for simplicity, have been chosen to be equal for all three phases. The example of the meso-level discretisation are presented in figs. 4.1, 4.2 and 4.3. The size of the meso-level elements have been chosen similar as in Chapter 4.

In order to be able to follow the solution into regimes of snap-back (when it appears) at macro-level[1] the arc-length control procedure, or more specifically, the indirect displacement control method (de Borst [22]) is employed.

Indirect displacement control

The indirect displacement control procedure can be presented as a sequence of the following steps:

1. Select two nodes m, n at the discretised macro-level on both sides of the imperfection. The constraint conditions then becomes

$$\Delta u_m - \Delta u_n = \Delta l \tag{5.24}$$

[1]Snap-back behaviour is expected because localisation of deformation in the meso-structure occurs. However, it is emphasized that in the analyses presented here snap-backs appear on the macro-level, not on the meso-level. Taking larger meso-level cells would lead to snap-back behaviour on the meso-level, but this leads to ambiguities in the homogenised stress-strain relation.

$$\mathrm{d}u_m - \mathrm{d}u_n = 0 \tag{5.25}$$

here Δu represents the incremental displacement, Δl is the user defined increment length along the load path and $\mathrm{d}u$ is the iteration correction of displacement.

FOR EACH LOADING STEP:

2. Split the displacement into two parts:

   a) first iteration

   $$\Delta u_1 = \Delta u_1^{\mathrm{I}} + \Delta\lambda_1 \Delta u_1^{\mathrm{II}}$$

   where

   $$\begin{aligned} \Delta u_1^{\mathrm{I}} &= (K_0^{\mathrm{M}})^{-1}(f_{\mathrm{ext}}^t - f_{\mathrm{int},0}) \equiv 0 \\ \Delta u_1^{\mathrm{II}} &= (K_0^{\mathrm{M}})^{-1} \hat{f}_{\mathrm{ext}} \end{aligned}$$

   as a result of the converged solution in the previous step $f_{\mathrm{ext}}^t = f_{\mathrm{int},0}$
   From the decomposition above it follows that

   $$\Delta\lambda_1 = \frac{\Delta l}{(\Delta u_1^{\mathrm{II}})_m - (\Delta u_1^{\mathrm{II}})_n} \tag{5.26}$$

   b) the subsequent iterations

   $$\mathrm{d}u_{j+1} = \mathrm{d}u_{j+1}^{\mathrm{I}} + \Delta\lambda_{j+1} \mathrm{d}u_{j+1}^{\mathrm{II}} \tag{5.27}$$

   where

   $$\begin{aligned} \mathrm{d}u_{j+1}^{\mathrm{I}} &= (K_j^{\mathrm{M}})^{-1}(f_{\mathrm{ext}}^t - f_{\mathrm{int},0}) \\ \mathrm{d}u_{j+1}^{\mathrm{II}} &= (K_j^{\mathrm{M}})^{-1} \hat{f}_{\mathrm{ext}} \end{aligned} \tag{5.28}$$

   From the decomposition above it follows that

   $$\Delta\lambda_{j+1} = \frac{(\mathrm{d}u_{j+1}^{\mathrm{I}})_m - (\mathrm{d}u_{j+1}^{\mathrm{I}})_n}{(\mathrm{d}u_{j+1}^{\mathrm{II}})_m - (\mathrm{d}u_{j+1}^{\mathrm{II}})_n} \tag{5.29}$$

3. Bring the two parts of the displacement back together

   $$\begin{aligned} \Delta u_1 &= \Delta\lambda_1 \Delta u_1^{\mathrm{II}} && \text{first iteration} \\ \mathrm{d}u_{j+1} &= \mathrm{d}u_{j+1}^{\mathrm{I}} + \Delta\lambda_{j+1} \mathrm{d}u_{j+1}^{\mathrm{II}} && \text{subsequent iterations} \end{aligned}$$

4. Then the macro-level displacement increment can be represented as

   $$\Delta u^{\mathrm{M}} = \begin{cases} \Delta u_1^{\mathrm{M}} & \text{first iteration} \\ \Delta u_j^{\mathrm{M}} + \mathrm{d}u_{j+1} & \text{subsequent iterations} \end{cases}$$

5. Macro-level strain increments for each integration point i can then be obtained: $\Delta\varepsilon^{\mathrm{M}}_{i,j+1} = \Delta\varepsilon^{\mathrm{M}}_{i,j+1}(\Delta u^{\mathrm{M}})$

6. Next, macroscopic total strains are translated into essential boundary conditions in terms of the vertex displacements of the meso-level cell: $\varepsilon^{\mathrm{M}}_{i,j+1} \rightarrow (u^p_k)^{\mathrm{m}}$; here $p = 1..4$ is the corner node number and $k = x, y$ is the degree of freedom (eq. (5.3)).

7. After solving the boundary value problem on the meso-level the homogenised values of stresses σ^{M} (eqs. (5.4-5.5)) and stiffnesses D^{M} (eq. (5.13)) are treated as macro-level stress $\sigma^{\mathrm{M}}_{i,j+1}$ and macro-level constitutive tangent stiffness $D^{\mathrm{M}}_{i,j+1}$.

8. The incremental force vector can be found as

$$f_{int,j+1} = \int_{\Omega} B^T \sigma^{\mathrm{M}}_{j+1} \mathrm{d}\Omega \tag{5.30}$$

9. The macro-level tangent stiffness matrix is computed as

$$K_{j+1} = \int_{\Omega} B^T D^{\mathrm{M}}_{j+1} B \mathrm{d}\Omega \tag{5.31}$$

10. Convergence check: if $\|\mathrm{d}u_{j+1}\| \leq \gamma \times \|\Delta u_1\|$, where γ is the prescribed tolerance, go to next loading step otherwise go to 2.

11. New load increment $\lambda_t = \lambda_t + \Delta\lambda_{j+1}$ and new external load is $f^t_{\mathrm{ext}} = \lambda_t \hat{f}^t_{\mathrm{ext}}$.

Note 16 *Arc-length control is not the only possible choice to control snap-back behaviour, Massart [64] has offered an alternative procedure, the idea of which is to introduce the non-local degree of freedom $\bar{\varepsilon}$ on the meso-level via the implicit gradient damage formulation and define the conjugate residual $f_{\bar{\varepsilon}}$. Adding the condition of $f_{\bar{\varepsilon}} = 0$, satisfying only upon macroscopic convergence, helps controlling the snap-back behaviour. Another possible procedure to control snap-back behaviour has been introduced by Gutiérrez [44]. The method is based on the energy released during failure. The idea of the approach, derived from the first principle of thermodynamics, is to introduce a new interpretation of the path following parameter. This parameter has to be related to a certain monotonically increasing variable, and as such dissipated energy satisfies this requirement in a natural way.*

As it has been done for the RVE size determination, the results of the multi-scale procedure are analysed in three regimes: linear-elasticity, hardening and softening. In all three of those regimes the issues of meso-level size dependence and macro-level mesh dependence are studied. Following the concept of the RVE, it is known, that with increasing size, the structural behaviour should not be affected. In other words, it should be verified whether the macroscopic response converges with increasing meso-level unit cell size. On the other hand, a proper reliable model should not be affected by changes

in finite element discretisation, i.e. the model should be mesh independent. These both issues have been studied in the framework of the multi-scale model. The response of the material is analysed in terms of the reaction forces on the macro-level for a given imposed displacement.

5.1.2 Influence of meso-level size and macro-level element size

The sensitivity of the results to the macro-level discretisation and meso-level size has been analysed.

Macro-level mesh dependence. The first issue to analyse is the macro-level mesh dependence. Four different meshes (tab. 5.2 [2]) have been used in order to discretise the macro-level. All macro-meshes have been combined with meso-level cell sizes of $10 \times 10\text{mm}^2$, $15 \times 15\text{mm}^2$, $20 \times 20\text{mm}^2$ and $25 \times 25\text{mm}^2$. Results of the multi-scale

MACRO M24	macro-level mesh 24 elements
MACRO M30	macro-level mesh 30 elements
MACRO M40	macro-level mesh 40 elements
MACRO M60	macro-level mesh 60 elements

Table 5.2: Macro-level meshes

procedure for different meshes on the macro-level are presented in fig. 5.4. Based on these results, the following observations can be made:

- in the **pre-peak** regime, according to fig. 5.4, the material does not show macro-level mesh sensitivity;
- on the contrary, in the **post-peak** or **softening** regime the material experiences mesh dependence: the brittleness is increasing with refining the mesh. Material even can exhibit a *snap-back* behaviour with increasing the number of elements: compare for example the macroscopic responses in cases of mesh M24 and mesh M60 in figs. 5.4–top-left. In figs. 5.4–top-right, bottom-left, bottom-right the snap-back behaviour is present for all macro-mesh densities and it is progressing with refining the mesh. Thus, in the softening regime the mechanical behaviour of the material is influenced by the discretisation scheme, irrespective of the meso-level cell size. The fact that the meso-level response is regularised by a length-scale parameter of the gradient damage model does not solve the problem.

Meso-level size dependence. In order to analyse meso-level size dependence, the sizes $10 \times 10\text{mm}^2$, $15 \times 15\text{mm}^2$, $20 \times 20\text{mm}^2$ and $25 \times 25\text{mm}^2$ (tab. 5.3) have been used for the meso-level. In combination, all four mesh densities MACRO M24 – MACRO M60 have been applied. The results are presented in fig. 5.5. The following observations can be made:

[2] Size of the imperfection on the macro-level scales with macro-element size.

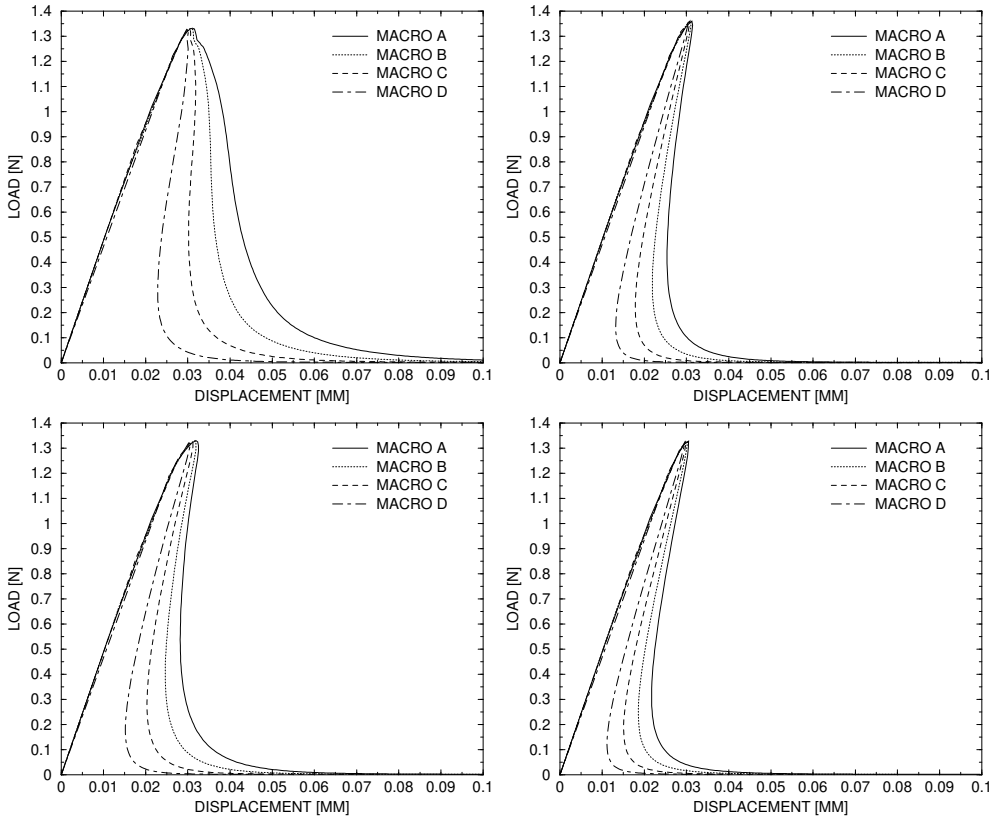

Figure 5.4: Macro-level mesh dependence (volume fraction of inclusions 45%); meso-level size 10 × 10mm^2 (top left), meso-level size 15 × 15mm^2 (top right), meso-level size 20 × 20mm^2 (bottom left), meso-level size 25 × 25mm^2 (bottom right).

MESO S10	meso-level size 10mm × 10mm
MESO S15	meso-level size 15mm × 15mm
MESO S20	meso-level size 20mm × 20mm
MESO S25	meso-level size 25mm × 25mm

Table 5.3: Meso-level sizes

- in the **pre-peak** regime the material is not sensitive to the changes in the meso-cell size.
- However, in the post-peak or **softening** regime increasing the size of the meso-

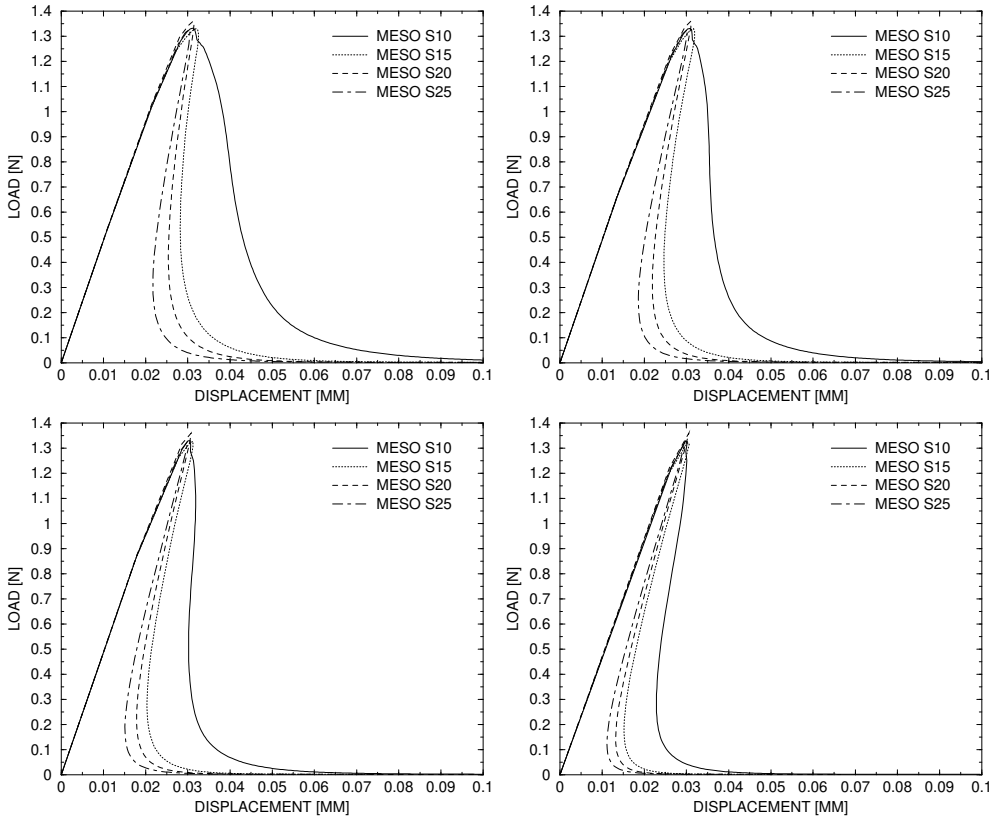

Figure 5.5: Meso-level size dependence (volume fraction of inclusions 45%); macro-level mesh M24 (top left), macro-level mesh M30 (top right), macro-level mesh M40 (bottom left), macro-level mesh M60 (bottom right).

level leads to a more brittle material behaviour. This holds for all macro-level mesh densities. The appearance (fig. 5.5-top) or increasing (fig. 5.5-bottom) of snap-back behaviour is again possible as a result of increasing the meso-level size. The big difference between MESO S10 and others (fig. 5.5) can be explained by the choice of the particular realisation. By increasing the size the difference between the realisations becomes smaller, however the average response still does not converge. A similar effect has been described in Chapter 4.

5.1.3 Discussion

In the pre-peak regime, material is not sensitive to changes in the macro-level mesh and meso-level size. On the contrary, in the softening regime the mechanical behaviour

of the material is highly influenced by the discretisation scheme and by the size of the meso-level. The results appear to be in a good agreement with the behaviour of the RVE analysed in Chapter 4: in linear elasticity and hardening the RVE size can be found and it has a unique lower bound, increasing the sample size would not lead to different results. Conversely, in material with localised deformations the unique size of the RVE cannot be found, thus increasing the sample size would lead to different results. Therefore the results from fig. 5.5 are in accordance with the results presented in Chapter 4.

However, one may argue, that if considering the finite mesostructural domain as such, then the size of this domain should play an intrinsic role, and the real physical response should be size dependent. Within the multi-scale approach, the meso-level size dependence should then be accounted for, as ideally the multi-scale response should converge to the unique mono-scale response (for example if considering the material using only the mesostructural description). This convergence is questionable if a non-unique response (the result of different meso-level size) is allowed. As such, a modification should be made within the multi-scale scheme. Moreover, since in softening the RVE does not exist, it is not appropriate to use this term and instead the meso-level cell is referred to as unit cell.

5.2 Non-local multi-scale modeling

In the previous Section, the local approach has been analysed: in each integration point of the macro-level the local strain is transferred into meso-level input, and in return the values of the homogenised meso-level stress and stiffness are transferred into a macro-level local stress and stiffness. Despite the fact that the underlying meso-structure of the material is taken into account, this local multi-scale approach suffers from both macro-level mesh dependence and meso-level size dependence. It is noted once again that the meso-level analyses are not mesh dependent because of the higher-order gradient model that is used. One of the ways to overcome these problems could be to introduce *nonlocality*[3] in the multi-scale model. Two major types of non-local models will be discussed here: an integral model and a differential formulation.

5.2.1 Integral and differential models: pro and contra

Initially introduced to include mesostructural effects and to solve the issue of the discretisation sensitivity, two non-local approaches can be distinguished:

- integral models (Bažant and Pijaudier-Cabot [15], Bažant [9], Bažant and Jirásek [12], Pijaudier-Cabot and Bažant [81], Pijaudier-Cabot [80]), where a non-local strain is introduced as

$$\bar{\varepsilon} = \frac{\int\limits_S \psi(s)\varepsilon(x+s)\mathrm{d}S}{\int\limits_S \psi(s)\mathrm{d}S} \tag{5.32}$$

[3]Here, the term nonlocality is used to specify the homogenisation technique (cf. Chapter 3), not to be confused with the non-local constitutive relation, used in Chapter 4 and beginning of Chapter 5.

in which $\psi(s)$ is the exponential weight function:

$$\psi(s) = \exp\left(-\frac{s^2}{2\ell^2}\right) \tag{5.33}$$

and ℓ is a length-scale parameter

- differential models, where higher-order gradients are included in the constitutive relation. This can be done directly in the stress-strain relation (Ru and Aifantis [85]) or in the nonlinear evolution laws of the state variables[4] (Peerlings [77], Simone [90]). This has inspired the development of numerical second-order homogenisation schemes (Kouznetsova [55], Kouznetsova et al. [53]), whereby not only the macroscopic strain but also its gradient is used to generate the meso-level boundary value problem. The conjugated variables are then the usual stress but also a higher-order stress, which are extracted from the meso-level together with the appropriate tangent stiffness tensors. The inclusion of strain gradients and higher-order stresses automatically results in the occurrence of a length-scale parameter in the macroscopic response, see also Chapter 3.

Not all of the various formats of the above models are suitable for implementation within a computational homogenisation scheme. For instance, a model should not employ both local strains and nonlocal strains within the same constitutive equation[5]. In Appendix C a typical example of each class is presented that could be implemented. The mechanical properties of these two types of models are studied by means of a dispersion analysis. It is found that the integral model is unstable and therefore should not be used. In contrast, the differential model is unconditionally stable.

It has been shown that the second-order homogenisation scheme is linked one-to-one to the differential model as mentioned above (Kouznetsova [55]). Indeed, the second-order homogenisation scheme overcomes dependence on the macro-level discretisation. However, this scheme suffers from two disadvantages:

- implementation of the second-order homogenisation scheme is considerably more involved than the first-order homogenisation. Apart from the additional strain gradient and the additional higher-order stress, also the higher-order equilibrium at the macro-scale should be accounted for.

- more importantly, the second-order homogenisation scheme does not solve the meso-level size dependence in case of softening response. Although the RVE ceases to exist in softening, the macroscopic length-scale in a second-order scheme is still proportional to the size of the meso-level sample, see eq. (3.17).

Obviously, a conceptually different approach is needed, which could resolve the macro-level discretisation sensitivity and the meso-level size dependency simultaneously.

[4] This type of modelling technique is used in the multi-scale framework of this thesis on the meso-level.
[5] See Appendix A for an explanation of this terminology.

5.2.2 Coupled–Volume approach: an alternative multi-scale scheme

As it has been shown the results of the local multi-scale technique are both macro-level mesh dependent and meso-level size dependent. One can try to overcome macro-level mesh dependency by exploiting non-local homogenisation techniques. Unfortunately, non-local multi-scale techniques as discussed in the previous paragraph seem not to provide a solution to both problems.

The present philosophy of the multi-scale material description has been formulated by Nemat-Nasser and Hori [73], who as the *scales separation principle* have offered the interaction between infinitesimal macro-material point and meso-material volume. However, once localisation occurs on the meso-level, the RVE for such a material can not be found (see Chapter 4). Thus the statistically representative meso- material volume does not exist any more; there is no longer a corresponding infinitesimal macro- material point; the *separation of scales* is no longer possible. In conclusion, the decoupling of a macro-level integration point and a meso-level volume is no longer admissible.

An alternative multi-scale model is introduced in this thesis. The main idea of this model and the main difference compared with the known multi-scale models is to abandon the idea that a finite meso-level cell size can be linked to an infinitely small macro-level material point. In contrast, the macro-level mesh and meso-level size are uniquely linked. This link, in terms of the given macro-level meshes and meso-level sizes, follows the rule that the macro-level element size *equals* the meso-level cell size. We introduce this approach as the *Coupled-Volume* approach. The attempt to connect model parameters and material parameters has already been made in Chapter 3, where the material length-scale has been found in terms of the model parameter RVE size (eq. 3.17). Here the connection is made between a model parameter (size of the meso-level) and a numerical parameter (size of the macro-level mesh element).

In the current formulation of the coupled-volume approach the one-dimensional case is studied[6]. However the approach can be extended to two- and three-dimensions. In fig. 5.6–top the two-dimensional case is presented. In the present case also only one integration point per element is allowed. In case when two or more integration points per element are used the formulation of the method changes and instead of element size on the macro-level the integration volume, i.e. the volume belonging to one integration point, is linked with the meso-level size. This situation is presented in fig. 5.6–middle. Here, attention should be given to the fact that the imperfection is concentrated only in one integration point. The coupled-volume approach can also be extended to the case of arbitrary shaped macro-level elements. The difficulty here would be in constructing the meso-level sample identical to the element on the macro-level (fig. 5.6–bottom). Once this is done, the assumption of periodicity of boundary conditions on the meso-level can not hold any longer. Instead of the periodic boundary conditions the essential boundary condition in the form of displacement on the meso-level can be used: $u_i^{\mathrm{m}} = \varepsilon^{\mathrm{M}} x_i$ where u_i^{m} is the displacement in the node i of the discretised meso-level. Note, that not only

[6] When comparing different meso-level sample sizes, the height of these samples will change. This change in height can be accounted for on the macro-level by adjusting the cross-sectional area that is used within the one-dimensional problem statement on the macro-level.

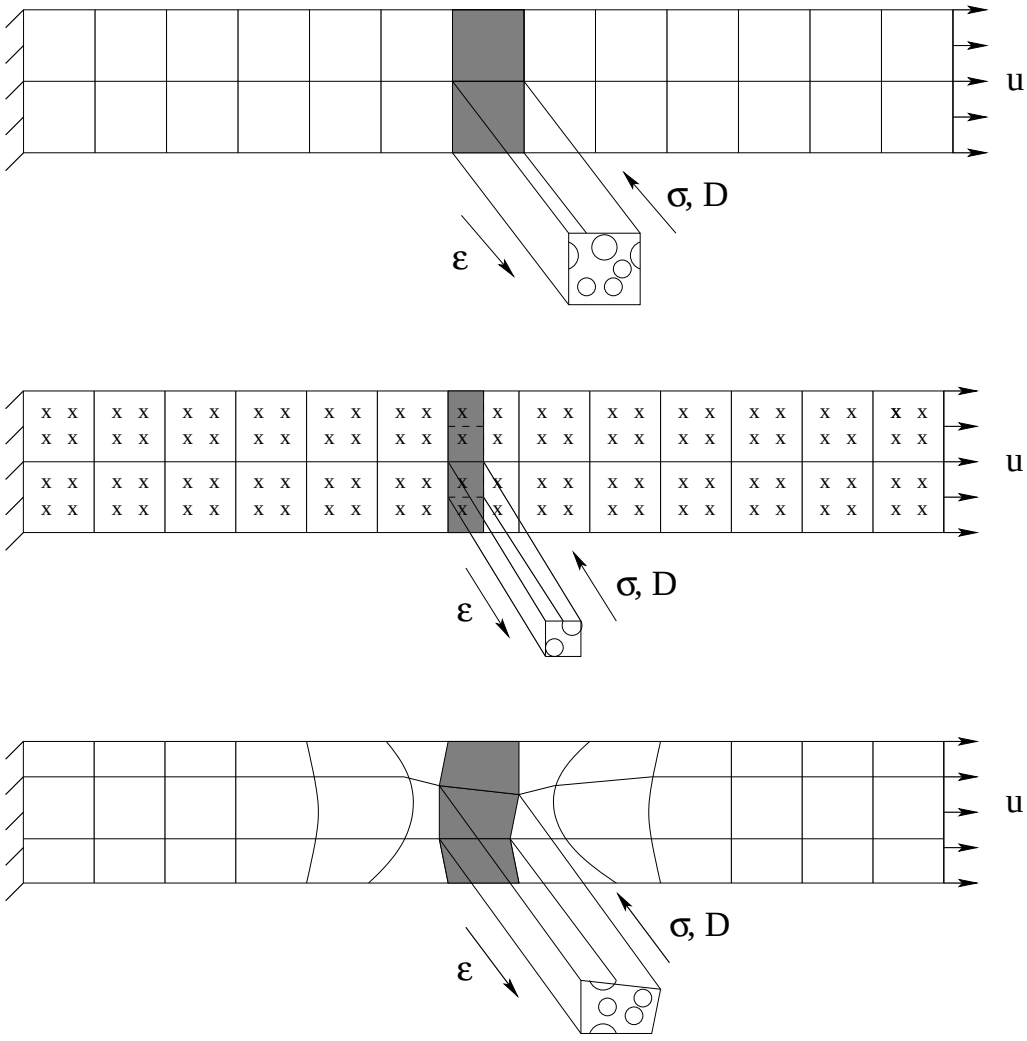

Figure 5.6: Coupled-volume multi-scale approach: two-dimensional case (top), more than one integration point per element (middle) and elements have arbitrary shape (bottom)

the corner node but all boundary nodes are taken into account, ε^{M} is the strain coming from the macro-level and x_i is the position of the node i.

Somewhat similar strategies of coupling meso (micro) and macro scales of observations have been independently reported by Markovic and Ibrahimbegovic [63] and Massart [64]. Both types of approaches are based on abandoning the separation of scales principle. In

their work Markovic and Ibrahimbegovic [63] have addressed the problem of coupling a *periodic* micro-structure with one or more (depending on the size of the micro unit cell) inclusions and the constant volume fraction of them within the cell. Displacement and traction (but not periodic) boundary conditions were applied on the micro-level. In their study the attention has been focused on elastic and elasto-plastic hardening regimes; as such no softening was included. Thus it is questionable whether the principle of separation of scales should be abandoned or not.

Periodic meso-structures have also been used in the work of Massart [64], although no variation of the size of the meso-level cell was studied. However, a methodology was proposed to investigate material response in case of softening. Periodic boundary conditions have been used in this work.

In contrast to the above works, in the present study random material has been used on the meso-level. Since randomly structured material is considered on the meso-level also the cases of different volume fractions of inclusions are investigated. As it will be discussed below, the statistical study of different meso-level sizes and its influence on the overall response is carried out. The coupled–volume approach is applicable for the case of softening, as will be demonstrated.

Coupled-volume approach versus fracture-energy-based approach

In this section the coupled-volume multi-scale approach is viewed in connection to the fracture-energy-based approach (Bažant and Oh [14], de Borst and Sluys [24]). The idea of the fracture-energy-based approach can be presented by means of the following characteristics:

- as a consequence of the local damage model, results in terms of stress-strain relation show sensitivity to the discretisation, i.e. mesh dependency – the finer the mesh the more brittle material behaves;

- by introducing a material parameter – the fracture energy i.e. the energy that is needed to create a unit area of a fully developed crack – as the area under the stress-displacement diagram, the softening modulus appears to be dependent on the size of the element;

- this brings the dependence of the constitutive behaviour on the element size: the smaller the element size the less brittle the material is

- as a conclusion the two above effects compensate each other, and the fracture energy model is mesh-objective in terms of dissipated energy.

Similar effects can be observed in the coupled-volume approach:

- on one hand, while considering different discretisations on the macro-level, keeping sizes of the meso-level constant, the effect of macro-level mesh dependency can be observed: the finer the mesh, the more brittle the macro-level response;

- on the other hand, while keeping the discretisation on the macro-level constant and changing the size of the meso-level the meso-level size dependence is obtained: the smaller the meso-level size the less brittle the macro-level response becomes; this meso-level size dependency can be understood as the constitutive behaviour of the material;
- as a consequence, by linking the size of the macro-level elements to the size of the meso-level, the macro-level element size influence (macro-level mesh dependence) is balanced by different constitutive behaviour coming from different sizes of the meso-level (meso-level size dependence). The macro-level response shows neither macro-level mesh dependency nor meso-level size dependency.

In order to analyse the coupled-volume approach, the academical example has been performed where the one-dimensional bar with an imperfection on the macro-level has been considered (as mentioned in Section 5.1.1). On the meso-level, however, instead of complicated three-phase material, a simplified meso-structure has been used: the material has been described as homogeneous with an imperfection to initiate the crack. Note, that later in this section also the multi-phase material will be discussed. The results of

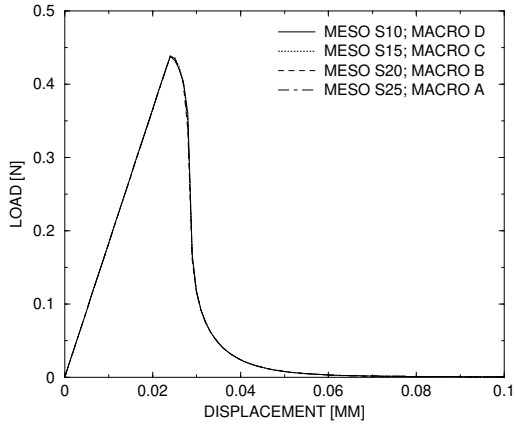

Figure 5.7: Coupled-volume multi-scale approach: academic example with homogeneous material

this coupled-volume multi-scale procedure for the academic homogeneous material are presented in fig. 5.7. Based on the unique response of the material on the macro-level (fig. 5.7) the conclusion can be made about the results being macro-level mesh insensitive and at the same time meso-level size independent.

Meso-level length-scale parameter

The coupled-volume approach is based on abandoning the separation of scales principle and linking a model parameter (size of the meso-level) to a numerical parameter (size of

the macro-level mesh element). The next step would be to estimate this model parameter and connect it with some material parameter. The only *material length scale* parameter remaining in the framework of the coupled-volume approach is the meso-level length-scale parameter – the parameter representing the information from the micro-level and responsible for the width of the fracture-process zone on the meso-level.

The influence of this meso-level length-scale parameter on the results of the multi-scale computations has been studied. The same one-dimensional bar as in the previous Section has been analysed. Different length-scale parameters were chosen for the analysis: starting from $\ell = 0.5$ mm, $\ell = 1.0$ mm, $\ell = 2.0$ mm, $\ell = 4.0$ mm and $\ell = 10.0$ mm, and the same macro-level meshes and meso-level size as in Section 5.1 were used (cf. tabs. 5.2–5.3). The results are presented in fig. 5.8. As it can be seen in fig. 5.8, with the growth of the meso-level length-scale parameter the results are losing uniqueness: the response remains insensitive to macro-level mesh and meso-level size only for small values of the length-scale parameter ($\ell = 0.5$mm and $\ell = 1$mm). Next (fig. 5.8–centre left), $\ell = 2$mm is a transition value. In the first stage of the post-peak behaviour the mesh-dependence is observed since the width of the fracture-process zone extends over the meso-size, however later on deformation localises further and mesh-objectivity is again found. This trend is even more pronounced for larger length-scales. Thus, starting from the smallest value $\ell = 0.5$mm the length-scale parameter is growing and eventually reaching and even exceeding the size of the tested sample size on the meso-level. However, bearing in mind that the meso-level length-scale carries the information from the micro-level and represents the fracture-process zone on the meso-level, it is obvious that the meso-level sample size should be considerably larger than the length-scale parameter in order to produce insensitive and reliable results on the macro-level. This last expression together with evidence in fig. 5.8 allows to make an estimation of the minimum size of the meso-level and consequently of the minimum mesh size on the macro-level. Both depend on the meso-level length-scale[7] as

$$L^{\mathrm{M}} > 10\ell \tag{5.34}$$

Here, L^{M} represents the macro-level mesh size[8]. Once the size of the macro-level mesh (and the corresponding meso-level sample size) is verified according to the meso-level length scale, the coupled-volume multi-scale procedure is fully defined.

[7] In this academical example the one-phase material has been considered on the meso-level, resulting in only one meso-level length-scale parameter. Though in the case of three- (or more)phase material each phase can actually have its own length-scale. However for simplicity in the framework of this study the length-scales of all three phases have been taken similar. The influence of different length-scales and the question of choosing the dominant one needs further investigation.

[8] Generally speaking, L^{M}, as it could be shown based on the procedure introduced in Chapter 4, should also be dependent on the volume fraction of inclusions, once the multi-phase material is considered. However for this academical case of one-phase material the relation 5.34 is enough. The relation of L^{M} and the volume fraction of inclusions of the multi-phase material is the subject for future research.

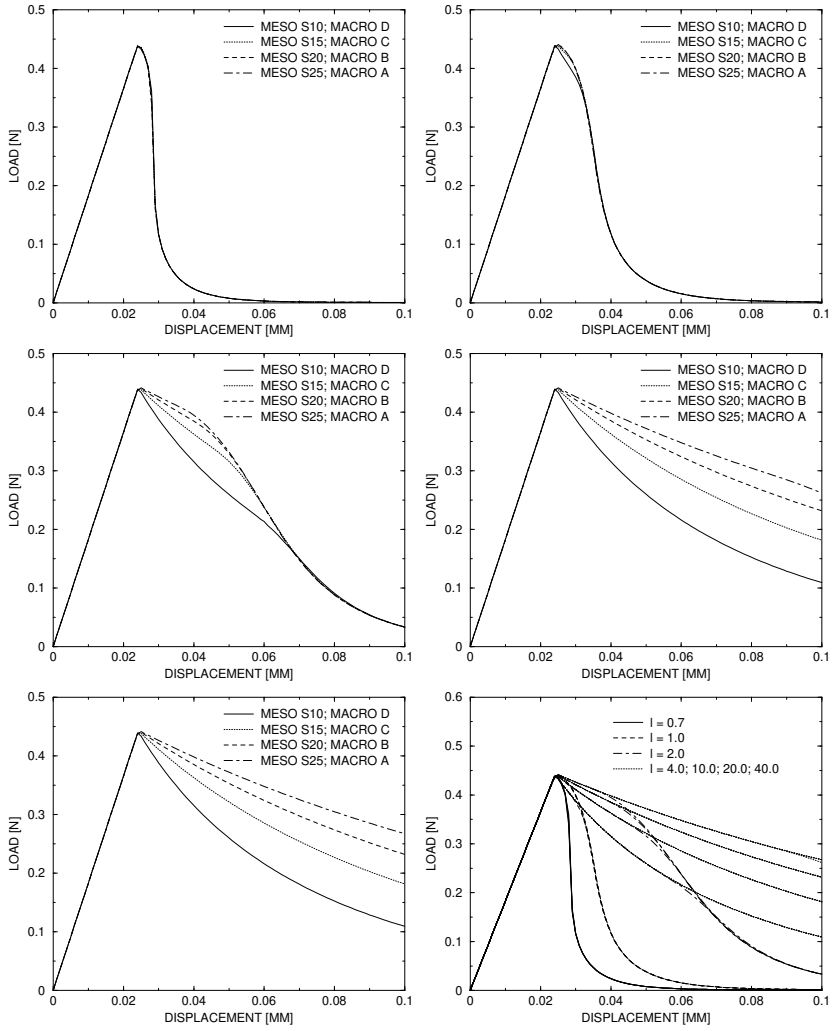

Figure 5.8: Meso-level length-scale parameter influence on the coupled-volume approach: $\ell = 0.5$ mm (top left), $\ell = 1.0$ mm (top right), $\ell = 2.0$ mm (centre left), $\ell = 4.0$ mm (centre right), $\ell = 10.0$ mm (bottom left), all ℓ (bottom right)

Multi-phase meso-structure

The results of the coupled-volume multi-scale framework for three-phase material (similar material as the one described in Chapter 4) on the meso-level with different volume fractions of inclusions are presented in figs. 5.9, 5.10 and 5.11. Again it can be seen, that both macro-level mesh sensitivity and meso-level size sensitivity are solved simulta-

neously. The difference in load-displacement diagrams, appearing in figs. 5.9, 5.10 and

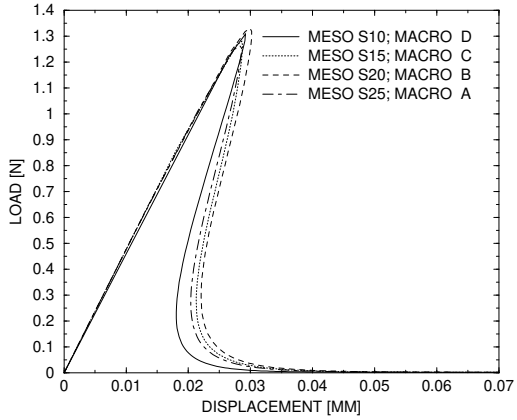

Figure 5.9: Coupled-volume multi-scale approach: volume fraction of inclusions 30%

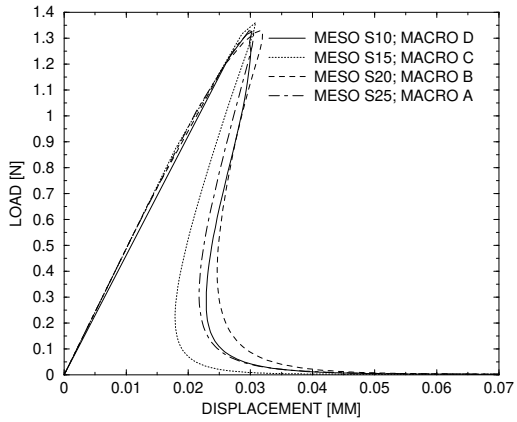

Figure 5.10: Coupled-volume multi-scale approach: volume fraction of inclusions 45%

5.11 can be explained by the statistical effects: the locations of inclusions in different meso-level samples are responsible for this small deviation of results. However, it has been shown in fig. 4.9 (Section 4.2) that with increasing the size of the unit cell the deviation of the results is decreasing. Thus, the conclusion can be made that the macro-level response sensitivity to the particular meso-level realisation will decrease with increasing the size of the meso-level. This last statement has been verified on the basis of the statistical analysis of the coupled-volume multi-scale results. A similar statistical analysis as

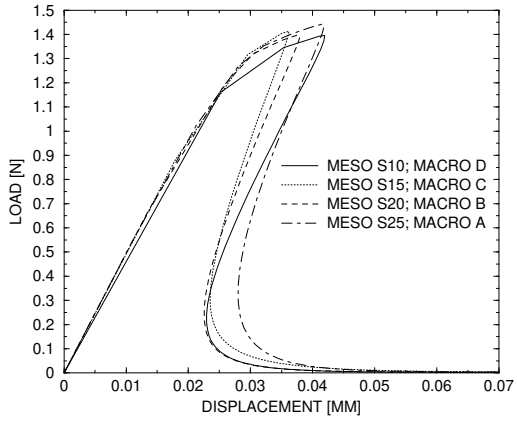

Figure 5.11: Coupled-volume multi-scale approach: volume fraction of inclusions 60%

presented in Section 4.2 has been used. Five different realisation of the meso-level unit cells for each meso-level size have been considered. Corresponding macro-level responses have been obtained in terms of dissipated energy. Then the statistical analysis based on the mathematical expectation and standard deviation has been performed. The result is presented in fig. 5.12. It can be seen from fig. 5.12, that with increasing the size of the

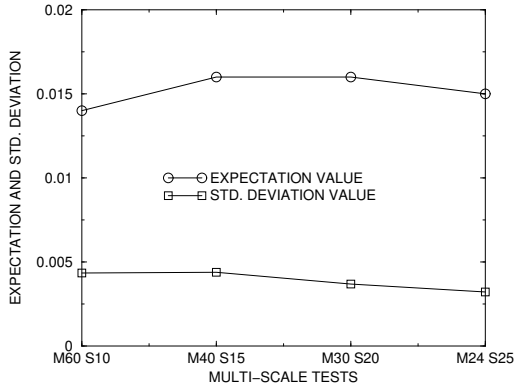

Figure 5.12: Expectation and standard deviation values of the dissipated energy for different coupled-volume multi-scale analysis ($\rho = 30\%$)

meso-level (i.e. increasing the size of the macro-level element) the mathematical expectation of the dissipated energy remains relatively constant. Also the value of the standard deviation is virtually the same for all tests. Thus, no conclusion can be drawn from the statistical point of view on what should be the size of the macro-level element size and

the corresponding meso-level cell size. In order to select macro-level element size and meso-level cell size, one should consider eq. 5.34. Furthermore, snap-back behaviour may occur on the meso-level in case the meso-level cell size is too large. Since snap-back on the meso-level implies that a macro-level strain cannot be uniquely related to a macro-level stress, the use of too large meso-level cells should be avoided. As such the **upper-bound** on the meso-level unit cell size and the conjugate macro-level mesh size can be found:

$$L^{\mathrm{m}} < \min L^{\mathrm{m}}_{\mathrm{sb}} \tag{5.35}$$

Here, L^{m} is the size of the meso-level unit cell and the conjugate macro-level element; and $\min L^{\mathrm{m}}_{\mathrm{sb}}$ represents the *smallest* meso-level unit cell that can exhibit snap-back behaviour.

Note 17 *Within the coupled-volume approach the issue of snap-back on the meso-level is treated as the possible condition on the meso-level size (and corresponding macro-level element size) as it is not desirable and may cause non-uniqueness in the relations between the macro-level strain and the macro-level stress. Other known multi-scale approaches may deal with the snap-back questions differently: for example Massart [64] offered a more complex multi-scale procedure, which allows the snap-back behaviour on the meso-level without the loss of the uniqueness.*

Note 18 *The results in figs. 5.9–5.11 have been generated by using one value for the length-scale, namely $\ell = 0.63$ mm. In the discussion of fig. 5.8 it was established that the macro-level ductility is set by the length-scale present on the meso-level. Thus, the ductility of the results in figs. 5.9–5.11 can be manipulated by varying the mesoscopic length-scale.*

The detailed analysis of the material evolution for the chosen macro-level mesh "MACRO M40" and meso-level size "MESO S15" with volume fraction of inclusion $\rho = 45\%$ is described below.

Overall remarks. Figs. 5.13–5.18 are built in the following way:

- several (6) steps are presented in these figures, corresponding to different loading regimes: figs. 5.13–5.15 corresponds to the pre-peak regimes, figs. 5.16–5.18 to the post-peak or softening behaviour; it should be emphasized, that the pre-peak non-linear response is a natural outcome of the coupled-volume multi-scale modelling technique; the pre-peak nonlinear response is also observed in experiments;
- on the top of all figures the global macro-level response in the form of load-displacement curve is presented;
- the meso-level behaviour is analysed for the elements outside the imperfection (fig. 5.13–5.18–left) and inside the imperfection (fig. 5.13–5.18–right), thus two sets of figures are needed. *Note, that the global macro-level response is similar for both sets*;

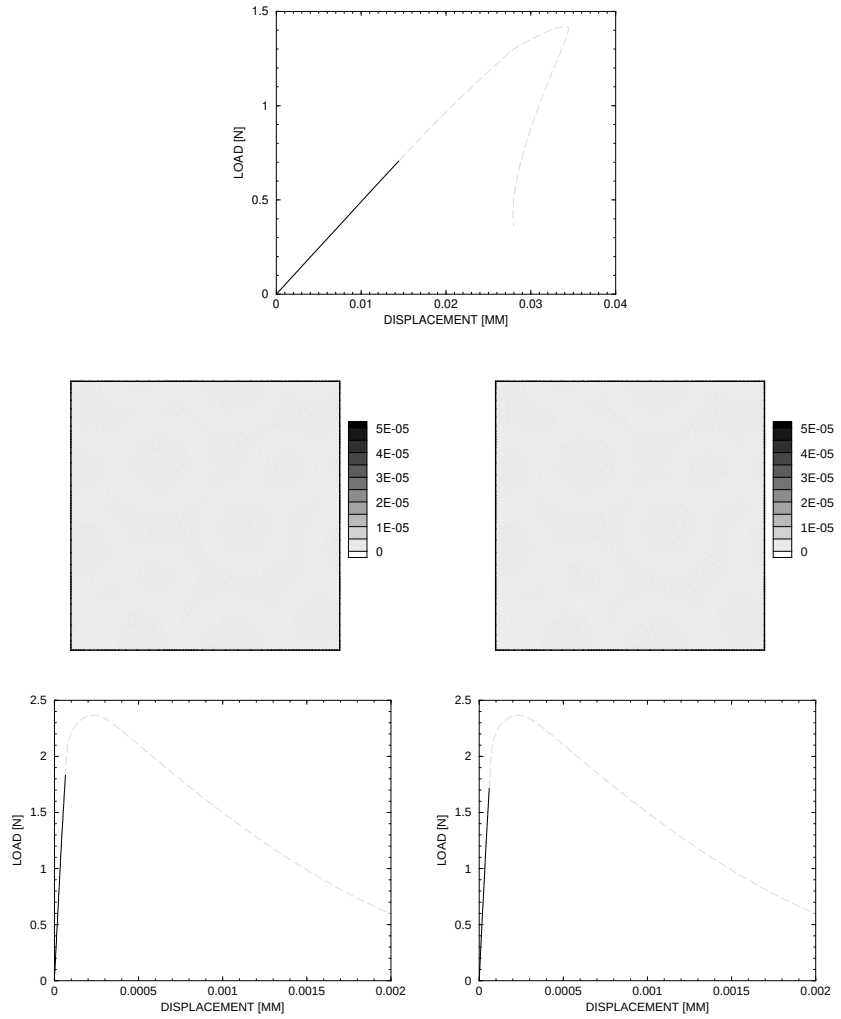

Figure 5.13: Multi-scale evolution. Top to bottom: macro-level response in the form of load-displacement curve, meso-level contour and the load-displacement curve of the element outside the imperfection (left) and inside the imperfection (right) in the linear-elastic regime.

- the meso-level responses are represented by means of the contour plots of equivalent strains as defined in eq. A.3 (the middle picture) and the load-displacement curves (the bottom picture).

Thus, analysing all figures correspondingly the following observations can be made:

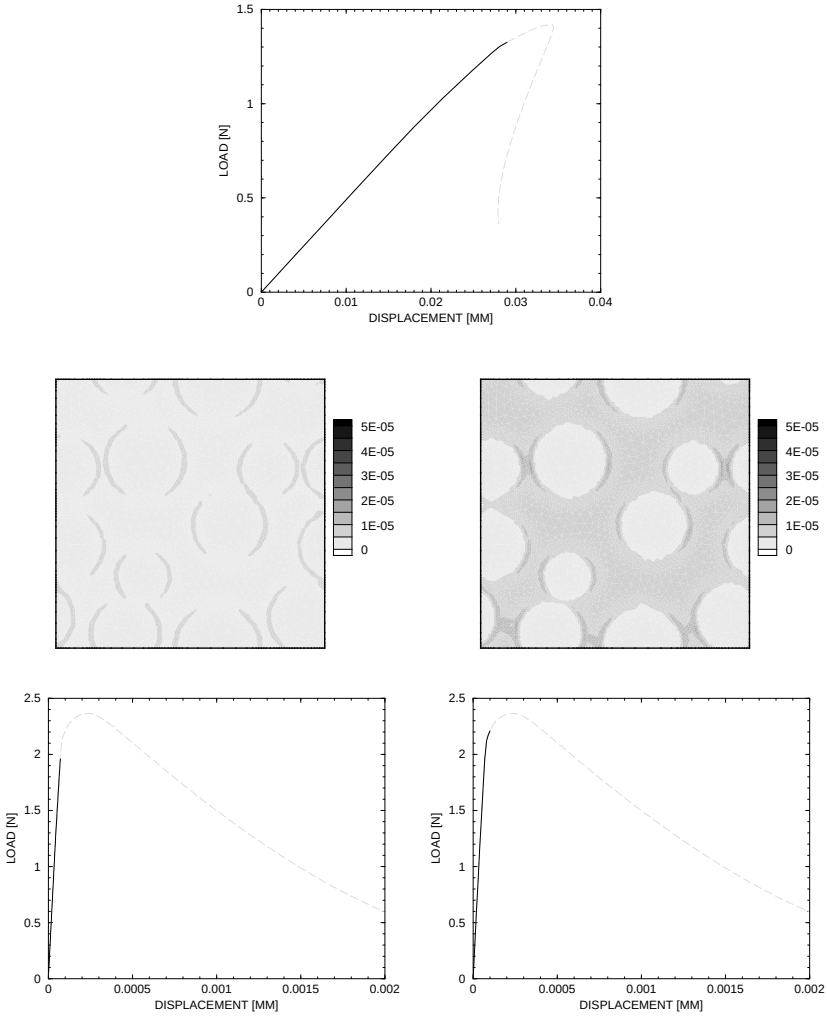

Figure 5.14: Multi-scale evolution. Top to bottom: macro-level response in the form of load-displacement curve, meso-level contour and the load-displacement curve of the element outside the imperfection (left) and inside the imperfection (right) in nonlinear pre-peak regime.

Pre-peak regime. It can be seen on the top picture of fig. 5.13 that the macro-level is in the linear-elastic regime. Corresponding to this macro-linear-elastic point, two meso-level elements outside (lower parts of fig. 5.13–left) and inside the imperfection zone (lower parts of fig. 5.13–right) also experience linear elastic behaviour. For both outside and inside meso-level elements contour plots (the middle pictures in figs. 5.13–left and 5.13–

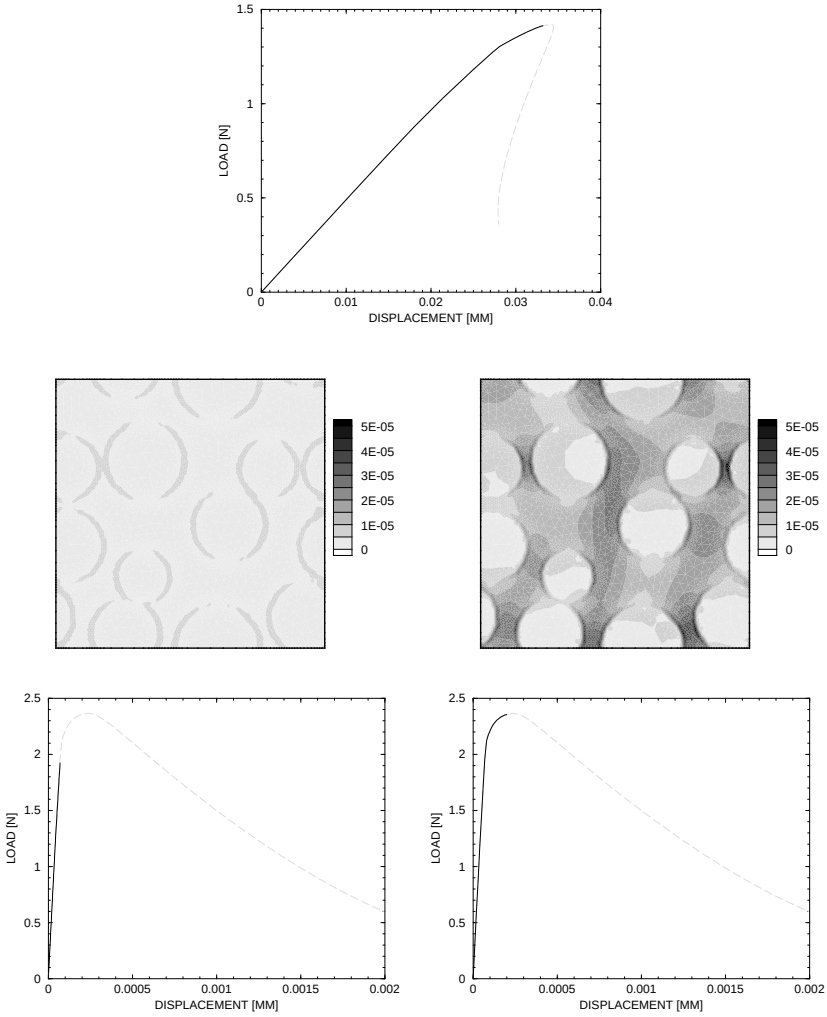

Figure 5.15: Multi-scale evolution. Top to bottom: macro-level response in the form of load-displacement curve, meso-level contour and the load-displacement curve of the element without localisation (left) and with localisation (right) at the peak.

right) look more or less similar, the small difference is dictated only by the different width of the corresponding macro-level elements: the width of the imperfection is 0.9 times the width of the rest of the bar. This difference in the macro-level element width influences the value of the strain field in the particular macro integration points: the strains in the element with imperfection are somewhat higher than in the element without imperfection.

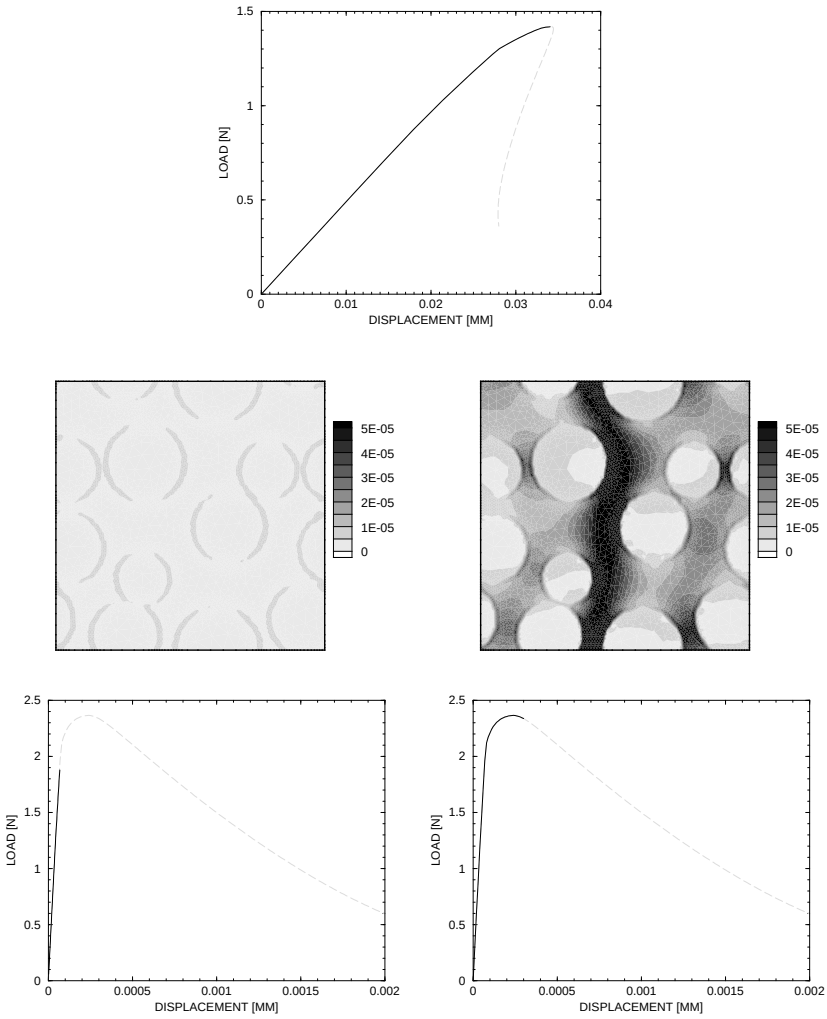

Figure 5.16: Multi-scale evolution. Top to bottom: macro-level response in the form of load-displacement curve, meso-level contour and the load-displacement curve of the element without localisation (left) and with localisation (right) in the post-peak regime.

And this difference in the strain field, in turn, slightly changes the boundary condition on the meso-level. This slight difference is also noticeable in the load-displacement curves (the bottom pictures in figs. 5.13–left and 5.13–right). Nevertheless, both outside the imperfection and inside the imperfection meso-level elements are still in the linear-elastic regime. All three components of the meso-level heterogeneous material are linear elastic.

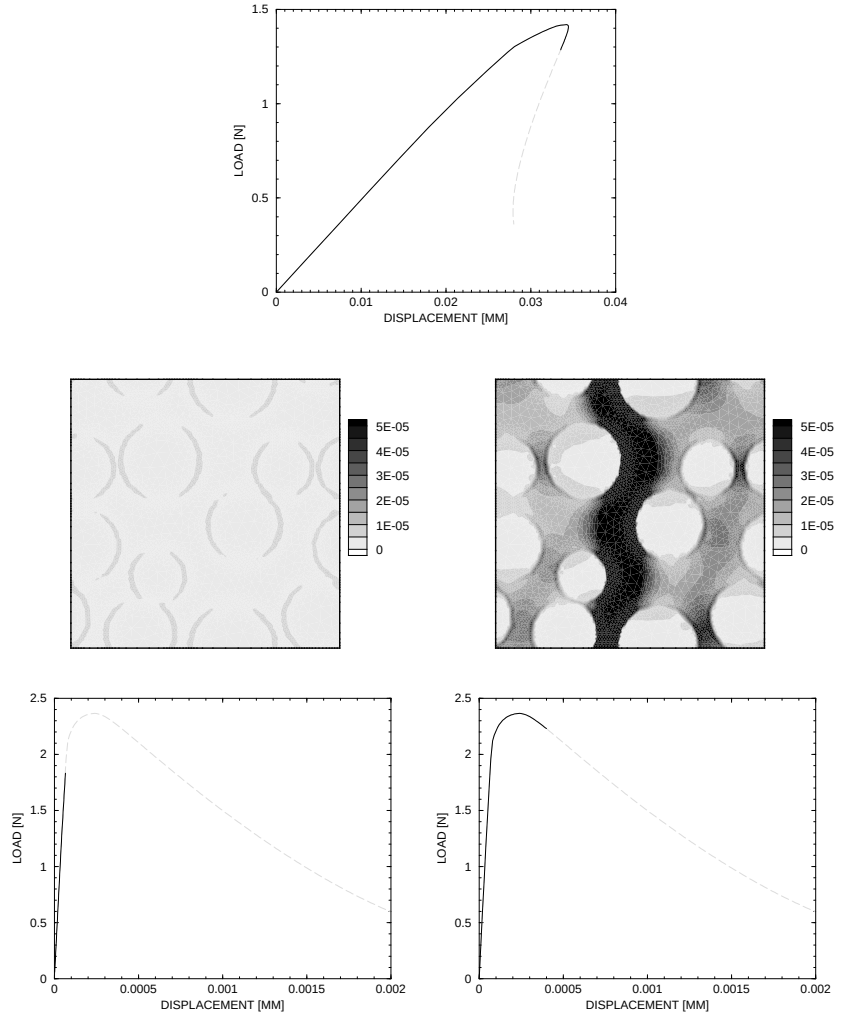

Figure 5.17: Multi-scale evolution. Top to bottom: macro-level response in the form of load-displacement curve, meso-level contour and the load-displacement curve of the element with localisation (left) and with localisation (right) in the softening regime close to the peak.

The picture changes in fig. 5.14. Here, as it can be seen from the load-displacement curve of the macro-level response (top of the figures), the macro-level starts experiencing the initiation of damage. The difference in the corresponding meso-level elements is larger. Now the equivalent strain in the interfacial transition zones of both inside and outside the imperfection has exceeded the critical value and started to soften causing the pre-

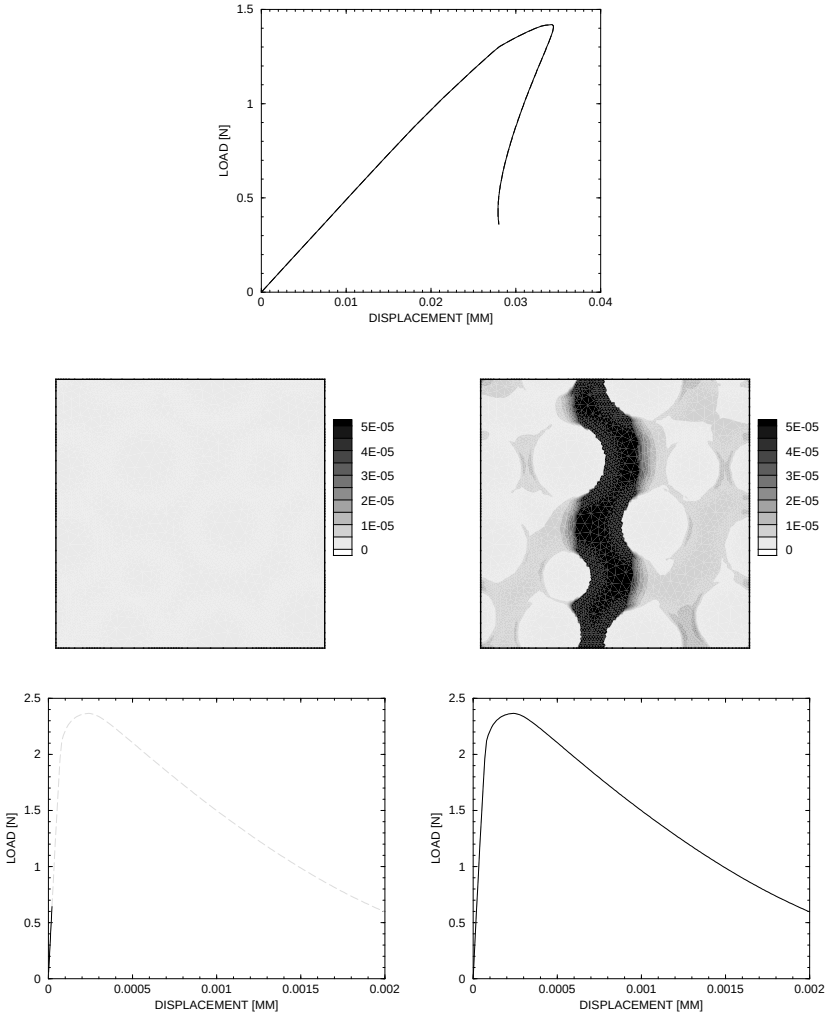

Figure 5.18: Multi-scale evolution. Top to bottom: macro-level response in the form of load-displacement curve, meso-level contour and the load-displacement curve of the element with localisation (left) and with localisation (right) in the fully damaged regime.

peak damage on the global meso response (the bottom pictures in figs. 5.14–left and 5.14–right): more on the meso-element inside imperfection and less on the outside meso-element. Still no localisation can be seen in the contour plots (the middle pictures in figs. 5.14–left and 5.14–right).

As the macro-level response approaches to the peak (the top of fig. 5.15), the meso-

level response starts being qualitatively different for inside and outside the imperfection elements. The pre-peak regime can be characterised by the first indication of the dominant crack in the meso-element inside the imperfection (the middle of fig. 5.15–right), the global meso-level load-displacement response shows *just before the peak* behaviour (the bottom of fig. 5.15–right). The meso-element outside the imperfection is still in the loading process and it is still in the ascending branch (the middle / bottom of fig. 5.15–left).

Post-peak regime. Starting from this point the meso-element outside the imperfection is in unloading regime (the middle / bottom of fig. 5.16–left). The meso-element inside the imperfection shows the localised region – the dominant crack has appeared (the middle of fig. 5.16–right) and the load-displacement curve is in softening regime (the bottom of fig. 5.16–right). As a result of this meso-level localisation, macro-level load-displacement curve has gone to the *just after the peak* region (the top of fig. 5.16).

The evolution of the material behaviour after localisation of deformation in the meso cell has occurred is presented in figs. 5.17-5.18. The softening regime close to the peak (fig. 5.17) and softening regime far from the peak (fig.5.18) have a similar character: the meso-element inside the imperfection has a clear localisation zone or dominant crack, and the material surrounding the localisation zone is experiencing unloading behaviour. This unloading behaviour further develops (it can be seen on the middle / bottom figs. 5.17–right) and eventually the fully damaged meso-level element is occurring (the middle of fig. 5.18–right): here, the crack has deep black color and the surrounding material is slightly grey. The meso-element outside the imperfection also experiencing the unloading regime (figs. 5.17-5.18–left).

6 Conclusions

The overall goal of this contribution was to introduce an objective model to describe, explain and predict the behaviour of a material with a composite structure subjected to mechanical loading in pre- and post-peak regimes.

Several different ways are available in order to describe the behaviour of a composite material. *Macrostructural modelling approaches* capture the influence of the underlying levels of observation by means of additional, phenomenological constitutive parameters. On the other hand, *mesostructural modelling approaches* provide a detailed description of the material at the lowest level of observation that is of interest. In spite of advantages, both of these approaches have critical disadvantages: it is not always possible to define or even estimate (or measure experimentally) phenomenological properties within a macrostructural approach and in a mesostructural approach problems with CPU time/memory could arise. As an alternative, it has been chosen to introduce the *multi-scale approach*, which would retain all advantages of the two parent methods and avoid disadvantages. In this thesis a multi-scale model was introduced with the macro-level described as homogeneous material and the meso-level as heterogeneous material.

In the framework of analytically derived multi-scale models two homogenisation schemes have been compared in terms of appearance of macroscopic length-scale and time-scale. It was found that in a local homogenisation scheme no macroscopic length-scale or time scale are introduced. On the other hand, in a non-local homogenisation scheme a length-scale (in statics and dynamics) and a time scale (in dynamics only) do appear. They are connected to higher-order spatial gradients and higher-order inertia terms, respectively. Moreover, the length-scale and the time-scale are one-to-one related to the size of the mesoscopic unit cell, which is supposed to be a Representative Volume Element. For softening applications it is well-known that a macroscopic length-scale parameter is required in order to obtain objective results. Thus, the second-order homogenisation technique seems to be preferable in case of softening.

Within the framework of this thesis, the Representative Volume concept, widely used in mechanics, has been given a closer look in two directions: first of all the question of an RVE overall existence has been elaborated, and, where proven to exist, the RVE size has been determined. Pre-peak and post-peak regimes of mechanical loading have been considered. Based on the statistical analysis the conclusions have been made about an RVE existence in these regimes. It appeared that RVE can be found in the pre-peak regime, but once in the post-peak (softening), material loses the "representative" properties, in other words an RVE cannot be found. This is not a striking conclusion since material in softening leads to highly localised strain patterns. A piece of material with strain localisation loses statistical homogeneity, whereas an RVE can be found only for statistically homogeneous materials. On the contrary, material in the pre-peak regime is statistically homogeneous, thus an RVE can be found there. Supporting the conclusion

of an RVE non-existence in the softening regime, the size effect theory shows a strong deterministic size effect in that the size of the strain localisation zone does not scale with the cell size, therefore the dissipated energy depends strongly on the cell size.

Next, attention has been given to RVE size determination. The case of linear elasticity has been considered. A procedure, based on the analysis of the variation coefficient has been presented in order to determine an RVE size.

Two different types of parameters influencing an RVE size have been investigated: parameters related to geometry and boundary conditions and material parameters. Several test parameters were chosen such as loading scheme (tension versus shear), periodicity versus non-periodicity (both boundary conditions and wall-effect issues) and criterion of interest (stiffness-based RVE versus stress-based RVE).

- The results showed that for the periodic material (no wall-effect) with periodic boundary conditions there is no significant sensitivity of the RVE size to the loading scheme.

- Regarding material periodicity (no wall-effect), the following observations have been made. In case of a tension test, it is desirable but not essential to have material without wall-effect. Conversely, in case of a shear test, the absence of wall-effects is essential in order to describe the material behaviour realistically. As for periodic boundary conditions, the results show that for a tension test the periodicity of boundary conditions is the more dominant condition: the RVE in case of non-periodic boundary conditions is much larger than the RVE for the same material with periodic boundary conditions. On the contrary, RVE sizes for material with and without wall-effect are relatively similar. Comparing shear test results, the conclusion can be made, that the material periodicity is the dominant condition compared to periodic boundary conditions.

- The RVE size sensitivity to the parameter of interest such as the homogenised stiffness and the average stress, has been analysed. It has been shown that taking any of these two parameters does not lead to a significant change in the RVE size.

- Material parameters have also been analysed with respect to their influence on the RVE size. The results show a strong dependence of the RVE size on the material properties such as changing stiffness ratio. The sensitivity of the RVE size to the volume fraction of inclusions supports this. For the case of a stochastic volume fraction of inclusions, RVEs have been computed for different values of the volume fraction of inclusions. In order to estimate the stability of the RVE sizes and analyse the RVE size dependence on the certain stochastic characteristics, the DH–stability concept has been employed. By means of DH–stability, it has been shown that for a DH-stable RVE, a small change in the stochastic initial data should not lead to a large change of the RVE size.

An overall conclusion can be made, that an RVE size does not depend on the parameters related to the geometry and boundary conditions, once the periodicity issues have been taken care of. On the contrary, the RVE size strongly depends on the materials

parameters. These conclusions are also valid in the nonlinear pre-peak regime, i.e. the hardening stage. However, the statistical analysis shows for a chosen accuracy, that the RVE size in the hardening stage is much larger than the RVE size in linear-elasticity.

Once the question of an RVE size determination has been worked out, both analytical and computational homogenisation schemes can be performed. The attention in the last part of this contribution has been given to the computational homogenisation technique in the framework of the multi-scale model. As an example, the behaviour of one-dimensional bar with an imperfection has been analysed. The meso-level has been described as a three-phase material with stiff inclusions, embedded in a softer matrix and surrounded by an interfacial transition zone. The global response has been analysed with respect to macro-level discretisation parameter (macro-level mesh dependence) and a meso-level model parameter (meso-level size dependence).

Following the logic used while analysing the analytical approach, a distinction between local and non-local numerical schemes has been made. The local multi-scale model has been analysed first. Again pre- and post-peak regimes were considered. In the pre-peak regime the macro-level response shows no signs of macro-level mesh dependency nor meso-level size dependency. This last observation supports the conclusion obtained earlier that an RVE exists in this regime. On the contrary, in the post-peak regime the results show strong macro-level mesh and meso-level size dependency, which in turn supports the conclusion of an RVE non-existence in this regime. No "representative" size can be found, thus with increasing the size the material behaves differently – this explains meso-level size dependency of the multi-scale results.

The dependency of the multi-scale results on the macro-level mesh size can be overcome by introducing a non-local multi-scale scheme, for example a gradient enhanced framework such as the second-order homogenisation scheme. Unfortunately, this type of models also have disadvantages. Firstly, the implementation is relatively complicated. Secondly and more importantly, the dependence on the meso-level sample size is not resolved.

A multi-scale model is desired that can describe the behaviour of a material with a composite structure based on the computational homogenisation but being independent on the macro-level mesh and meso-level size. Such a model has been introduced in the framework of non-local multi-scale as the *coupled-volume* approach. The key idea is that the size of the meso-level sample should be identical to the size of the macro-level integration volume that is associated with this meso-level sample. This unique link of macro-level mesh size and meso-level sample size abandons the concept of separation of scales, which was present in the local model and previous non-local models. Since this approach does not relay upon the existence of an RVE, it can also be used in softening. With the coupled-volume approach results can be obtained that do not depend on the macro-level mesh size nor the meso-level sample size. Thus the conclusion can be drawn that the coupled-volume multi-scale model is an objective tool to describe the behaviour of the composite material.

Future perspectives

Although in this thesis contributions have been made with regards to homogenisation schemes and length-/time-scales, the existence and size determination of RVEs, and a novel multi-scale framework to analyse composite materials, some interesting and rather important issues have been left aside.

Firstly, the existence and size determination of RVEs should be tested in a wider variety of loading cases. In this thesis, the concept of an RVE has been analysed in the case of static loading (Chapter 4). Questions that remain include (*i*) *does* RVE exist in dynamic loading, and if positive, then (*ii*) *how* will it behave in the case of dynamic loading? Not less important is the issue of the RVE concept in the case of a porous medium with water content. The physical importance of this question arises once analysing the composite material with porous structure under the mechanical loading in humid surroundings.

The multi-scale procedure presented in this thesis has only been tested in a one-dimensional application. However, as it has been mentioned in Chapter 5, the extension of the procedure to two- and three-dimensions is possible. The implementation and analysis of the procedure in case of two- and three-dimensional formulation can be another direction of the future research, which includes the case of arbitrary shaped macro-elements and, as a consequence, in the coupled-volume approach also leads to arbitrary shaped meso-level unit cells.

While considering a multi-phase material, several length-scale parameters, different for each material component, are to be expected. In the present contribution, the same unique value of the parameter has been chosen for all material phases. Possible future research would be to analyse how the difference in length-scale parameters for different material components influences the result and which material component has the most influential length-scale.

A Damage models

In this appendix, the damage theory is presented starting from the local damage model and following by the short overview of non-local integral and differential models.

A.1 Local damage model

An elasticity based damage model can be represented via the constitutive relation

$$\sigma = (1-\omega)D^e : \varepsilon \tag{A.1}$$

with D^e an isotropic elastic stiffness matrix and ω a scalar parameter describing the amount of damage which the material has experienced: $\omega = 0$ and $\omega = 1$ correspond to virgin, undamaged material and completely damaged material, respectively. The damage grow is controlled by the damage loading function

$$f(\tilde{\varepsilon}, \kappa) = \tilde{\varepsilon} - \kappa \tag{A.2}$$

Here κ is a history-dependent parameter and $\tilde{\varepsilon}$ is a local equivalent strain following, here, Mazars criterion[1]

$$\tilde{\varepsilon} = \sqrt{\sum_{i=1}^{3} (< \varepsilon_i >)^2} \tag{A.3}$$

with ε_i the principle strains and $< \varepsilon_i >= \varepsilon_i$ if $\varepsilon > 0$ and $< \varepsilon_i >= 0$ otherwise. The damage history of the material is described by the history-dependent parameter κ which is by definition increasing during the loading with non-negative rate. The damage grows is possible if $\dot{\kappa} > 0$. The evolution of this parameter follows the Kuhn-Tucker conditions:

$$\dot{\kappa} \geq 0, \qquad f(\tilde{\varepsilon}, \kappa) \leq 0, \qquad \dot{\kappa} f(\tilde{\varepsilon}, \kappa) = 0. \tag{A.4}$$

The damage parameter ω is described as a function of the history-dependent parameter κ: $\omega = \omega(\kappa)$. The exponential softening law is employed here as an evolution law:

$$\omega = \begin{cases} 0 & \text{if} \quad \kappa < \kappa_0 \\ 1 - \frac{\kappa_0}{\kappa}\left(1 - \alpha + \alpha \exp\left(-\beta(\kappa - \kappa_0)\right)\right) & \text{if} \quad \kappa \geq \kappa_0 \end{cases} \tag{A.5}$$

model parameters α and β represent the residual stress level and the slope of the softening curverepresent respectively.

[1] The Mazars criterion is often employed for the description of granular media of which the behaviour in tension is different from that in compression. As the description of heterogeneous material (also such as a concrete) is the goal of this contribution, the Mazars criterion seems to be a reasonable choice. However other applications may be better represented by the elastic energy criterion: $\tilde{\varepsilon} = \frac{1}{2}\varepsilon^T D^e \varepsilon$.

A.2 Non-local damage model

The Nonlocal damage model was introduced by Bažant and Pijaudier-Cabot [15], Bažant [9], Bažant and Jirásek [12], Pijaudier-Cabot and Bažant [81], Pijaudier-Cabot [80]. The model describes the growth of the damage no longer as a function of the local equivalent strain $\tilde{\varepsilon}$, but as a function of the equivalent strain average over the RVE, surrounding each point in the material.

The loading function and the damage evolution law are then replaced by

$$f(\bar{\varepsilon}, \kappa) = \bar{\varepsilon} - \kappa \tag{A.6}$$

and

$$\dot{\omega} = g(\omega, \bar{\varepsilon})\dot{\tilde{\varepsilon}} \tag{A.7}$$

The averaged strain, or so-called, non-local strain now reads

$$\bar{\varepsilon} = \frac{1}{V_r(x)} \int_{\tilde{\Omega}} \Psi(x - s)\tilde{\varepsilon}(s) \, \mathrm{d}V \tag{A.8}$$

where $\Psi(x - s)$ is the weight function

$$\Psi(x - s) = \Psi_0 \exp\left(-\frac{\|x - s\|^2}{2l_c^2}\right) \tag{A.9}$$

l is the internal length of the non local continuum, related to the scale of the microstructure, and Ψ_0 is a normalising factor such, that for infinite body

$$V_r(x) = \int_{\tilde{\Omega}} \Psi(x - s) \, \mathrm{d}V = 1 \tag{A.10}$$

Note, that l

1. represents the lower scale of observation;
2. regularises mathematical model;
3. avoids mesh dependency;
4. its functioning is connected to the length scale parameter ℓ from the eq. (3.17).

A.3 Gradient damage model

The integral representation of the non-local equivalent strain, given in eq. A.8, can be rewritten in terms of gradients. This can be done by expanding $\tilde{\varepsilon}$ into a Taylor series

(Peerlings [77]):

$$\begin{aligned}\tilde{\varepsilon}(s) = \tilde{\varepsilon}(x) \quad &+ \quad \frac{\partial \tilde{\varepsilon}}{\partial x_i}(s_i - x_i) + \frac{1}{2!}\frac{\partial^2 \tilde{\varepsilon}}{\partial x_i \partial x_j}(s_i - x_i)(s_j - x_j) \\ &+ \quad \frac{1}{3!}\frac{\partial^3 \tilde{\varepsilon}}{\partial x_i \partial x_j \partial x_k}(s_i - x_i)(s_j - x_j)(s_k - x_k) \\ &+ \quad \frac{1}{4!}\frac{\partial^4 \tilde{\varepsilon}}{\partial x_i \partial x_j \partial x_k \partial x_l}(s_i - x_i)(s_j - x_j)(s_k - x_k)(s_l - x_l) + ...\end{aligned} \tag{A.11}$$

After the substitution of this relation into the eq. A.8, the non-local equivalent strain expression reads

$$\bar{\varepsilon}(x) = \tilde{\varepsilon}(x) + c_i \frac{\partial^2 \tilde{\varepsilon}}{\partial x_i^2} + c_{ij} \frac{\partial^4 \tilde{\varepsilon}}{\partial x_i^2 \partial x_j^2} + ... \tag{A.12}$$

with

$$c_i = \frac{1}{2! V_r} \int_{\tilde{\Omega}} \Psi(x - s)(s_i - x_i)^2 \, \mathrm{d}V \tag{A.13}$$

and

$$c_{ij} = \frac{1}{4! V_r} \int_{\tilde{\Omega}} \Psi(x - s)(s_i - x_i)^2 (s_j - x_j)^2 \, \mathrm{d}V. \tag{A.14}$$

Neglecting the fourth and higher order terms and keeping in mind that for the case of isotropy of the weight function all coefficients c_i (where $i = 1..3$) are equal, thus the index i can be dropped. Eq. (A.8) can now be rewritten as

$$\bar{\varepsilon} = \tilde{\varepsilon} + c\nabla^2 \tilde{\varepsilon} \tag{A.15}$$

here the dependence on the coordinates x has been dropped for brevity. The coefficient c represents here the internal length scale of the non-local model, it has the dimension of length squared: for example for the Gaussian weight function (Peerlings [77]) $c = \frac{1}{2} l^2$.

An alternative gradient formulation can be derived from eq. (A.12). After differentiating it twice, then premultiplying the result by c, subtracting the obtained expression from eq. (A.12) and neglecting the fourth-order term, the resulting relation reads

$$\bar{\varepsilon} - c\nabla^2 \bar{\varepsilon} = \tilde{\varepsilon} \tag{A.16}$$

This last expression is called an implicit gradient damage formulation on the contrary to explicit formulation, given in eq. (A.15).

In this contribution the non-local model, based on implicit gradient damage formulation, introduced as an additional second-order partial differential equation in terms of non-local strain $\bar{\varepsilon}$ is employed.

Non-local boundary conditions Higher-order models require the introduction of additional boundary conditions. In order to obtained a unique solution, the value of $\bar{\varepsilon}$, its normal derivative, or a linear combination of them should be specified on the boundary. The natural boundary condition, according to Peerlings [77] is the best choice:

$$\frac{\partial \bar{\varepsilon}}{\partial n} \equiv n_i \frac{\partial \bar{\varepsilon}}{\partial x_i} = 0 \tag{A.17}$$

Adopting this boundary condition, the non-local $\bar{\varepsilon}$ is equal to the local $\tilde{\varepsilon}$ on the boundary and as it follows, the gradient approximation is then consistent with the non-local expression (A.5).

B Forward and Inverse problems of DH–stability

In some applications not only the question arises whether the process is stochastically stable or not, sometimes it is needed to find out under which conditions a stochastic process *is* DH-stable. Thus, it makes sense to make a devision on the forward and inverse problems.

As it follows from the definition of DH-stability, there are four values which make impacts on whether the solution is stochastically stable or not, i.e. two confidence levels (P^* and P^{**}) and two numbers (ε and δ) corresponding to maximal possible deviation of solution and initial data from some fixed given values. This, in turn, brings us to the division of the inverse problem on several different types.

Forward problem All four values (P^*, P^{**}, ε and δ)are given and it is needed to find whether the solution is stochastically stable or not. It is possible to solve this problem directly following the definition of the DH-stability.

Inverse problems For the inverse problem, there can be distinguish four types of inverse problems. All four of them will be formulated here.

- **Type 1** For DH-stable system, define the confidence level of the solution P^* with the given maximal possible deviation ε of the solution from the exact value, for the given maximal possible deviation δ of the initial data from the given value, with the confidence level of the initial data P^{**}.

- **Type 2** For DH-stable system, define the maximal possible deviation ε of the solution from the exact value with the confidence level of the solution P^*, for the given maximal possible deviation δ of the initial data from the given value, with the confidence level of the initial data P^{**}.

- **Type 3** For DH-stable system, define the confidence level of the initial data P^{**} with the given maximal possible deviation δ of the initial data from the given value, for given maximal possible deviation ε of the solution from the exact value, with the confidence level of the solution P^*.

- **Type 4** For DH-stable system, define the maximal possible deviation δ of the initial data from the given value with the confidence level of the initial data P^{**}, for given maximal possible deviation ε of the solution from the exact value, with the confidence level of the solution P^*.

In order to find a solution for any of above problems one could use standard Monte-Carlo method.

Note 19 *As it was already mentioned, in all above problems initial data (namely initial conditions, boundary conditions, right-hand-side etc.) could have different maximal possible deviations δ_i and different confidence levels P_i^{**} for $i = 1..N$ where N is the number of initial data. Thus it yields N problems of types 3 and 4.*

Schematically, all information above could be summarized in the table B.1: here "+"

Type		DH-st.	P^*	ε	P_1^{**}	P_2^{**}	δ_1	δ_2
Forward	F	**?**	+	+	+	+	+	+
Inverse	I.T.1	+	**?**	+	+	+	+	+
	I.T.2	+	+	**?**	+	+	+	+
	I.T.3.a	+	+	+	**?**	+	+	+
	I.T.3.b	+	+	+	+	**?**	+	+
	I.T.4.a	+	+	+	+	+	**?**	+
	I.T.4.b	+	+	+	+	+	+	**?**

Table B.1: Formulation Scheme

refers to the given data, and "?" is data to be found.

Obviously, the table above can grow in both directions, if one considers more than two initial data.

C Dispersion analysis

Dispersion analysis is a simple yet insightful method to verify the stability, wave propagation characteristics and localisation properties of a material model. A dispersion analysis is carried out in a sequence of steps:

1. Introduce the equation of motion, which for the one-dimensional case reads

$$\varrho \ddot{u} = \frac{\partial \sigma}{\partial x} \tag{C.1}$$

where ϱ is the mass density.

2. Insert the constitutive relation of the model. In this thesis, physical nonlinearities are taken into account. However, on the macroscopic level no material model is explicitly defined. In order to incorporate a dissipation mechanism, a damage framework is assumed. The damage ω does not appear explicitly on the macro-level but is merely a representation of the nonlinear processes that occur on the meso-level. The constitutive relation then reads

$$\sigma = (1 - \omega) E \varepsilon \tag{C.2}$$

3. The damage parameter ranges from $\omega = 0$, corresponding to the intact material, to $\omega = 1.0$ representing the complete failure of the material. The loading function describes the evolution of damage: $f(\varepsilon_{\text{eq}}) = \varepsilon_{\text{eq}} - \kappa(\varepsilon_{\text{eq}})$ where the equivalent strain is chosen according to the Mazars positive principle strain formulation, see also Appendix A. Assuming the growth of damage, i.e. $f = 0, \dot{\kappa} \geq 0$ and bearing in mind the assumption of a one-dimensional tension test the following can be stated: $\varepsilon_{\text{eq}} = \kappa = \varepsilon$. As both pre-peak and post-peak behaviour are of interest, the damage evolution function has been chosen as (fig. C.1):

$$\omega = \frac{\varepsilon}{\kappa_u} \tag{C.3}$$

where κ_u is the critical strain level, corresponding to the completely damaged material. The resulting stress-strain relation is plotted in fig. C.1. From eq. (C.3), the constitutive equation is elaborated as

$$\sigma = \left(1 - \frac{\varepsilon}{\kappa_u}\right) E \varepsilon \tag{C.4}$$

therefore

$$\frac{\partial \sigma}{\partial \varepsilon} = \left(1 - \frac{2\varepsilon}{\kappa_u}\right) E \tag{C.5}$$

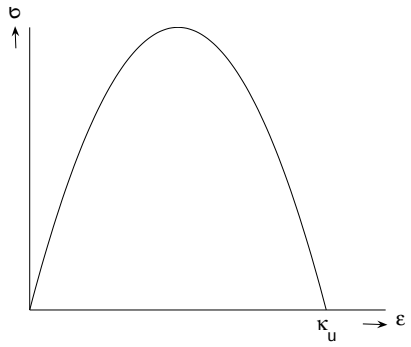

Figure C.1: Quadratic stress-strain relation

by which it is found that the peak is attained for $\omega = \dfrac{\varepsilon}{\kappa_u} = \dfrac{1}{2}$. Thus, the transition to the softening regime occurs when $\omega = 0.5$.

4. Substitute the constitutive equation (C.2) together with the damage evolution law (C.3) into the equation of motion (C.1).

5. Apply a harmonic perturbation on the displacement in the form of

$$\delta u = \hat{u} \exp(\mathrm{i} n(x - ct)) \tag{C.6}$$

where $\hat{u}$ is the amplitude, n is the wave number and c is the phase velocity of the wave.

6. Elaborate eq. (C.1) accordingly and present the result in the form of

$$\frac{c^2}{c_e^2} = g(\omega, n, ..) \tag{C.7}$$

Here the elastic bar velocity is $c_e = \sqrt{E/\varrho}$ and $g(\omega, n, ..)$ is a function depending on the model under consideration. Based on eq. (C.7) the conclusion can be made on the stability of the treated non-local model. In particular, the occurence of imaginary phase velocities could under certain conditions indicate the loss of stability.

C.1 Integral model

The first class of non-local model to be analysed in this Section is integral non-local models. The distinctive property of these models is the representation of the non-local

strain in the integral form. The non-local strain $\bar{\varepsilon}$ is written in the integral form as (Pijaudier-Cabot [80], Pijaudier-Cabot and Bažant [81])

$$\bar{\varepsilon} = \frac{\int\limits_S \psi(s)\varepsilon(x+s)\mathrm{d}S}{\int\limits_S \psi(s)\mathrm{d}S} \tag{C.8}$$

where $\psi(s)$ is the exponential weight function:

$$\psi(s) = \exp\left(-\frac{s^2}{2\ell^2}\right) \tag{C.9}$$

and ℓ is the length-scale parameter of the non-local continuum, which sets the neighbouring volume contributing to the damage of the particular point.

Both constitutive relation and damage evolution law employ the non-local strain $\bar{\varepsilon}$ in this integral non-local model formulation:

$$\sigma = (1-\omega)E\bar{\varepsilon} \tag{C.10}$$

$$\omega = \frac{\bar{\varepsilon}}{\kappa_u} \tag{C.11}$$

The equation of motion in this case can be elaborated as:

$$\varrho\ddot{u} = \frac{\partial\sigma}{\partial x} = (1-\omega)E\frac{\partial\bar{\varepsilon}}{\partial x} - \frac{\partial\omega}{\partial\kappa}\frac{\partial\bar{\varepsilon}}{\partial x}E\bar{\varepsilon} \tag{C.12}$$

where the derivative of the non-local strain can be found as:

$$\frac{\partial\bar{\varepsilon}}{\partial x} = \frac{2}{\ell\sqrt{2\pi}}\int\limits_S \frac{\partial^2 u(x+s)}{\partial x^2}\exp\left(-\frac{s^2}{2\ell^2}\right)\mathrm{d}S \tag{C.13}$$

After substitution of eq. (C.13) into eq. (C.12) and using the harmonic perturbation (C.6), the elaborated equation of motion results in the following expression for the phase velocity:

$$\frac{c^2}{c_e^2} = 2(1-2\omega)\exp\left(-\frac{n^2\ell^2}{2}\right) \tag{C.14}$$

As it can be seen from eq. (C.14) the model loses its stability for $\omega > 0.5$, i.e. in softening all phase velocities become imaginary (fig. C.2).

C.2 Differential models

Another class of non-local models is the model in differential formulation. It is obvious that the integral and differential types of non-local models are connected to each other (cf. Appendix A). The constitutive equation of the differential model is written as

$$\sigma = (1-\omega)E(\varepsilon - \ell^2\nabla^2\varepsilon) \tag{C.15}$$

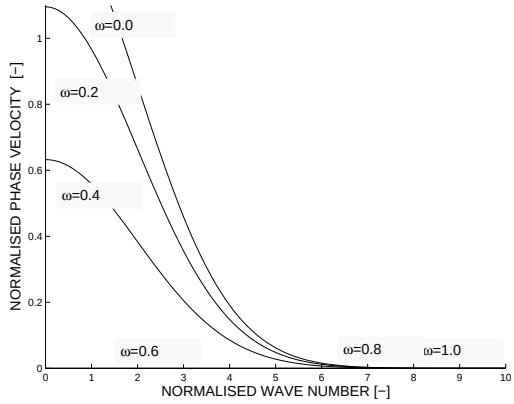

Figure C.2: Strain- and damage-based integral non-local model: normalised phase velocity versus the normalised wave number for different damage levels

The damage evolution law remains local:

$$\omega = \frac{\varepsilon}{\kappa_u} \tag{C.16}$$

After the dispersion analysis procedure, the equation of motion (C.1) together with eqs. (C.15) and (C.16) yields the phase velocity

$$\frac{c^2}{c_e^2} = (1-\omega)(1+\ell^2 n^2) - \omega \tag{C.17}$$

This behaviour is plotted for different damage values in fig. C.3. In the pre-peak regime ($\omega < 0.5$) all wave numbers have real phase velocities. In the post-peak regime ($\omega > 0.5$) some wave numbers have real phase velocities whereas others have imaginary phase velocities. The zone in which strain localisation takes place is set by the condition $c = 0$, and the corresponding wave number is denoted the critical wave number. It is important to realise that the wave numbers with imaginary phase velocities are the ones that are *smaller* than the critical wave number. Those unstable wave numbers correspond to wave lengths that *do not fit* within the localisation zone. Therefore, these unstable waves cannot exist within the softening zone, and it is concluded that this model is stable.

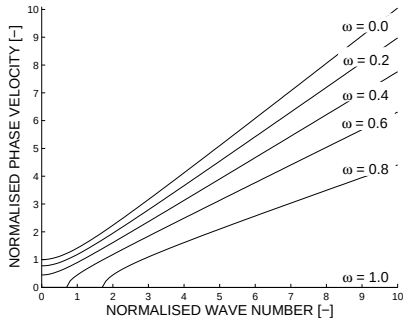

Figure C.3: Strain-gradient model: normalised phase velocity versus the normalised wave number for different damage levels

Summary

Representative Volumes and Multi-scale Modelling in Quasi-brittle Materials

Several different approaches are available in order to describe material behaviour. Considering material on the higher (macro) level of observation constitutes the macroscopic approach. However, the key to understand a macro materials behaviour lies in its mesostructure. As such the mesoscopic approach can be used which is based on the detailed material description of the lower (meso) observational level. The main focus of this dissertation is the combination of the two above techniques – the multi-scale approach. The idea is, by means of a hierarchical multi-scale procedure, to bring the homogenised information of the detailed mesostructural description to the macro-level in the form of effective properties. Thus, the homogeneous macrostructural behaviour is driven by the heterogeneous mesostructure. Traditionally, the size of a Representative Volume Element (RVE) of the material on the meso-level is chosen as a model parameter within the multi-scale framework. Two questions arise: what should this size be and how stable is this multi-scale model based on an RVE? As an answer to the first question, a unique procedure to determine the RVE size is proposed in the dissertation. An extensive study of this size sensitivity to different test and material parameters, both deterministic and stochastic, has been discussed. With knowledge of the RVE size, the multi-scale procedure can be introduced, in which the meso-level RVE plays the role of a macro-level length-scale parameter. However, the answer to the second question is not always positive. As an example the material behaviour due to mechanical loading can be considered. Although the results are stable and reliable in the linear-elastic and hardening regimes, the picture changes in softening. This is caused by the material developing strain localisation and as a consequence losing its statistical homogeneity. For such a material a Representative Volume cannot be found and as an inference cannot be used in the multi-scale framework. A conceptually new so-called coupled-volume multi-scale approach is introduced, based on abandoning the separation of scales principle. This approach does not require an RVE be a model parameter. The idea of the approach is to uniquely link the size of the mesostructural unit cell and element size of the discretised macrostructure. The results of this coupled-volume approach show stable and reliable behaviour in all mechanical regimes.

Inna Gitman

Samenvatting

Representative Volumes and Multi-scale Modelling in Quasi-brittle Materials

Er zijn verschillende methoden beschikbaar om materiaalgedrag te beschrijven. De macroscopische aanpak bestaat er uit het materiaal op het hoogste (macro) observatieniveau te beschouwen. De sleutel tot begrip van macroscopisch materiaalgedrag ligt echter in de mesostructuur. De mesoscopische aanpak kan aldus gebruikt worden, welke gebaseerd is op een gedetailleerde materiaalbeschrijving op het lagere (meso) observatieniveau. De nadruk van dit proefschrift ligt op de combinatie van de bovengenoemde technieken – de multischaal aanpak. Het idee hiervan is door middel van een hiërarchische multischaal procedure de gehomogeniseerde informatie van de gedetailleerde mesostructuurbeschrijving naar het macroniveau te brengen middels effectieve eigenschappen. Het homogene macrostructuurgedrag wordt dus gestuurd door een heterogene mesostructuur. De afmeting van een Representatief Volume Element (RVE) van het materiaal op mesoniveau wordt traditioneel gekozen als een modelparameter in het multischaal raamwerk. Twee vragen komen op: wat moet deze afmeting zijn en hoe stabiel is dit multischaal model gebaseerd op een RVE? Als antwoord op de eerste vraag is in dit proefschrift een éénduidige procedure voorgesteld om de RVE-grootte te bepalen. Een uitgebreide studie naar de gevoeligheid van de grootte voor verschillende test- en materiaalparameters, zowel deterministic als stochastisch, volgt erna. Met kennis van de RVE-grootte kan de multischaal procedure ingevoerd worden, waarbij de mesoscopische RVE optreedt als macroscopische lengteschaal parameter. Het antwoord op de tweede vraag is echter niet altijd positief. Als voorbeeld dient materiaalgedrag onder mechanische belasting. Hoewel de resultaten stabiel en betrouwbaar zijn in de lineair-elastische en hardeningtrajecten, verandert het beeld voor softening materiaalgedrag. Dit wordt veroorzaakt doordat het materiaal reklocalisatie ontwikkeld en daardoor zijn statistische homogeniteit verliest. Voor dit soort materiaal kan geen RVE gevonden worden en dientengevolge ook niet gebruikt worden in een multischaal raamwerk. Een conceptueel nieuw, zogenaamd gekoppeld-volume, multischaal aanpak is geïntroduceerd op basis van het loslaten van het principe van schaalscheiding. Deze aanpak vereist niet dat de RVE een modelparameter is. De idee van deze aanpak is om de mesostructurele eenheidscel één-op-één te koppelen aan de elementgrootte van de gediscretiseerde macrostructuur. De resultaten van de gekoppeld-volume aanpak laten stabiele resultaten zien in alle mechanische trajecten.

Inna Gitman

Acknowledgements

The research presented in this dissertation has been carried out in the framework of a doctoral studies at the Faculty of Civil Engineering and Geosciences of Delft University of Technology.

Using this opportunity I would like to express acknowledgements to my supervisor Bert Sluys for his guidance and support during these research years. I am also most grateful to Harm Askes for his constant encouragements not only in research but also in everyday life.

I would like to thank all my colleagues and friends within and outside the university whose company made my life in Delft much more enjoyable. In particular, I would like to mention Andrei Metrikine, Sandra Pel, Miguel Gutiérrez, Terry Bennett, Ronnie Pedersen, Ellen Kuhl, Yulia Efimova, Alexey Andrianov, Svetlana Ponomaryeva, Tanyada Pannachet, Oriol Lloberas Valls, Ahmed Elkadi, Ivan Markovic, Garth Wells, Angelo Simone, Martijn Stroeven, Hans Welleman, Erik Schlangen, Jaap Weerheijm, Hans van der Weide and of course my room-mate Cecilia Iacono. I am especially grateful to Frank Everdij for his patience and willingness to help.

Further words of thanks I would like to address to Perm State Technical University, especially to the Department of Mathematical Modelling of Systems and Processes for the excellent basis for my research career in the form of MSc and BSc studies.

And finally I deeply thank my parents and brother for their inexpressible and unconditional support.

The financial support by Delft Cluster through project 01.07.02 "Nieuwe Numerieke Technieken" is gratefully aknowledged.

Inna Gitman

Bibliography

[1] E.C. Aifantis. On the microstructural origin of certain inelastic models. *ASME Journal of Engineering Materials and Technology*, 106:26–330, 1984.

[2] E.C. Aifantis. The physics of plastic deformation. *International Journal of Plasticity*, 3:211–247, 1987.

[3] E.C. Aifantis. On the role of gradients in the localization of the deformation and fracture. *International Journal of Engineering Science*, 30:1279–1299, 1992.

[4] B.S. Altan and E.C. Aifantis. On some aspects in the special theory of gradient elasticity. *Journal of the Mechanical Behavior of Materials*, 8:231–282, 1997.

[5] V.N. Ashihmin, M.G. Bojarshinov, M.B. Gitman, I.E. Keller, O.B. Naimark, V.U. Stolbov, P.V. Trusov, and P.G. Frik. *Introduction to Mathematical Modelling*. Intermet Engineering, Moscow, 2000. In Russian.

[6] V.N. Ashihmin and I.A. Povyshev. Statisticheskie zakonomernosti raspredeleniia napriajenii v polikristalah. *Mathematical modelling od system and processes*, 3: 11–18, 1995. In Russian.

[7] H. Askes and A.V. Metrikine. One-dimensional dynamically consistent gradient elasticity models derived from a discrete microstructure. Part 2: Static and dynamic response. *European Journal of Mechanics A/Solids*, 21:573–588, 2002.

[8] H. Askes and A.V. Metrikine. Higher-order continua derived from discrete media: continualisation aspects and boundary conditions. *International Journal of Solids and Structures*, 42:187–202, 2005.

[9] Z.P. Bažant. Why continuum damage is nonlocal: micromechanics arguments. *Journal of Engineering Mechanics*, 117:1070–1087, 1991.

[10] Z.P. Bažant. Size effect. *Inernational Journal of Solids and Structures*, 37:69–80, 2000.

[11] Z.P. Bažant. Probabilistic modeling of quasibrittle fracture and size effect. In Corotis, editor, *Structural safety and reliability*, 2001.

[12] Z.P. Bažant and M. Jirásek. Damage nonlocality due to microcrack interactions: statistical determination of crack influence function. In Z.P. Bažant, Z. Bittnar, M. Jirásek, and J. Mazars, editors, *Fracture and damage in quasibrittle structures*. E& FN Spon, 1994.

[13] Z.P. Bažant and D. Novák. Stochastic models for deformation and failure of quasibrittle structures: recent advances and new directions. In N. Bićanić, R. de Borst, H. Mang, and G. Meschke, editors, *Computational Modelling of Concrete Structures*, 2003.

[14] Z.P. Bažant and B.H. Oh. Crack band theory for fracture of concrete. *Material Structures. RILEM*, 16:155–177, 1983.

[15] Z.P. Bažant and G. Pijaudier-Cabot. Measurement of characteristic length of nonlocal continuum. *Journal of Engineering Mechanics*, 115(4):755–767, 1989.

[16] Z.P. Bažant and A. Yavari. Is the cause of size effect on structural strength fractal or energetic–statistical? *Engineering Fracture Mechanics*, 72:1–31, 2005.

[17] A. Borbely, H. Biermann, and O. Hartmann. FE investigation of the effect of particle distribution on the uniaxial stress–strain behaviour of particulate reinforced metal-matrix composites. *Materials Science and Engineering A*, 313:34–45, 2001.

[18] R.G.M. Breuls, B.G. Sengers, C.W.J. Oomens, and C.V.C. Bouten. Predicting local cell deformations in engineered tissue constructs: A multilevel finite element approach. *ASME Journal of Biomechanical Engineering*, 124:198–207, 2002.

[19] V.N. Bulsara, R. Talreja, and J. Qu. Damage initiation under transverse loading of unidirectional composites with arbitrarily distributed fibers. *Composites Science and Technology*, 59:673–682, 1999.

[20] A. Carpinteri, B. Chiaia, and G. Ferro. *Multifractal scaling law: an extensive application to nominal strength size effect of concrete structures.* Politecnico di Torino, Torino, 1995.

[21] C.S. Chang and J. Gao. Second-gradient constitutive theory for granular material with random packing structure. *International Journal of Solids and Structures*, 32: 2279–2293, 1995.

[22] R. de Borst. Computation of post-biefurcation and post-failure behaviour of strain-softening solids. *Computers & Structures*, 25:211–224, 1987.

[23] R. de Borst and H.B. Muhlhaus. Gradient-dependent plastisity - formulation and algorithmic aspects. *International Journal for Numerical Methods in Engineering*, 35:521–539, 1992.

[24] R. de Borst and L.J. Sluys. *Computational methods in non-linear solid mechanics.* Delft University of Technology, Delft, 2001.

[25] W.J. Drugan. Micromechanics-based variational estimates for a higher-order nonlokal constitutive equation and optimal choice of moduli for elastic composites. *Journal of the Mechanics and Physics of Solids*, 48:1359–1387, 2000.

[26] W.J. Drugan and J.R. Willis. A micromechanics-based nonlocal constitutive equation and estimates of representative volume element size for elastic composites. *Journal of the Mechanics and Physics of Solids*, 44(4):497–524, 1996.

[27] K. Duan, X. Hu, and F.H. Wittmann. Boundary effect on concrete fracture and non-constant fracture energy distribution. *Engineering Fracture Mechanics*, 70: 2257–2268, 2003.

[28] P. Evesque. Fluctuations, correlations and representative elementary volume (rev) in granular materials. *Poudres & Grains*, 11:6–17, 2000.

[29] P. Evesque and F. Adjemian. Stress fluctuations and macroscopic stick-slip in granular materials. *The European Physics Journal E*, 9:253–259, 2002.

[30] J. Fatemi, P.R. Onck, G. Poort, and F. Van Keulen. Cosserat moduli of anisotropic cancellous bone: A micromechanical analysis. *Journal de Physique IV*, 105:273–280, 2003.

[31] F. Feyel and J.L. Chaboche. FE^2 multiscale approach for modelling the elastoplastic behaviour of long fibre sic/ti composite materials. *Computer Methods in Applied Mechanics and Engineering*, 183:309–330, 2000.

[32] M.G.D. Geers, R. de Borst, W.A.M. Brekelmans, and R.H.J. Peerling. On the use of local strain fields for the determination of the intrinsic length scale. *Journal de Physique IV*, 8:167–174, 1998.

[33] N.M. Ghoniem and K. Cho. The emerging role of miltiscale modeling in nano- and micro-mechanics of materials. Technical report, University of California and Stanford University, 2000.

[34] S. Ghosh, K. Lee, and P. Raghavan. A multi-level computational model for multi-scale damage analysis in composite and porous materials. *International Journal of Solids and Structures*, 38:2335–2385, 2001.

[35] I.M. Gitman, H. Askes, and E.C. Aifantis. The representative volume size in static and dynamic micro-macro transitions. *International Journal of Fracture*, 135:3–9, 2005.

[36] I.M. Gitman, H. Askes, and E.C. Aifantis. Gradient elasticity with internal length and internal inertia based on the homogeniastion of a representative volume element. *Journal of the Mechanical Behavior of Materials*, 2006. accepted.

[37] I.M. Gitman, H. Askes, and L.J. Sluys. Representative volume size as a macroscopic length scale parameter. In V.C. Li, C.K.Y. Leung, K.J. Willam, and S.L. Billington, editors, *Fifth international conference on fracture mechanics of concrete and concrete structures*, volume 1, pages 483–491, 2004.

[38] I.M. Gitman, H. Askes, L.J. Sluys, and M. Stroeven. Multiscale modelling of granular materials. In N. Bićanić, R. de Borst, H. Mang, and G. Meschke, editors, *Computational Modelling of Concrete Structures*, 2003.

[39] I.M. Gitman, M.B. Gitman, and H. Askes. Quantification of stochastically stable representative volumes for random heterogeneous materials. *Archive of Applied Mechanics*, 2005. in press.

[40] M.B. Gitman and I.M. Gitman. A new approach to stochastic stability. DH-stability. *Computational and Applied Mechanics*, 2004. in press.

[41] S. Graham and N. Yang. Representative volumes of materials based on microstructural statistics. *Scripta Materialia*, 48:269–274, 2003.

[42] J.M. Guedes and N. Kikuchi. Preprocessing and postprocessing for materials based on the homogenization method with adaptive finite element methods. *Computer Methods in Applied Mechanics and Engineering*, 83:143–198, 1990.

[43] A.A. Gusev. Representative volume element size for elastic composites: a numerical study. *Journal of the Mechanics and Physics of Solids*, 45(9):1449–1459, 1997.

[44] M.A. Gutiérrez. Enegry release control for numerical simulations of failure in quasi-brittle solids. *Communications in Numerical Methods in Engineering*, 20: 19–29, 2004.

[45] Z. Hashin. Analysis of composite materials – a survey. *Journal of Applied Mechanics*, 50:481–505, 1983.

[46] R. Hill. Elastic properties of reinforced solids: some theoreticel principles. *Journal of the Mechanics and Physics of Solids*, 11:357–372, 1963.

[47] R. Hill. The essential structure of constitutive laws for metal composites and polycristals. *Journal of the Mechanics and Physics of Solids*, 15:79–95, 1967.

[48] R. Hill. On macroscopic effects of heterogeneity in elastoplastic media at finite strain. *Mathematical Proceedings of the Cambridge Philosophical Society*, 95:481–494, 1984.

[49] E.T. Jaynes. *Probability theory: the logic of science*. Washington University in St. Louis, USA, 1995.

[50] T. Kanit, S. Forest, I. Galliet, V. Mounoury, and D. Jeulin. Determination of the size of the representative volume element for random composites: statistical and numerical approach. *International Journal of Solids and Structures*, 40:3647–3679, 2003.

[51] B.L. Karihaloo. Size effect in shallow and deep notched quasi-brittle structures. *International Journal of Fracture*, 95:379–390, 1999.

[52] V. Kouznetsova, W.A.M. Brekelmans, and F.P.T. Baaijens. An approach to micro-macro modeling of heterodeneous materials. *Computational Mechanics*, 27:37–48, 2001.

[53] V. Kouznetsova, M.G.D. Geers, and W.A.M. Brekelmans. Multi-scale constitutive modelling of heterogeneous materials with a gradient-enhanced computational homogenization scheme. *International Journal for Numerical Methods in Engineering*, 54:1235, 2002.

[54] V. Kouznetsova, M.G.D. Geers, and W.A.M. Brekelmans. Size of a representative volume element in a second-order computational homogenization framework. *International Journal for Multiscale Computational Engineering*, 2:575–598, 2004.

[55] V.G. Kouznetsova. *Computational homogenization for the multi-scale analysis of multi-phase materials*. PhD thesis, Technical University Eindhoven, 2002.

[56] F. Kozin. A survey of stability of stochastic systems. *Automatica*, 5:95–112, 1969.

[57] T.E. Lacy, D.L. McDowell, and R. Talreja. Gradient concept for evolution of damage. *Mechanics of Materials*, 31:831–860, 1999.

[58] D. Lasry and T. Belytschko. Localization limiters in transient problems. *International Journal of Solids and Structures*, 4:581–597, 1988.

[59] K. Lee and S. Ghosh. Multiple scale analysis of heterogeneous elastic structures using homogenization theory and voronoi cellfinite element method. *International Journal of Solids and Structures*, 32:27–62, 1995.

[60] K. Lee and S. Ghosh. Small deformation multi-scale analysis of heterogeneous materials with the voronoi cell finite element model and homogenization theory. *Computational Materials Science*, 7:131–146, 1996.

[61] J. Lemaitre. *Continuum Damage Mechanics Theory and Applications*. Springer, Wien-New York, 1987.

[62] J. Lemaitre and J.-L. Chaboche. *Meshanics of solid materials*. Cambridge University Press, Cambridge, 1990.

[63] D. Markovic and A. Ibrahimbegovic. On micro-macro interface conditions for micro scale based FEM for inelastic behaviour of heterogeneous materials. *Computer Methods in Applied Mechanics and Ebgineering*, 193:5503–5523, 2004.

[64] T.J. Massart. *Multi-scale modeling of damage in masonry structures*. PhD thesis, Technical University Eindhoven, 2003.

[65] A.V. Metrikine and H. Askes. One-dimensional dynamically consistent gradient elasticity models derived from a discrete microstructure. Part 1: Generic formulation. *European Journal of Mechanics A/Solids*, 21:555–572, 2002.

[66] J.C. Michel, H. Moulinec, and P. Suquet. Effective properties of composite materials with periodic microstructure: a computational approach. *Computer Methods in Applied Mechanics and Engineering*, 16:109–143, 1999.

[67] C. Miehe and A. Koch. Computational micro-to-macro transitions of discretized microstructures undergoing small strains. *Archive of Applied Mechanics*, 72:300–317, 2002.

[68] C. Miehe, J. Schotte, and J. Schröder. Computational micro-macro transitions and overall moduli in the analysis of polycrystals at large strains. *Computational Materials Science*, 16:372–382, 1999.

[69] C. Miehe, J. Schröder, and M. Becker. Computational homogenization analysis in finite elasticity: material and structural instabilities on the micr- and macro-scales of periodic composites and treir interaction. *Computer Methods in Applied Mechanics and Engineering*, 191:4971–5005, 2002.

[70] R.D. Mindlin. Micro-structure in linear elasticity. *Archive for Rational Mechanics and Analysis*, 16:51–78, 1964.

[71] H.-B. Mühlhaus and F. Oka. Dispersion and wave propagation in discrete and continuous models for granular materials. *International Journal of Solids and Structures*, 33:2841–2858, 1996.

[72] H.B. Mühlhaus and E.C. Aifantis. The influence of microstructure-induced gradients on the localization of deformation in viscoplastic materials. *Acta Mechanica*, 89:217–231, 1991.

[73] S. Nemat-Nasser and M. Hori. *Micromechanics: overall properties of heterogeneous materials*. ELSEVIER, 1999.

[74] M. Ostoja-Starzewski. Random field models of heterogeneous materials. *Internation Journal of Solids and Structures*, 35:2429–2455, 1998.

[75] M. Ostoja-Starzewski. Scale effects in materials with random distributions of needles and cracks. *Mechanics of Materials*, 31:883–893, 1999.

[76] M. Ostoja-Starzewski. Microstructural randomness versus representative volume element in thermomechanics. *ASME Journal of Applied Mechanics*, 69:25–35, 2002.

[77] R.H.J. Peerlings. *Enhanced damage modelling for fracture and fatigue*. PhD thesis, Technical University Eindhoven, 1999.

[78] R.H.J. Peerlings, R. de Borst, W.A.M. Brekelmans, and J.H.P. de Vree. Gradient-enchanced damage for quasi-brittle materials. *International Journal for Numerical Methods in Engineering*, 39:3391–3403, 1996.

[79] R.H.J. Peerlings and N.A. Fleck. Computational evaluation of strain gradient elasticity constants. *International Journal for Multiscale Computational Engineering*, 2:599–619, 2004.

[80] G. Pijaudier-Cabot. Non local damage. In H.-B. Mühlhaus, editor, *Continuum models for materials with microstructure*. John Wiley & Sons Ltd., 1995.

[81] G. Pijaudier-Cabot and Z.P. Bažant. Nonlocal damage theory. *Journal of Engineering Mechanics*, 113:1512–1533, 1987.

[82] Z.-Y. Ren and Q.-S. Zheng. A quantitative study of minimum size of reprezentative volume elements of cubic polycrystals – numerical experiments. *International Journal of Physics of Solids*, 50:881–893, 2002.

[83] Z.-Y. Ren and Q.-S. Zheng. Effects of grain sizes, shapes, and distribution on minimum sizes of representative volume elements of cubic polycrystals. *Mechanics of Materials*, 36:1217–1229, 2004.

[84] P. Romero and E. Masad. Relationship between the representative volume element and machanical properties of asphalt concrete. *Journal of Materials in Civil Engineering*, 13:77–84, 1999.

[85] C.Q. Ru and E.C. Aifantis. A simple approach to solve boundary-value problems in gradient elasticity. *Acta Mechanica*, 101:59–68, 1993.

[86] M.B. Rubin, P. Rosenau, and O. Gottlieb. Continuum model of dispersion caused by an inherent material characteristic length. *Journal of Applied Physics*, 77:4054–4063, 1995.

[87] J.P. Schaffer, A. Saxena, S.D. Antolovich, T.H. Sanders Jr., and S.B. Warner. *The Science and Design of Engineering Materials*. McGraw-Hill, Chicago, 2001.

[88] H.L. Schreyer and Z. Chen. One-dimensional softening with localization. *ASME Journal of Applied Mechanics*, 53:791–797, 1986.

[89] Z. Shan and A.M. Gokhale. Representative volume element for non-uniform microstructure. *Computational Materials Science*, 24:361–379, 2002.

[90] A. Simone. *Continuous-discontinuous modelling of failure*. PhD thesis, Delft University of Technology, 2003.

[91] A. Simone, H. Askes, R.H.J. Peerlings, and L.J. Sluys. Interpolation requirements for implicit gradient-enchanced continuum damage model. *Communications in Numerical Methods in Engineering*, 19:563–572, 2003.

[92] L.J. Sluys. *Wave propagation, localisation and dispersion in softening solids*. PhD thesis, Delft University of Technology, 1992.

[93] R.J.M. Smit, W.A.M. Brekelmans, and H.E.H. Meijer. Prediction of the mechanical behavior of nonlinear heterogeneous systems by multi-level finite element modeling. *Computer Method in Applied Mechanics and Engineering*, 55:181–192, 1998.

[94] M. Stroeven, H. Askes, and L.J. Suys. Numerical determination of representative volumes for granular materials. *Computer Methods in Applied Mechanics and Engineering*, 193:3221–3238, 2004.

[95] A. Subramanian and A.H. Sayed. Robust exponential filtering for uncertain systems with stochastic and polytopic uncertainties. In *Proc. CDC, Las Vegas, NY*, 2002.

[96] A.S.J. Suiker, R. de Borst, and C.S Chang. Micro-mechanical modelling of granular material. Part 1: derivation of a second gradient micro-polar constitutive theory. *Acta Mechanica*, 149:161–180, 2001.

[97] A.V. Svishchuk and A.V. Kalemanova. The stochastic stability of interest rates with jump changes. *Theory of Probability and Mathematical Statistics*, 61, 2000.

[98] K. Terada and N. Kikuchi. A class of general algorithms for multi-scale analyses of heterogeneous media. *Computer Methods in Applied Mechanics and Engineering*, 190:5427–5464, 2001.

[99] A. Trukozko and W. Zijl. Complementary finite element methods applied to the numerical homogenization of 3d absolute permeability. *Communications in Numerical Methods in Engineering*, 18:31–41, 2002.

[100] P.V. Trusov and I.E. Keller. *The theory of constitutive relations. Part I.* Perm State Technical University, Perm, 1997. In Russian.

[101] O. van der Sluis. *Homogenisation of structured elastoviscoplastic solids*. PhD thesis, Technical University Eindhoven, 2001.

[102] J.G.M. van Mier. *Fracture processes of concrete*. CRC Press,Inc., USA, 1997.

[103] J.G.M. van Mier. Microstructural effects on fracture scaling in concrete, rock and ice. In *IUTAM Symposium on Scaling Laws in Ice Mechanics and Ice Dynamics*, 2000.

[104] J.G.M. van Mier. Reality behind fictitious crack? In V.C. Li, C.K.Y. Leung, K.J. Willam, and S.L. Billington, editors, *Fifth international conference on fracture mechanics of concrete and concrete structures*, volume 1, pages 11–30, 2004.

[105] M.R.A. van Vliet. *Size effect in tensile fracture of concrete and rock*. PhD thesis, Delft University of Technology, 2000.

[106] I. Vardoulakis and E.C. Aifantis. On the role of microstructure in the behavior of soils - effects of higher-order gradients and internal inertia. *Mechanics of Materials*, 18:151–158, 1994.

[107] O. Vinogradov. On a representative volume in the micromechanics of particulate compusites. *Mechanics of Composite Materials*, 37:245–250, 2001.

[108] M. Wang, P.H.S.W. Kulatilake, J. Um, and J. Narviz. Estimation pf rev size and three-dimensional hydraulic conductivity tensor for a fracturesd rock mass through a single well packer test and discrete fracture fluid flow modeling. *International Journal of Rock Mechanics & Mining Sciences*, 39:887–904, 2002.

[109] Z.-P. Wang and C.T. Sun. Modeling micro-inertia in heterogeneous materials under dynamic loading. *Wave Motion*, 36:473–485, 2002.

[110] W. Weibull. *A statistical theory of the strength of materials*. Royal Technical University, Stockholm, 1939.

[111] W. Weibull. A statistical representation of fatigue failures in solids. In *Royal institute of technology*, volume 27, 1949.

[112] W. Weibull. A statistical distribution function of wide applicability. *Journal of Applied Mechanics*, pages 293–297, 1951.

[113] V.E. Wildemann, U.V. Sokolkin, and A.A. Tashkinov. *Mechanis of non-elastic deformation and damage of composite materials*. Science, Moscow, 1997. In Russian.

[114] S. Zimmermann, C.S. Kleinman, and D.A. Hordijk. Multi-scale modeling of concrete-like composites. In *9th International conference of the mechanical behaviour of materials*, 2003.

[115] T.I. Zohdi, P. Wriggers, and C. Huet. A method of substructuring large-scale computational mecromechanical problems. *Computer Methods in Applied Mechanics and Engineering*, 190:5639–5656, 2001.

Stellingen

1. De klassieke definitie van een Representatief Volume geldt niet voor een materiaal met reklocalisatie.

   The classical definition of a Representative Volume does not hold for a material with strain localisation.

2. Multischaalmodellering gebaseerd op het principe van schaalscheiding leidt niet tot unieke en betrouwbare resultaten in het geval van softening materialen. Daarom moet het principe van schaalscheiding worden losgelaten en de multischaalprocedures worden aangepast voor softening materialen

   Multi-scale modelling based on the separation of scales principle fails to obtain unique and reliable results in the case of softening materials. As such, the separation of scales principle should be abandoned and the multi-scale procedure should be revised for softening materials.

3. Resultaten die falsificeren zijn net zo belangrijk als resultaten die verifiëren.

   Results that falsify are as important as results that verify.

4. Een probleem moet eerst analytisch aangepakt worden en alleen wanneer dit niet lukt numeriek.

   A problem should first be approached analytically and, only if it fails, numerically.

5. Verschillende wetenschappelijke scholen in hetzelfde wetenschapsgebied zijn als verschillende landen — ze spreken verschillende wetenschappelijke talen. Om deze reden moet moeite worden gedaan om kennis te unificeren, minimaal wat betreft vergelijkbare (unieke) terminologie.

   Different scientific schools within the same scientific area are as different countries – they speak different languages of science. For this reason, an effort should be made to unify knowledge, at least in terms of similar (unique) terminology.

6. Alle onderzoekers mogen en moeten hun eigen mening hebben binnen de grenzen der redelijkheid. ("De waarheid komt voort uit een discussie" — Socrates)

   All researchers can and should have their own opinions staying within the limitation of common sense*. ("The truth is born of an argument" — Socrates)*

7. De wiskundige formulering van een probleem moet de kern van de modellering zijn. Zonder een zorgvuldige theoretische basis is het niet mogelijk de juistheid van de oplossing te bediscussiëren.

The mathematical formulation of a problem should be at the heart of the modelling. Without a sound theoretical basis it is impossible to discuss correctness of the solution.

8. De kunst van onderzoek is de "gouden" balans te vinden tussen gewenste nauwkeurigheid en materiaal- en tijdsinvestering die nodig is voor deze nauwkeurigheid.

   The art of research is to find the "golden" compromise between desired accuracy, and material and time expenses necessary for obtaining that accuracy.

9. Kennis van verschillende bestaande methoden helpt in het vinden van nieuwe en innovatieve procedures om een probleem op te lossen, hoewel het ook het aantal vragen en onzekerheden doet toenemen.

   The knowledge of different available methods helps in finding new and innovative approaches to solving a problem, although it also increases the amount of arising questions and uncertainties.

10. Een promovendus moet de gelegenheid worden gegeven om onderwijservaring op te doen.

    A PhD student should be given the opportunity to develop teaching experience.

These propositions are regarded as defendable, and have been approved as such by the supervisor prof. dr. ir. L.J. Sluys.

Curriculum vitæ

Nov. 17$^{\text{th}}$, 1979	Born in Kaluga, Russia (USSR), as Inna Mikhailovna Gitman.
Sept. 1994 – June 1996	Lyceum of the Perm State Technical University, Russia. Distinction: cum laude.
Sept. 1995 – June 1997	Frederikssund Gymnasium, Denmark
Sept. 1996 – June 2000	Bachelor degree in Applied Mathematics and Computer Science, Department of Mathematical Modelling of System and Processes, Perm State Technical University, Russia. Graduation thesis on *Instability and Loss of the symmetry of potential stream of viscous incompressible liquid near stagnation point.* Distinction: cum laude.
Sept. 2000 – June 2002	Master degree in Applied Mathematics and Computer Science, Department of Mathematical Modelling of System and Processes, Perm State Technical University, Russia.Graduation thesis on *Modelling of the behaviour of the three-phase medium.* Distinction: cum laude.
Sept. 2001 – Jan. 2006	PhD researcher in Faculty of Civil Engineering and Geosciences, Delft University of Technology, The Netherlands, under supervision of Prof. L.J. Sluys. Research topic *Representative volumes and multi-scale modelling in quasi-brittle materials*
June 2005 – present	Research associate, School of Mechanical, Aerospace and Civil Engineering, Faculty of Engineering and Physical Science, University of Manchester, United Kingdom